PERFORMANCE CONSIDERATIONS OF WIRELESS MULTIPLE-ACCESS DIGITAL IMPULSE RADIO UNDER REALISTIC MULTIPATH CHANNELS

by

Ali Taha

A Dissertation Presented to the

FACULTY OF THE GRADUATE SCHOOL

UNIVERSITY OF SOUTHERN CALIFORNIA

In Partial Fulfillment of the

Requirements for the Degree

DOCTOR OF PHILOSOPHY

(ELECTRICAL ENGINEERING)

May 2003

Dedication

To my parents, Parviz and Mahanz, who always encouraged me and sacrificed so much to provide me with ease and comfort towards my educations.

To my wife, Elmira, who has always been there for me and filled my life with love and happiness.

Acknowledgements

This dissertation could not come through without the help of many wonderful people around me. First, I would like to express my sincere gratitude to my parents who always encouraged me to study hard and never hesitated to provide me with ease and comfort towards my educations. They sacrificed so much to support me through my first few semesters at the University of Southern California.

God has blessed me with such a wonderful wife who was always there for me through my higher educations and brought me peace of mind and love through hardship and life's fluctuations. She always asked me to enjoy being a student and never rush to finish my Ph.D. She not only supported me emotionally and provided me with a life style far beyond a student's life, but also helped me technically with my computer simulations and saved me a lot of time by applying her programming expertise to my C^{++} programs.

My special thanks go to my kind and intelligent advisor, Professor Keith M. Chugg, who not only taught me how to approach unsolved hard engineering problems, but also supported me financially during my four years of Ph.D.

studies. He inspired me how to write and present highly technical subjects with plain English words. I deeply appreciate what he taught me during these years and I will carry those experiences through my whole life.

I do not know how to thank Professor Robert A. Scholtz who always gave me valuable feedbacks on my research papers. I am honored to have Dr. Scholtz, the prominent expert in ultra wide bandwidth radio, in my Ph.D. committee. I will never forget the wonderful parties at his house at the beginning of each academic year.

My deep appreciation goes to Professor Gary Rosen who taught me the fundamental concepts of analysis and supported me through a teaching assistant position at the Department of Mathematics for one full academic year. He revolutionized my sense of mathematics and opened my eyes towards a way of mathematical thinking that I would never imagine. It is my great pleasure to have him in my Ph.D. committee.

I would like to thank Milly Montenegro, Mayumi Thrasher, and Gerrielyn Ramos for being so nice and creating a friendly atmosphere at the Communication Sciences Institute. Special thanks go to Diane Demetras, Tim Boston, and James Davis who always go beyond their duties in resolving student affairs.

Last but not least, I am pleased to thank my sister and brother, Nazila and Nima, for being kind and supportive during my graduate studies.

Contents

List Of Figures

Abstract

Ultra Wide Bandwidth (UWB) radio has recently been considered as a candidate for short range, high data rate wireless multiple-access communication systems. UWB radio promises a great multiple-access capacity under ideal propagation conditions. In this thesis, performance of wireless multiple access digital impulse radio under realistic multipath channels is investigated. Both time-hopping and direct-sequence spreading schemes along with pulse position and antipodal data modulations are analyzed.

The optimal template waveform design for use at the receiver correlator in order to capture the most amount of energy out of the multipath received signal with the least number of correlations is studied. Since this template waveform algorithm processes only the received signal, channel characteristics and the effects of the antennas on the received pulse shape are implicitly embedded in the design of the optimal template, which are difficult to account for with mathematical models.

UWB radio performance in the presence of an arbitrary external interference source is evaluated and narrow band interference rejection using doublet

pulses is described. Power spectral density of multiple access digital impulse radio for both time-hopping pulse position modulation and direct-sequence bit flipping modulation in the presence of multipath is derived. UWB radio under new spectral masks imposed by regulatory authorities is discussed followed by future research directions of interest.

Chapter 1

Introduction

Multiple access communication allows many users to communicate with each other with tolerable interference. Today, the demand for accessing the internet from virtually anywhere motivates a reliable wireless multiple access scheme. Code division multiple access (CDMA) systems have been extensively investigated in the last two decades [62, 31]. In realistic propagation conditions, multipath phenomena cause degradation in the performance and, even with large fading margin design, an ongoing communication may be disconnected. Multipath phenomenon happens due to the electromagnetic wave reflections from objects, persons, buildings, trees, mountains or anything in the surrounding environment at which the wireless communication takes place.

Multipath channel characteristics of wireless narrow band communication systems have been studied by numerous researchers. A comprehensive study

on this subject can be found in [17, 18, 19, 20, 21, 22, 23, 24, 40, 41]. The models developed for such narrow bandwidth communication systems are not appropriate to be used for Ultra Wide Bandwidth (UWB) communication systems. This is due to the fact that unlike narrow bandwidth systems, the UWB multipath received signal consists of many resolvable paths. However, fading phenomenon is more severely observed for narrow band systems for which many arriving paths may overlap causing Rayleigh or Rician multipath fading distributions depending on whether a strong line of sight path is present or not, respectively.

Finding a solution to combat multipath phenomenon is vital. The most proposed digital impulse radio transmits very narrow pulses, less than a nanosecond wide, which implies an ultra wide bandwidth. This feature makes digital impulse radio a very promising candidate for future multiple access communication needs. Specifically, ultra wide bandwidth radio can resolve multipath phenomenon up to the paths that differ in distance by as low as a fraction of one foot. This unique feature of digital impulse radio also suggests very accurate ranging applications. According to the Federal Communication Commission (FCC) First Report And Order on UWB devices and applications, a UWB device is one where the fractional bandwidth is greater than 25% or occupies 1.5 GHz or more of spectrum. The fractional bandwidth is calculated as $2\frac{f_H - f_L}{f_H + f_L}$ where f_H is the upper frequency of -10 dB emission point

and f_L is the lower frequency of -10 dB emission point. The center frequency of the transmission was simply defined as $\frac{f_H+f_L}{2}$.

Ultra wide bandwidth radio communication systems have the potential for great capacity and robustness. Time-hopping (T-H) impulse radios are among the most developed UWB prototype systems [57] . The multiple access capacity of digital impulse radio employing a time-hopping modulation format under ideal propagation conditions has been investigated [46]. The time-hopping pattern is a way of spreading the signal spectrum. It also adds security with low probability of detection or interception. This is due to the fact that each user has his/her own time-hopping pattern that looks random to all other users, except for the receiver of interest. With ideal propagation conditions, ultra wide band radio promises a great multiple access capacity. In this thesis, the performance of multiple access digital impulse radio under realistic multipath channels is considered, and it is shown that the multiple access capacity is degraded under realistic propagation conditions using a selective combining receiver [58]. This is due to the fact that any ultra wide band time-hopping system will have many resolvable multipath delays because of the very narrow pulses used for this kind of radio, and the delay spread is many times the pulse duration, even indoors [67, 73].

A selective multiple combining receiver [45], which selects the few strongest of many independent multipath components, is considered. The strongest received path may not necessarily be the line of sight path signal [75]. Bit error rate performance of multiple access digital impulse radio is derived. We assume that the receiver of the user of interest is synchronized to the time-hopping pattern and the selected path delays of the user of interest. Each data symbol is repeated several times to attain processing gain at the receiver [72]. Also, each user has his/her own time-hopping pattern, and the data symbol adds an additional pulse position modulation in each frame time. A signal consisting of the dominant paths of the user of interest along with all other dominant multipath components from other users plus the additive white Gaussian noise is received. The receiver correlates this signal against the appropriate template waveform associated to the user of interest. Employing longer frame times reduces the chance of multipath collisions, but this introduces a reduction in data rate for a fixed number of pulses per data symbol.

The organization of this dissertation is as follows. Chapter Two deals with designing the optimal template waveform used at the receiver of ultra wide bandwidth radio. Using an appropriate template waveform matched to the received signal allows extracting the energy of the received signal efficiently. This efficiency becomes vital for ultra wide bandwidth impulse radio in the presence of multipath, where each path undergoes a different channel causing

distortion in the received pulse shape due to a variety of factors such as different amounts of attenuation for different frequencies [44, 42, 43]. In such a situation, using a clean ideal line of sight path signal as a template may degrade the performance due to the mismatches between the template waveform and the received signal. Furthermore, because of inherent filtering in the RF processing (i.e., antennas, amplifiers, etc.), it is often difficult to determine even such a clean line of sight pulse. Algorithms for designing optimal template waveforms for UWB impulse radio are developed and the improvement over a more traditional template waveform used for this kind of radio is illustrated. The template waveform design algorithm developed in this chapter is not limited to UWB systems, and can be applied to any kind of communication system.

Multiple access performance of digital impulse radio in the presence of multipath is derived and discussed in Chapter Three. Digital impulse radio has been recently considered as a new technology for short range high data rate indoor wireless communications [63, 81, 53, 52]. Researchers have published papers on the performance of digital impulse radio under various simplifying assumptions in order to use a tractable approach to the problem. In [46, 77, 78, 74, 72], no multipath has been assumed for the performance of multiple access impulse radio, instead, only one line of sight path exists between each user's transmitter and the receiver of the user of interest. In many other

articles, such as [6, 4, 5, 29, 37, 42, 10, 71, 1, 50, 76], multipath characteristics without consideration of multiuser collisions have been investigated. In this chapter, the multiple access performance of digital impulse radio under realistic propagation conditions is investigated. Signals transmitted by different users experience different channels depending on the position of each user.

In Chapter four, the effects of an external interference on multiple-access digital impulse radio is analytically investigated. Ultra wide bandwidth impulse radio occupies huge bandwidth. This suggests that many coexisting communication systems working simultaneously at different regions of impulse radio's bandwidth cause interference. In this chapter, the effects of an arbitrary external interference as SNR and bit error rate degradation of multiple access UWB radio versus interference frequency is theoretically evaluated and pulse shape design for narrow band interference rejection is presented. Using doublet pulses [14] and computing 99% energy bandwidth, it is shown how narrow bandwidth interference is mitigated significantly. Effects of amplitude mismatches and gap time offset from the nominal value in a doublet pulse are investigated.

According to new rules imposed by the FCC on ultra wide bandwidth systems and devices, the radiated power should be restricted within specific spectral masks for different applications. For multiuser indoor wireless UWB

networking, the aggregate interference should be less than specified limits allowing other narrow band systems to operate reliably. This motivates deriving the power spectral density of multiple access digital impulse radio in the presence of realistic propagation conditions. This task is carried on in Chapter five.

Chapter six studies the UWB impulse radio under FCC regulations. A pulse shape fit to the spectral mask is used to investigate the performance of multiple access UWB radio in the presence of multipath channels. Chapter seven gives an overview for future research directions.

Chapter 2

Template Waveform Design

2.1 Introduction

Using an appropriate template waveform matched to the received signal allows extracting the energy of the received signal efficiently. This efficiency becomes vital for Ultra Wide Bandwidth (UWB) impulse radio in the presence of multipath, where each path undergoes a different channel causing distortion in the received pulse shape due to a variety of factors such as different amounts of attenuation for different frequencies [44, 42]. In such a situation, using a clean ideal line of sight path signal as a template may degrade the performance due to the mismatches between the template waveform and the received signal. Furthermore, because of inherent filtering in the RF processing (i.e., antennas, amplifiers, etc.), it is often difficult to determine even such a clean

line of sight pulse. In this chapter, algorithms for designing optimal template waveforms for UWB Impulse Radio are developed and the improvement over a more traditional template waveform used for this kind of radio is illustrated.

Due to sending a sub-nanosecond pulse in each frame period, impulse radio enjoys a very high multipath resolution capability and a very low duty cycle signal with huge spread spectrum processing gain [77, 46, 74]. On the other hand ultra-wide bandwidth suggests that the higher frequencies attenuate more than the lower frequencies [44, 42, 43], causing distortion in the shape of the received pulse. The delay spread of the impulse radio received signal is many pulse durations even for indoor applications. These phenomena motivate the design of an algorithm which derives an optimal template waveform at the receiver that captures the most amount of energy with the least number of correlations. Since the effects of the channel are somehow embedded in the received signal, we can compute the optimal template waveform based on the received signal online. This makes our algorithm adaptive, since with changes in the channel, the received signal changes, and so does our template based on the received signal. We show the improvement achieved by this template waveform compared to more traditional second order derivative of Gaussian waveform [73], by applying our iterative algorithm to real data obtained from measurement experiments taken in the Wireless Radio Lab of the University of Southern California. Using our template waveform algorithm

helps us adapt our template to different environments based on the received signal which embodies all the channel characteristics, including those of the antennas on the waveforms which are sometimes not well-understood. The algorithm developed in this chapter is not limited to UWB systems only, and can be applied to any kind of communication system.

First, optimal long-tailed template waveform design is presented, which then leads us to design optimal single path template waveform. After that, convergence and robustness of the template waveform design algorithm are discussed, followed by concluding remarks at the end of this chapter.

2.2 Long-Tailed Template

Using a digital sampling oscilloscope, 9 measurements have been taken in the Wireless Radio Lab of the University of Southern California. These measurements are shown in Fig. 2.1. These are the received signals from a pulser that generates Gaussian pulses. It is worth mentioning that each measurement is the average of 256 received profiles at the same location to get a more stable measurement and neglect some transient effects. We sample each measurement at a rate greater than the Nyquist rate and normalize them to have unit energy. After these procedures, we represent each measurement by a vector,

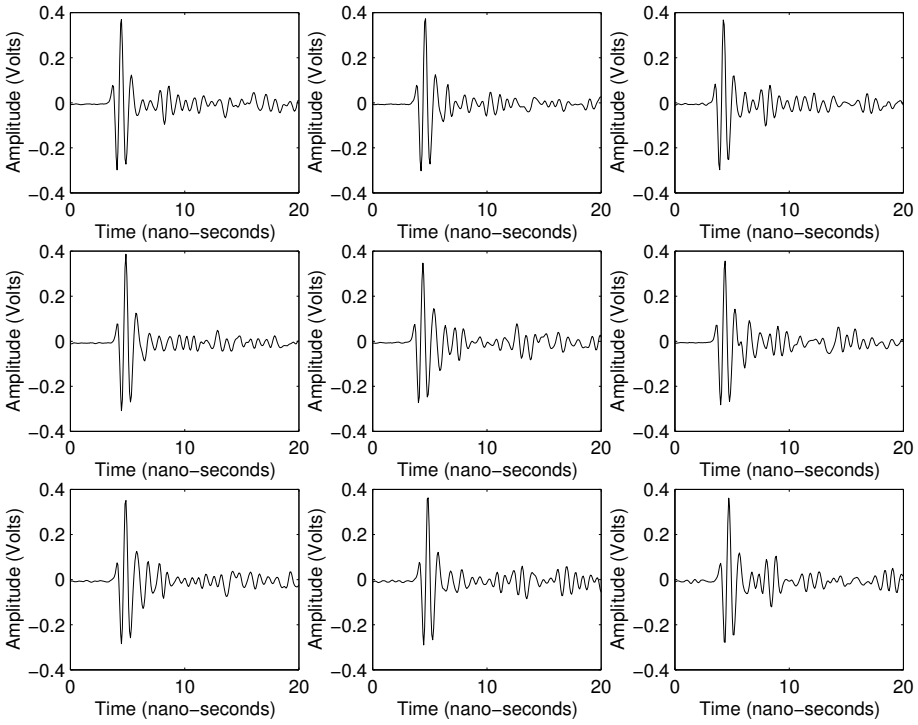

Figure 2.1: Measurements from the UWB radio received waveform taken at the Wireless Radio Lab at the University of Southern California

namely, $\mathbf{r}_i = [r_{i1} r_{i2} ... r_{in}]^t$, for $i = 1, 2, ..., 9$. Define the vector $\mathbf{w} = [w_1 w_2 ... w_n]^t$ for which the function,

$$F = \sum_{i=1}^{N} | < \mathbf{r}_i, \mathbf{w} > |^2 \tag{2.1}$$

is maximum. In this case, we find the nearest vector to all the measurement vectors in the sense that it captures the most amount of energy out of the measurements if we just do a single correlation at the receiver. [1] We set $\mathbf{w}$ to be of unit energy for normalization purposes. This is a constrained optimization problem (see appendix C in [25]) with $\|\mathbf{w}\| = 1$.

2.3 Solving the Constrained Optimization Problem

Rewrite F as

$$F = \sum_{i=1}^{N} (\sum_{j=1}^{n} r_{ij} w_j)^2 = f(\mathbf{w}) \tag{2.2}$$

[1] This is equivalent to a L.S. criterion when $\|\mathbf{w}\|$ is constrained to be constant.

where $f(\mathbf{w})$ explicitly shows that F is a function of $\mathbf{w}$. Solving a constrained optimization problem, we have to work with $h(\mathbf{w})$, where

$$h(\mathbf{w}) = f(\mathbf{w}) + \lambda c(\mathbf{w}) \tag{2.3}$$

where

$$c(\mathbf{w}) = \mathbf{w}^t.\mathbf{w} - 1 \tag{2.4}$$

is our constraint subject to $c(\mathbf{w}) = 0$. Rewrite $h(\mathbf{w})$ as

$$h(\mathbf{w}) = \sum_{i=1}^{N}(\sum_{j=1}^{n} r_{ij}w_j)^2 + \lambda((\sum_{j=1}^{n} w_j^2) - 1) \tag{2.5}$$

Taking the derivatives of $h(\mathbf{w})$ with respect to $w_k, k = 1, 2, ..., n$, we have

$$\frac{\partial h(\mathbf{w})}{\partial w_k} = 2((\sum_{i=1}^{N}(\sum_{j=1}^{n} r_{ik}(r_{ij}w_j))) + \lambda w_j) \tag{2.6}$$

In order to obtain the optimized values for w_k's, we need to set each derivative $\frac{\partial h(\mathbf{w})}{\partial w_k}, k = 1, 2, ..., n$, equal to zero. Therefore,

$$(\mathbf{A} + \lambda\mathbf{I})\mathbf{W} = \mathbf{0} \tag{2.7}$$

where

$$\mathbf{A} = \mathbf{M} * \mathbf{M}^t \tag{2.8}$$

and $\mathbf{M}$ is a matrix whose ith column is $\mathbf{r}_i$. Hence, $\mathbf{w}$ is simply the normalized eigen vector of matrix $\mathbf{A}$ corresponding to its largest eigen value since

$$F = \sum_{i=1}^{N}(\sum_{j=1}^{n}\sum_{l=1}^{n}(r_{ij}w_j w_l r_{il})) = \sum_{j=1}^{n}\sum_{l=1}^{n}(w_j(\sum_{i=1}^{N} r_{ij}r_{il})w_l) \tag{2.9}$$

or

$$F = \sum_{j=1}^{n}\sum_{l=1}^{n}(w_j(A_{jl})w_l) = \mathbf{w^t A w} = \mathbf{w^t}(-\lambda \mathbf{w}) = -\lambda\|\mathbf{w}\|^{\mathbf{2}} = -\lambda \tag{2.10}$$

where we have used the fact that $\mathbf{w}$ is the eigen vector of matrix $\mathbf{A}$ with associated eigen value $-\lambda$ according to (2.7) and that the pqth element of matrix $\mathbf{A}$ can be defined as $A_{pq} = \sum_{i=1}^{N}(r_{ip}r_{iq})$ for $p, q = 1, 2, ..., n$.

We see from (2.10) that the maximum of F can be obtained by choosing the eigen vector of matrix $\mathbf{A}$ associated to its largest eigen value. So our algorithm works according to the following steps:

1- Compute matrix $\mathbf{A}$. This can be done as soon as the measurements become available using (2.8).

2- Compute the largest eigen value of matrix **A**.

3- Obtain the eigen vector of matrix **A** associated to its largest eigen value and normalize it to have a unit norm to satisfy the constraint of the optimization.

This normalized eigen vector is simply the optimal template waveform when we want to do only one correlation against the received signal at the receiver. This problem can be generalized in a straight forward manner to the case when we want to design two or more orthogonal template waveforms that capture the energy of the received signal optimally. The solution is the eigen vectors corresponding to the largest eigen values of matrix **A**. Since matrix **A** is symmetric, these template waveforms can be selected orthogonal. Fig 2.2 shows 9 orthonormal template waveforms corresponding to the nine nonzero eigen values of matrix **A**. The first template waveform at the upper left corner of the figure captures 58.39% of the total energy contained in all the measurements by just one correlation with each measurement. The second template in the upper middle of the figure, captures 23% of the total energy out of all the measurements with just one correlation with each measurement. The rest of the templates capture $8.38\%, 3.61\%, 2.21\%, 1.71\%, 1.20\%, 0.83\%, 0.67\%$ of the total energy out of all the measurements, respectively. For nine measurements, we should be able to capture the whole energy with at most nine single

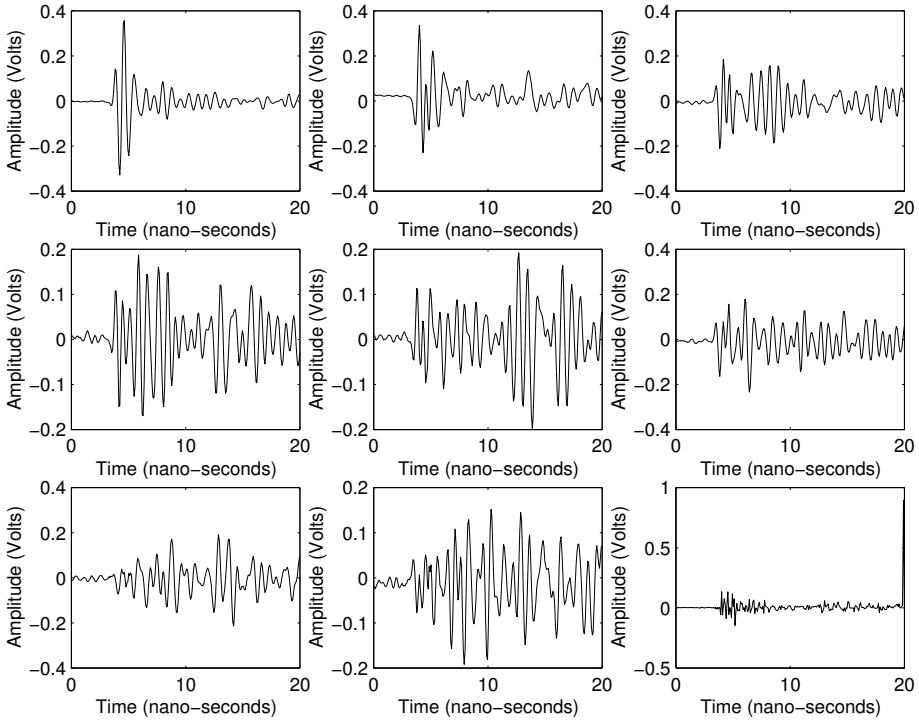

Figure 2.2: Orthonormal templates as the output of the algorithm

long-tailed orthonormal template waveforms. By looking at matrix $\mathbf{A}$, we see that each element somehow computes the average of the correlation between two specified components of each measurement, over all the measurements. In other words, matrix $\mathbf{A}$ represents the average of autocorrelations of different measurements, because $\mathbf{A}$ can be written as:

$$\mathbf{A} = \sum_i \mathbf{r}_i \mathbf{r}_i^t \tag{2.11}$$

2.4 Single Path Template

As Fig. 2.1 shows, there are a lot of paths in the received signal. We want to resolve the paths and find the optimal template waveform based on these individual paths. In that case we desire a short-tailed template waveform (i.e., with support much less than the delay spread) and we may use it to do a selective multiple combining [45] for the most dominant paths. Define the new objective function F as

$$F = ||r(t) - \sum_{j=1}^{L} c_j w(t - n_j)||^2 \tag{2.12}$$

where $r(t)$ is a typical received waveform, n_j is the delay associated to its jth path and c_j is its corresponding amplitude. As the above formula suggests, we

assume only the first L dominant paths in our model. In order to minimize F with respect to $w(t)$, c_j's, and n_j's, we first minimize F conditioned on a given waveform $w(t)$ as an initial estimation. A good initial estimation can be the truncated version of the long-tailed template waveform obtained in the last section. After finding the optimized values of c_j's and n_j's for $j = 1, 2, ..., L$ based on this initial waveform, we use these values of the coefficients c_j's and delays n_j's to find the optimized waveform $w(t)$ with support T_m. Now we use this new optimized waveform $w(t)$ to compute the new values of the coefficients and delays and we repeat this procedure again and again until convergence occurs for the waveform $w(t)$. The support of $w(t)$, T_m, is a design parameter. If we assign a very small width for the template waveform, then it will not be efficient, since it requires more correlations against the received signal to capture the same amount of energy. Therefore, we can choose an initial value for T_m, and then obtain the template waveform and compute the number of correlations to capture a specified amount of energy out of the received signal. Then we increase T_m, and repeat the same procedure again. If the reduction in the number of correlations to capture the same amount of energy is significant, we increase T_m again up to the point where the reduction is not worth choosing a longer template waveform or we get negligible values for the template waveform after some point. For the case when we know the width of one received pulse, we can simply choose T_m such that it meets the width of

the pulse. So $F = ||(r(t) - \sum_{j=1}^{L} c_j w_I(t - n_j))||^2$ where subscript I means the initial estimation for $w(t)$. Assume the received signal as $r(t) = s(t) + \tilde{n}(t)$ where $\tilde{n}(t)$ is the additive white Gaussian noise with power spectral level of $\frac{N_0}{2}$. The received signal $r(t)$ consists of several paths at specific delays n_i's, and amplitudes c_i's, for $i = 1, 2, ..., L$. Assuming selective combining for the first L dominant paths, we ignore the rest of the paths:

$$r(t) = \sum_{i=1}^{L} c_i w(t - n_i) + \tilde{n}(t) \tag{2.13}$$

Finding the maximum likelihood (ML) estimator is equivalent to finding the Minimum Mean Squared Estimates (MMSE) of c_i's and n_i's, because $\tilde{n}(t)$ is AWGN [36]. These MMSE can be found such that $\int_0^T |r(t) - \sum_{i=1}^{L} c_i w(t - n_i)|^2 \, dt$ is minimized. Defining $\mathbf{c} = [c_1 c_2 ... c_L]^t$ and $\mathbf{n} = [n_1 n_2 ... n_L]^t$ and ignoring the irrelevant term of the above integral in calculating the MMSE of $\mathbf{c}$ and $\mathbf{n}$ we get the following function that should be minimized [73]:

$$f(\mathbf{c}, \mathbf{n}) = \mathbf{c}^+ \mathbf{R} \mathbf{c} - \mathbf{c}^+ \mathbf{X}(\mathbf{n}) - \mathbf{X}^+(\mathbf{n}) \mathbf{c} \tag{2.14}$$

where

$$\mathbf{X}(\mathbf{n}) = \int_0^T r(t) \begin{pmatrix} w(t-n_1) \\ w(t-n_2) \\ \cdots \\ w(t-n_L) \end{pmatrix} dt \tag{2.15}$$

and the correlation matrix $\mathbf{R}$ is

$$\mathbf{R} = \begin{pmatrix} R(n_1-n_1) & R(n_1-n_2) & \ldots & R(n_1-n_L) \\ R(n_2-n_1) & R(n_2-n_2) & \ldots & R(n_2-n_L) \\ \vdots & & & \\ R(n_L-n_1) & R(n_L-n_2) & \ldots & R(n_L-n_L) \end{pmatrix} \tag{2.16}$$

where

$$R(n_i - n_j) = \int_0^T w(t-n_i)w(t-n_j)\,dt \tag{2.17}$$

Notice that the ith component of $\mathbf{X}$ represents the correlation between the received signal $r(t)$ and $w(t-n_i)$. Define

$$\Lambda(\mathbf{n}) = \mathbf{R}^{-1}\mathbf{X}(\mathbf{n}) \tag{2.18}$$

Adding and subtracting $\Lambda^{+}(\mathbf{n})\mathbf{R}\Lambda(\mathbf{n})$ to (2.14) and regrouping the like terms,

$$f(\mathbf{c},\mathbf{n}) = (\mathbf{c}-\Lambda(\mathbf{n}))^{+}\mathbf{R}(\mathbf{c}-\Lambda(\mathbf{n})) - \Lambda^{+}(\mathbf{n})\mathbf{R}\Lambda(\mathbf{n}) \tag{2.19}$$

Define

$$\mathbf{D} = (\mathbf{c}-\Lambda(\mathbf{n}))^{+}\mathbf{R}(\mathbf{c}-\Lambda(\mathbf{n})) \tag{2.20}$$

As can be observed, $\mathbf{D}$ is non-negative definite [54], so $f(\mathbf{c},\mathbf{n})$ will be minimum if $\mathbf{D}=\mathbf{0}$. Define

$$\mathbf{B} = \Lambda^{+}(\mathbf{n})\mathbf{R}\Lambda(\mathbf{n}) = \mathbf{X}^{+}(\mathbf{n})\mathbf{R}^{-1}\mathbf{X}(\mathbf{n}) \tag{2.21}$$

In order $f(\mathbf{c},\mathbf{n})$ to be minimum, $\mathbf{B}$ should be maximum. From $\mathbf{D}=\mathbf{0}$, it is concluded

$$\mathbf{c} = \Lambda(\mathbf{n}) = \mathbf{R}^{-1}\mathbf{X}(\mathbf{n}) \tag{2.22}$$

Therefore Maximum Likelihood Estimates of the delay vector $\mathbf{n}$ and amplitude vector $\mathbf{c}$ are

$$\hat{\mathbf{n}} = \arg\max(\mathbf{X}^{+}(\mathbf{n})\mathbf{R}^{-1}\mathbf{X}(\mathbf{n})) \tag{2.23}$$

and

$$\hat{\mathbf{c}} = \mathbf{R}^{-1}\mathbf{X}(\hat{\mathbf{n}}) \tag{2.24}$$

Now we will use the values obtained for delays and amplitudes in (2.23) and (2.24) to compute the optimum $w(t)$, and then we will repeat the whole procedure using our new $w(t)$ instead of $w_I(t)$ until the designed template waveform converges to its final format. Working in the discrete domain, we sample each waveform with a rate higher than the Nyquist rate, and represent the discrete version of the F as

$$F = ||\mathbf{r} - \sum_{j=1}^{L} \hat{c_j}\mathbf{w}(n - \hat{n_j})||^2 \tag{2.25}$$

In order to compute the new $w(t)$, we need to minimize F with respect to vector $\mathbf{w}$. In the above equation, $\mathbf{r}$ is an $q \times 1$ vector, and $\mathbf{w}$ is an $m \times 1$ vector, and in order to write the above equation correctly, we need to add zeros to each $\mathbf{w}(n - \hat{n_j})$ such that it becomes a vector of order $q \times 1$ too, i.e.,

$$\mathbf{w(n - \hat{n}_j)} = [\mathbf{0\ \ 0 \cdots 0\ \ x_1\ \ x_2\ \ x_3 \cdots x_m\ \ 0\ \ 0\ \ 0 \cdots 0}]^{\mathbf{t}} \tag{2.26}$$

where we have added $\hat{n_j}$ zeros at the beginning of the matrix, and then we have the unknown coefficients, x_j's, which are to be determined, and finally

we add $q - m - \hat{n_j}$ zeros to complete the dimension as an $q \times 1$ vector. Write F as

$$F = \mathbf{r}^t\mathbf{r} + \sum_{k=1}^{L}\sum_{i=1}^{m} c_k^2 x_i^2 + 2\sum_{k=1}^{L}\sum_{l<k}\sum_{i=0}^{m-\delta_{lk}-1} c_k c_l x_{1+\delta_{lk}+i} x_{i+1} - 2\sum_{i=1}^{L}\sum_{j=1}^{m} r_{n_i+j} c_i x_j \tag{2.27}$$

where

$$\delta_{lk} = |n_k - n_l| \tag{2.28}$$

In order to maximize F with respect to x_j's for $j = 1, 2, ..., m$, we need to take the derivatives of F with respect to each x_j and equate them to zero.

$$\frac{\partial F}{\partial x_p} = 2\sum_{k=1}^{L} c_k^2 x_p + 2\sum_{k=1}^{L}\sum_{l<k} c_k c_l (x_{p-\delta_{lk}} + x_{p+\delta_{lk}}) - 2\sum_{i=1}^{L} r_{n_i+p} c_i = 0 \tag{2.29}$$

In the above equation set $x_j = 0$ for $j > m$, or $j < 0$. The above linear system of equations can be solved for the given values of c_i's and n_j's using any standard algorithm for solving a linear system of equations available in any numerical computation book such as [3], however, we can give a closed form solution for each unknown x_j, $j = 1, 2, ..., m$ if we assume a sufficient

condition that $\delta_{lk} + 1 > m$ for which we get the following diagonal system of linear equations:

$$\begin{pmatrix} \sum_{i=1}^{L} c_i^2 & 0 & ... & 0 \\ 0 & \sum_{i=1}^{L} c_i^2 & ... & 0 \\ \vdots & & & \\ 0 & 0 & ... & \sum_{i=1}^{L} c_i^2 \end{pmatrix} \begin{pmatrix} x_1 \\ x_2 \\ . \\ . \\ . \\ x_m \end{pmatrix} = \begin{pmatrix} \sum_{i=1}^{L} r_{n_i+1} c_i \\ \sum_{i=1}^{L} r_{n_i+2} c_i \\ . \\ . \\ . \\ \sum_{i=1}^{L} r_{n_i+m} c_i \end{pmatrix} \tag{2.30}$$

which leads to the solution

$$x_p = \frac{\sum_{i=1}^{L} r_{n_i+p} c_i}{\sum_{i=1}^{L} c_i^2} \tag{2.31}$$

for $p = 1, 2, ..., m$. Assuming $\delta_{lk} + 1 > m$ means no two different paths overlap with each other. Particularly for UWB digital impulse radio, two paths with length difference of only a fraction of a foot will not overlap due to the very narrow pulses with very large bandwidth. Therefore, this assumption for outdoor environments, where the length differences of multipath are considerably large, is quite valid.

The last step is to normalize the optimal template waveform that we get from all the above steps in order to make it of unit energy, so that we can

compare its performance with any other unit energy template in terms of the amount of captured energy after correlation.

$$\mathbf{w}_{\text{des}} = \frac{\mathbf{w}}{\|\mathbf{w}\|} \tag{2.32}$$

where $\mathbf{w}_{\text{des}}$ is the designed template waveform as the output of our algorithm.

In order to determine whether the algorithm has converged to $\mathbf{w}_{\text{des}}$ or not, we can use the following criterion: If $\|\mathbf{w}_{\text{des}}^{(k+1)} - \mathbf{w}_{\text{des}}^{(k)}\| < \alpha$ for some small positive α, then stop running the algorithm, otherwise continue from step two. The output of the algorithm after the kth iteration has been denoted by $\mathbf{w}_{\text{des}}^{(k)}$. Here, α depends on the accuracy needed. The smaller the α, the better the approximation. Fig. 2.3 demonstrates the output of the algorithm, $\mathbf{w}_{\text{des}}$, along with the second-order derivative of Gaussian waveform. Fig. 2.4 shows the flow chart of the algorithm.

As (2.23) suggests, there is a nonlinear complexity associated to the exhaustive search for finding the optimal values of the dominant paths's arrival times. However, we can simply use a suboptimal linear search when we assume a negligible overlap between adjacent paths. This can be explained by looking at (2.16). In this case, we can see that matrix R becomes strongly diagonal, so does its inverse in (2.23). Therefore, (2.23) suggests that we need to search for those values of $\mathbf{n}$ where $\|\mathbf{X}\|^2$ becomes maximum. Since we can

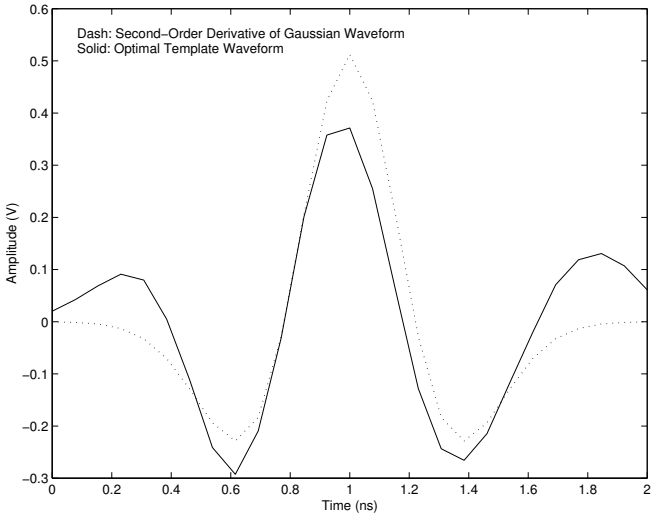

Figure 2.3: Optimal template along with the second-order derivative of Gaussian waveform

search for each dominant path independently in this case, this simply means to find those values of $\mathbf{n}$ for which the magnitude of each component of $\mathbf{X}$ is maximum. This is a linear complex search in terms of the number of components of $\mathbf{X}$. It is worth mentioning that this suboptimal algorithm becomes optimal for the case when there is no overlap between the adjacent paths at all. Because of the excellent multipath resolution capability of impulse radio due to its ultra wide bandwidth, we can employ the suboptimal algorithm with some confidence. Since the results obtained by the suboptimal algorithm match those of optimal algorithm with a high precision, the results presented here reflect those obtained by running the fast linear suboptimal algorithm.

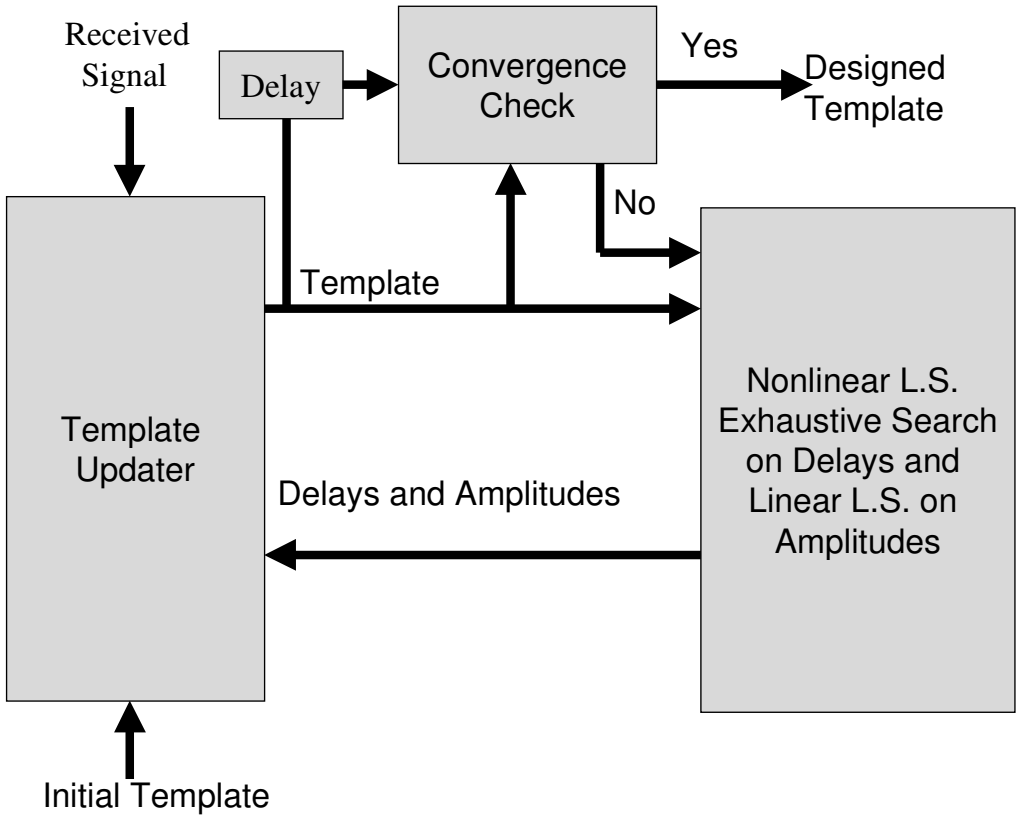

Figure 2.4: Flow chart of the algorithm

Running the suboptimal algorithm on a various generated data using computer simulations has shown that the algorithm resolves the paths successfully under different multipath scenarios where two different paths can even overlap with each other.

2.5 Convergence and Robustness

For any given $w(t)$ at each iteration of the algorithm, $\hat{c_i}$'s and $\hat{n_i}$'s are the maximum likelihood estimates of the amplitudes and delays of different paths. Specifically, $\hat{n_i}$'s are obtained through an exhaustive search to minimize the magnitude of the difference between $\sum_{i=1}^{L} c_i \mathbf{w}(t - n_i)$ and the received waveform $r(t)$. Also at the same time, due to the AWGN nature of the problem, $\hat{c_i}$'s are mean squared estimations which minimize the mean squared error. By these explanations, we see that after estimating the amplitudes and delays of different paths, the mean-squared error becomes smaller during any iteration. For the second part of each iteration, given the estimates of amplitudes and delays, we compute the shape of the template waveform by taking derivatives to minimize the mean-squared error; therefore, we get a smaller mean-squared error after the second half of each iteration. Since the sequence of mean-squared errors is a decreasing sequence bounded from below by zero, we conclude that this sequence is convergent.

In order to make sure that the algorithm converges to a global minimum and not a local one, we need to prove that our objective function is convex with respect to the designed template. To show this, we compute the second order derivative of F with respect to $\mathbf{w}$ using the already available first order derivative in (2.29).

$$\frac{\partial^2 F}{\partial x_p^2} = 2\sum_{k=1}^{k=L} c_k^2 > 0 \tag{2.33}$$

Since this second order derivative is positive for $p = 1, 2, ..., m$, we can conclude that F is convex and therefore, the local and global minima are the same.

Running the algorithm when $L = 3$ for the measurement shown in the upper left corner of Fig. 2.1 and with the initial estimation as the input to the algorithm to be the second-order derivative of Gaussian waveform, demonstrates about 0.93 dB improvement in terms of the captured energy out of the three most dominant paths with respect to that of second-order derivative of Gaussian. Similar results are obtained by running the algorithm on the rest of the measurements. Also, the algorithm converges very fast, and in fact after the second iteration, there is no more improvement. This verifies the optimality of our template waveform shown in Fig. 2.3 over the second order derivative of Gaussian.

Fig. 2.5 shows how our algorithm resolves the three dominant paths of the received signal using an initial estimation of the second-order derivative of Gaussian pulse [73] shown in Fig. 2.6 as the input to the algorithm. Fig. 2.7

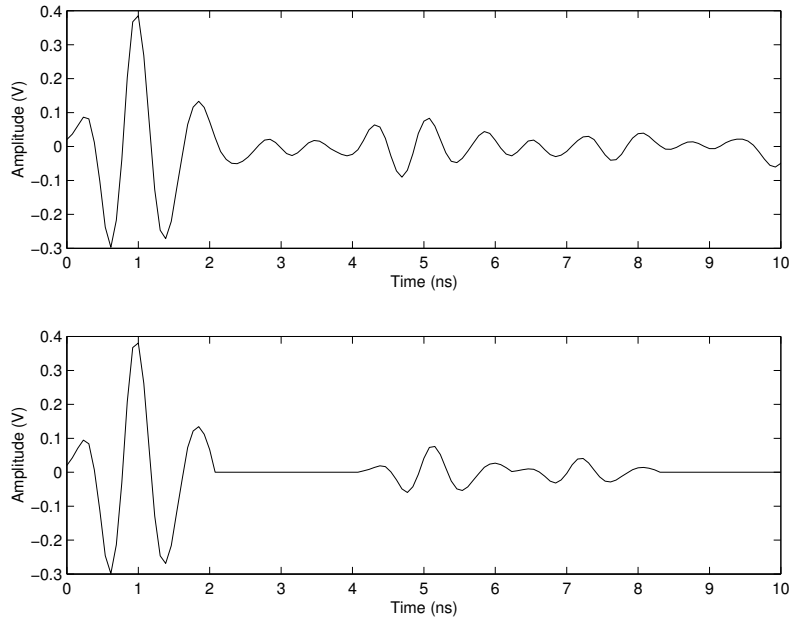

Figure 2.5: Received waveform along with its dominant resolved paths

demonstrates the output of the algorithm, $\mathbf{w_{opt}}$.

To demonstrate the robustness of the algorithm, we consider a simple initial estimation of the template waveform shown in Fig. 2.8, which is just a unit energy rectangular pulse (Flat Template Waveform) over the interval $0 \leq t \leq 2$ nanoseconds. Fig. 2.9 demonstrates the resolved multipath using this flat template waveform. As we observe, the performance is very poor and the captured energy using this template waveform is only 7 percent of the total

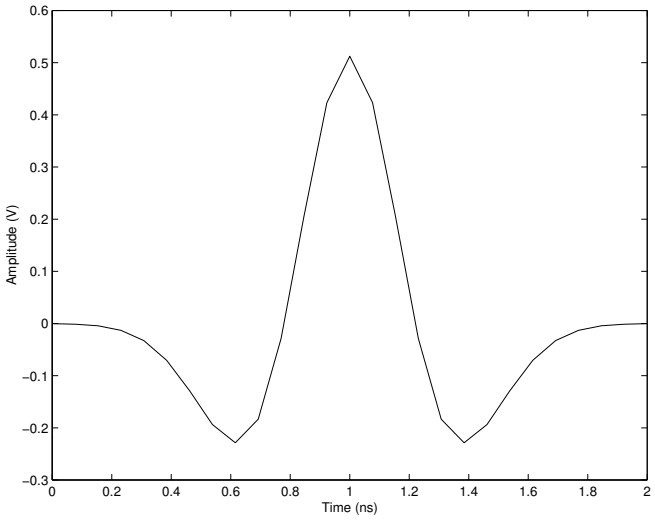

Figure 2.6: Initial waveform as the input of the algorithm (second order derivative of Gaussian waveform)

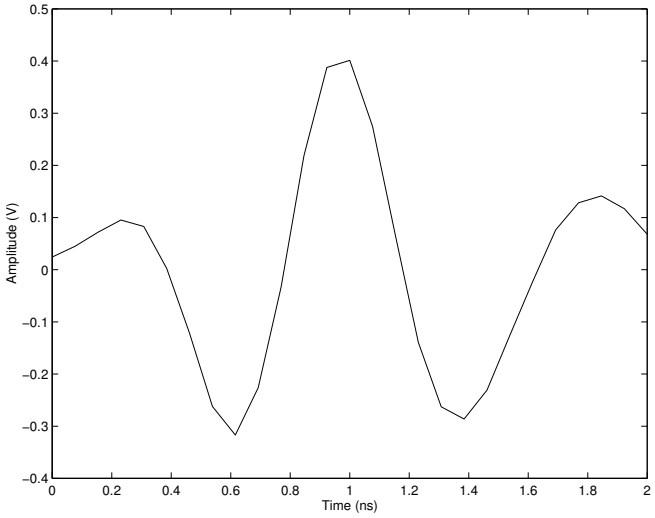

Figure 2.7: Optimal template waveform (output of the algorithm after two iterations)

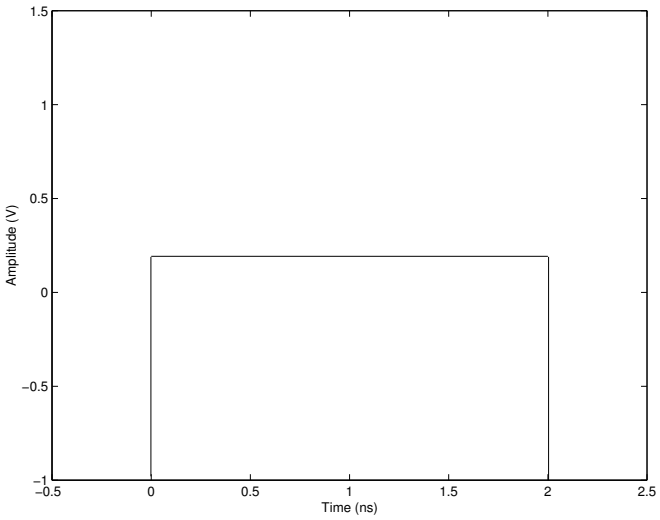

Figure 2.8: A simple initial estimation as the input to the algorithm

energy. Fig. 2.10 illustrates the resolved multipath using the initial template of Fig. 2.8 after two iterations of the algorithm. As can be seen, after just two iterations, the three dominant paths of the received signal has been finely resolved and the output template captures 97 percent of the energy and is identical to the template waveform obtained using the second-order derivative of Gaussian as the initial estimation. The 0.9 dB improvement in extracting the energy out of the received signal using the optimal template waveform compared to the second-order derivative of Gaussian, can even further mitigate the already low fading margin in UWB impulse radio.

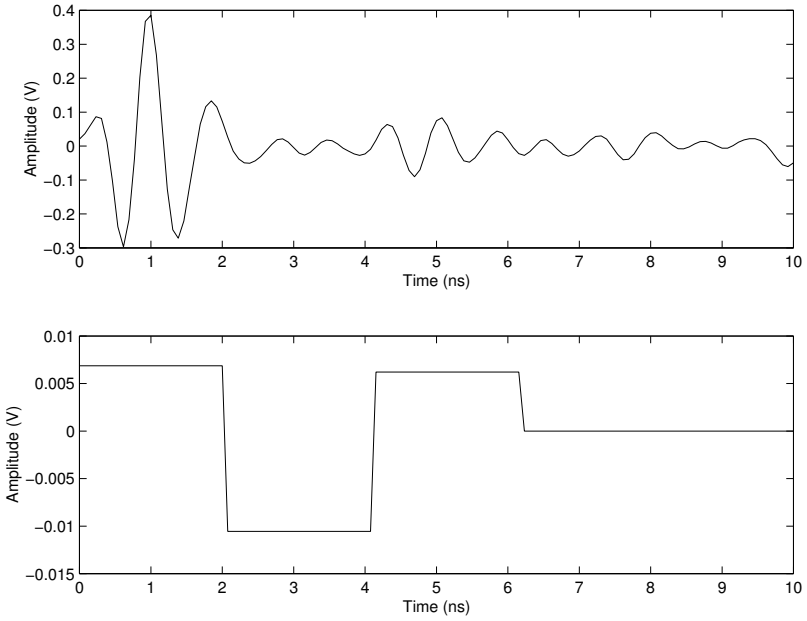

Figure 2.9: Resolved multipath using the template waveform shown in Fig. 2.8

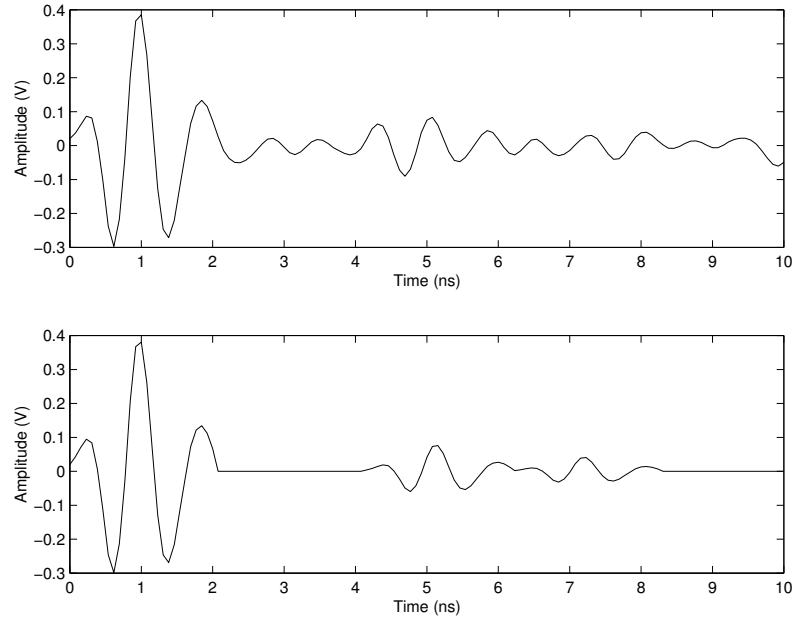

Figure 2.10: Resolved multipath after the two iterations of the algorithm using the initial template of Fig. 2.8

2.6 Conclusion

The effects of the propagation medium along with those of antennas on the transmitted pulse shape are either sometimes not well understood or very hard to model mathematically, specially for typical indoor wireless channels which involve the multipath phenomena due to reflections from the objects present in the medium. Also, penetration of a transmitted pulse into a wall or any other material distorts the transmitted pulse shape. To investigate the mismatches between the transmitted and received pulse shapes, we suggest to extract the received pulse shape based on the received signal. This allows to capture the energy out of the received signal more efficiently using a template waveform that is better matched to the received pulse shape.

Two algorithms to design optimal template waveforms were introduced: One for optimal one-time correlation long-tailed templates and the other for multi-correlation short-tailed templates. We showed how we can design optimal templates in the sense of capturing the most amount of energy with the least number of correlations against the received signal in the presence of multipath. Simulation results verifies the robustness and accuracy of our iterative algorithm. Applying our algorithm to real data obtained from measurements, we notice the capability of the algorithm in resolving the dominant paths of the multipath along with estimating the optimal template waveform

shape which showed around 0.9 dB improvement over more traditionally used templates in captured energy out of the three dominant paths. This is a general algorithm that can be used for any communication system and not just the impulse radio; however, due to the very fine multipath resolution of the impulse radio, we can use suboptimal algorithm in which an exhaustive search can be replaced by a linear complexity block in the algorithm.

Chapter 3

UWB Multiple Access in the Presence of Multipath

3.1 Introduction

Digital impulse radio has been recently considered as a good candidate for short range high data rate indoor wireless communications [63, 81, 53, 52]. Huge bandwidth of this kind of radio helps to resolve differential delays as low as a fraction of a nanosecond. In this chapter, the multiple access performance of digital impulse radio under realistic propagation conditions is investigated. Signals transmitted by different users experience different channels depending on the position of each user. To avoid multiple access collisions, each user is assigned his/her own random spreading sequence; however, we assume that the multiple selective combining receiver of the user of interest

perfectly knows and is synchronized to the spreading code of the user of interest. Both time-hopping and direct-sequence spread spectrum multiple access digital impulse radio in the presence of multipath channels are investigated. In a direct-sequence spread spectrum impulse radio the amplitude of each user's transmitted pulse in a given frame is randomly multiplied by ± 1 according to that user's random sequence generator.

We describe constructive and destructive collisions and evaluate them in terms of being fatal or recoverable in the way they contribute towards the soft decision statistic. If only one pulse is transmitted per bit, then a fatal collision will result in a detection error.

3.2 Introducing the Pulse Position Modulated Time-Hopped Signal

Fig. 3.1 shows the signal transmitted by the kth user. Fig. 3.1.a shows the situation without any time-hopping code or data modulation. Fig. 3.1.b shows the circumstance when time-hopping code is being used without sending any data modulation. Fig. 3.1.c demonstrates the pulse position modulated data when the transmitted data is zero and the time-hopping pattern of the kth user is also utilized at the same time. Fig. 3.1.d shows the pulse position modulated

transmitted signal by the kth user exploiting his/her time-hopping pattern when the transmitted data is one. As can be seen, there is an additional δ shift in time when the transmitted data is one compared to sending a zero.

To avoid catastrophic collisions each user is assigned his/her own time-hopping code. Here we assume that the receiver knows the time-hopping code of the user of interest, and it has synchronized to that perfectly. However, all the other users' time-hopping patterns look random to the receiver. Without loss of generality, we assume that the user of interest is User 1. Fig. 3.2 demonstrates the return link of the wireless multiple-access digital impulse radio in the presence of multipath. Each user's multipath profile has been denoted by a separate channel between that user's transmitter and the receiver of the user of interest.

The pulse position parameter, δ, is optimized such that the cross-correlation between the two received pulse position modulated signals, i.e., $w_{rec}(t)$ and $w_{rec}(t-\delta)$ is minimized. In other words,

$$\delta = \arg\min_{\delta'}\left(\int_0^{T_m+\delta'} w_{rec}(t)w_{rec}(t-\delta')\,dt\right) \tag{3.1}$$

where, T_m is the received pulse width. This optimization leads to the answer $\delta = 0.223T_m$ for the second-order derivative of Gaussian received pulse shape.

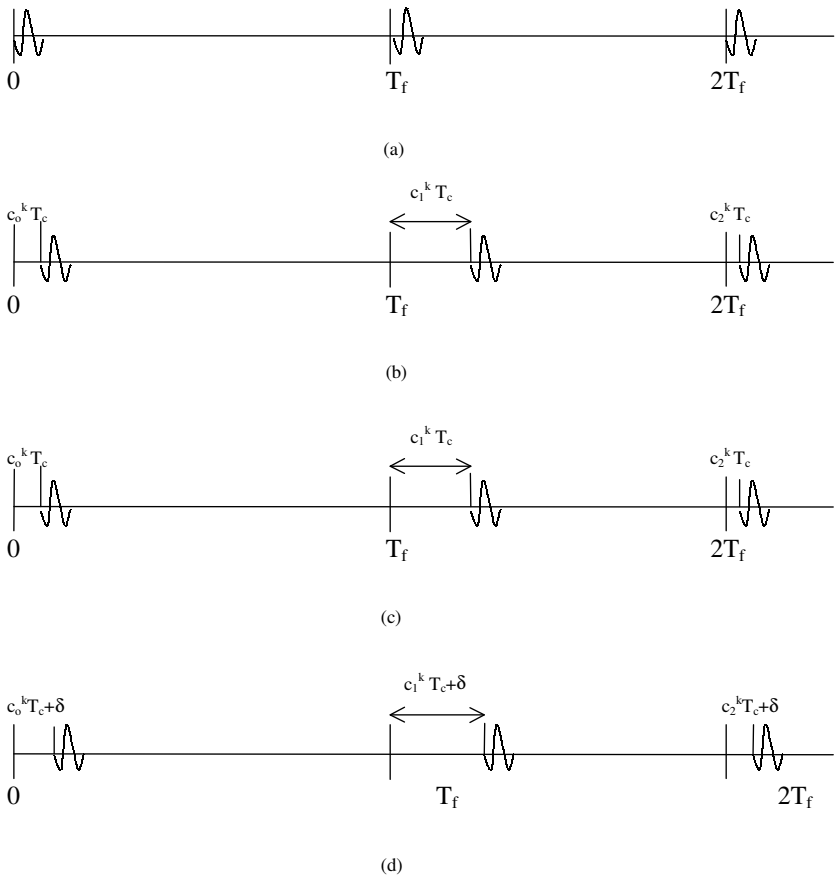

Figure 3.1: Demonstrating the kth user's frames (a)without any time-hopping code or data modulation, (b)with time-hopping code but without any data modulation, (c)with time-hopping code and pulse position data modulation when $D_j^k = 0$, and (d)with time-hopping code and pulse position data modulation when $D_j^k = 1$

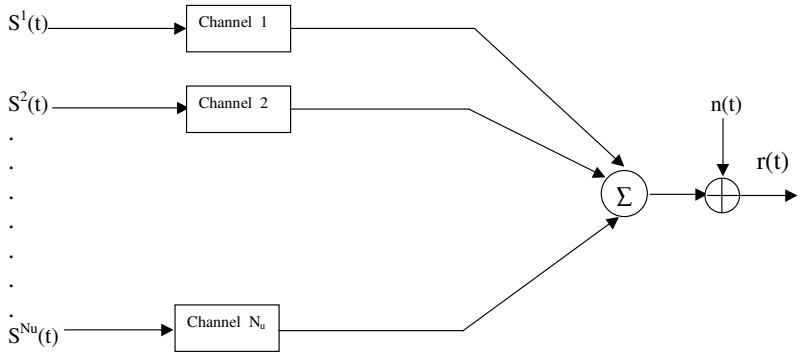

Figure 3.2: Return link (no base-station)

One simple solution is $\delta = T_m$, which leads to orthogonal pulse position modulated signals, however, with optimized value of δ in (3.1), we get performance gain since the cross-correlation in (3.1) will be negative instead of zero. This shows that although using pulse position modulation with antipodal signals is not feasible, using an optimized δ will lead to a better performance than simply orthogonal pulse position modulation.

3.3 Receiver Processing

Assuming N_u active users communicating through the multiple access time-hopping impulse radio, each experiencing a different channel, and considering the first L^k dominant paths for the kth user, the received signal is

$$r(t) = \sum_{k=1}^{N_u} \sum_{m=0}^{L^k-1} g_m^k S_{rec}^k(t - \tau_m^k) + n(t) \tag{3.2}$$

where g_m^k denotes the amplitude of the mth path of the kth user. Also, τ_m^k accounts for its corresponding delay relative to τ_0^1. Therefore, without loss of generality, we assume $\tau_0^1 = 0$. The received signal of user k with no delay with respect to the line of sight path signal of the user of interest (User 1) is denoted by $S_{rec}^k(t)$. The additive white Gaussian noise, $n(t)$, is assumed to have a two-sided power spectral density of $\frac{N_0}{2}$ and

$$S_{rec}^k(t) = \sum_j w_{rec}(t - jT_f - c_j^k T_c - \delta D_j^k) \tag{3.3}$$

where $w_{rec}(t)$ is the received pulse [77] shown in Fig. 3.3. Each data symbol is transmitted repeatedly in N_s consecutive frames in order to attain processing

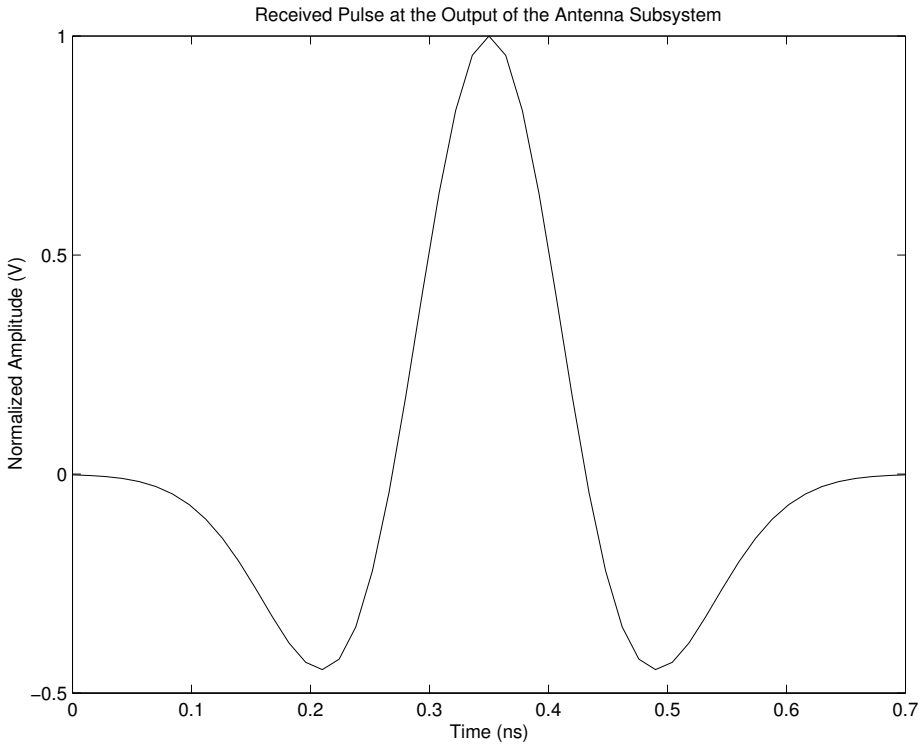

Figure 3.3: Received pulse waveform (second derivative of Gaussian waveform)

gain and make soft decisions at the receiver. Therefore, $D^k_{iN_s} = D^k_{iN_s+1} = \cdots = D^k_{(i+1)N_s-1} = d^k_i$ for all integer i's and $k = 1, 2, ..., N_u$. Here d^k_i is the ith transmitted symbol of user k and D^k_j is the ith repeated transmitted symbol of user k in the jth frame for $j = iN_s, iN_s + 1, ..., (i+1)N_s - 1$. In each frame period T_f, one pulse is transmitted; however, due to multipath phenomenon, several pulses with different amplitudes and delays are received at the receiver of the user of interest. The position of the kth user's pulse in the jth frame is determined by the time-hopping pattern of user k in the jth frame, c^k_j, and his/her transmitted data, $d^k_{\lfloor \frac{j}{N_s} \rfloor}$. The time-hopping codes are assumed random

and independent. Each frame is divided into several time slots with duration T_c [46, 77, 55].

Assuming a multiple selective combining RAKE receiver, the P dominant paths of the user of interest are selected [58, 45], and each is processed in a separate branch as shown in Fig. 3.4. The following correlation is made at the branch corresponding to the qth selected path:

$$A_q(i) = \int_{t=iN_sT_f+\tau_q^1}^{(i+1)N_sT_f+\tau_q^1} r(t) \sum_{j=iN_s}^{(i+1)N_s-1} g_q^1 v(t - jT_f - c_j^1 T_c - \tau_q^1)\, dt \tag{3.4}$$

where

$$v(t) = w_{rec}(t) - w_{rec}(t - \delta) \tag{3.5}$$

is the template waveform [77] used at the receiver shown in Fig. 3.5. Rewriting (3.2) as

$$r(t) = g_q^1 S_{rec}^1(t - \tau_q^1) + \sum_{k=1}^{N_u} \sum_{m=0(k=1,m\neq q)}^{L^k-1} g_m^k S_{rec}^k(t - \tau_m^k) + n(t) \tag{3.6}$$

and replacing it in (3.4), followed by a change of variable,

$$A_q(i) = S_q(i) + M_q(i) + N_q(i) \tag{3.7}$$

Figure 3.4: Block diagram of the multiple selective combining RAKE receiver

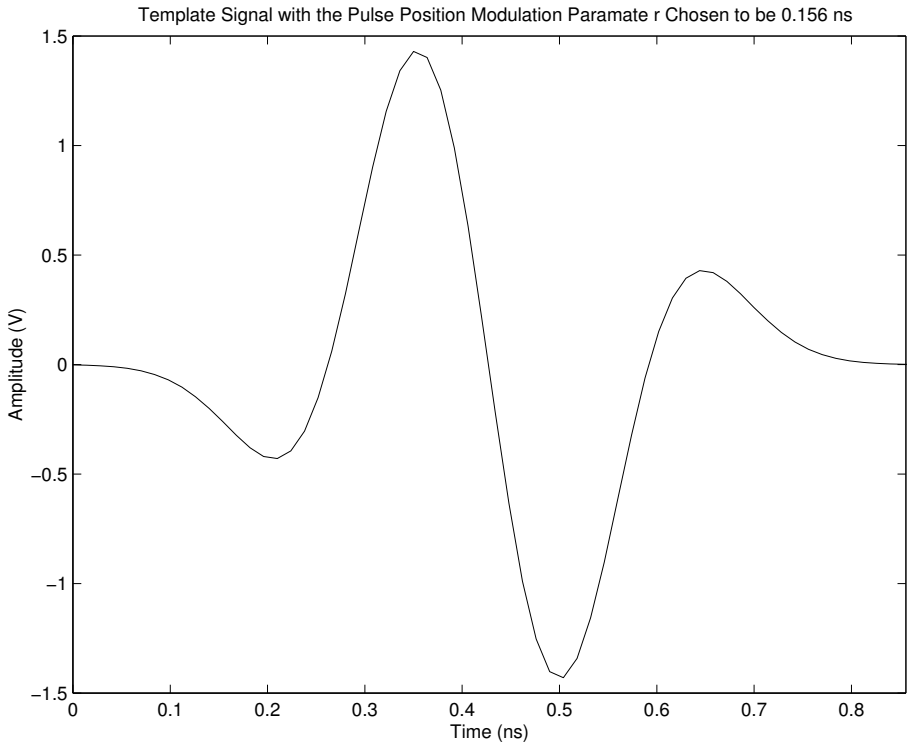

Figure 3.5: Template waveform used at the receiver of time-hopping digital impulse radio

where

$$S_q(i) = \sum_{j=iN_s}^{(i+1)N_s-1} {g_q^1}^2 R_{vw_{rec}}(\delta D_j^1) = N_s {g_q^1}^2 R_{vw_{rec}}(\delta d_i^1) \tag{3.8}$$

$$M_q(i) = \sum_{j=iN_s}^{(i+1)N_s-1} \sum_{k=1}^{N_u} \sum_{m=0(k=1,m\neq q)}^{L^k-1} \sum_{l=\lceil (j-1.5-\frac{\tilde{\tau}}{T_f})\rceil}^{l=\lfloor (j+1.5+\frac{\tilde{\tau}}{T_f})\rfloor} g_q^1 g_m^k$$

$$R_{vw_{rec}}((l-j)T_f + (c_l^k - c_j^1)T_c + \delta D_l^k + (\tau_m^k - \tau_q^1)) \tag{3.9}$$

and parameter $\tilde{\tau}$ is the maximum delay spread of multipath profiles (see Appendix A). $\lceil(x)\rceil$ is the smallest integer greater or equal to x and $\lfloor(x)\rfloor$ is the greatest integer less than or equal to x. Also,

$$R_{vw_{rec}}(\tau) = \int_{-\infty}^{\infty} v(t) w_{rec}(t-\tau)\, dt \tag{3.10}$$

is the cross-correlation between the template waveform $v(t)$ and the received pulse $w_{rec}(t)$ and can have non-zero values only on the interval $[-T_m, T_m + \delta]$, because the support of $v(t)$ is $[0, T_m + \delta]$. Also,

$$N_q(i) = \sum_{j=iN_s}^{(i+1)N_s-1} \int_{-\infty}^{\infty} g_q^1 n(t + jt_f + c_j^1 T_c + \tau_q^1) v(t)\, dt \tag{3.11}$$

accounts for AWGN contribution to the decision statistic.

If $A(i) = \sum_{p=1}^{P} A_{q_p}(i)$ is greater than zero we decide in favor of H_0, that is, the transmitted symbol d_i^1 has been a zero, otherwise we decide the hypothesis H_1. It is worth noting that in all the above signal processing, we have assumed that the receiver is synchronized to the first user's hoping code and selected paths delays. Writing $\tau_m^k = \tau_0^k + \lambda_m^k$, where τ_0^k is the asynchronous delay of user k with respect to the user of interest and λ_m^k is the excess delay of the mth path of the kth user, and assuming $\frac{T_f}{2}$ to be much greater than δ and with careful inspection of the integral and summation intervals, considering:

(i) $w_{rec}(t) = 0$ for $t < 0$, or $t > T_m$

(ii) $T_m > \delta$

(iii) $|c_j^p - c_l^q| T_c < 0.5T_f - \tilde{\tau} - 2T_m - \delta$

we can conclude (see Appendix B)

$$A_q(i) = N_s {g_q^1}^2 R_{vw_{rec}}(\delta d_i^1) + \sum_{j=iN_s}^{(i+1)N_s-1} \sum_{k=1}^{N_u} \sum_{m=0(k=1,m\neq q)}^{L^k-1} g_q^1 g_m^k R_{vw_{rec}}(\delta D_j^k + \tau_0^k + (\lambda_m^k - \lambda_q^1) - (c_j^1 - c_j^k)T_c) + \sum_{j=iN_s}^{(i+1)N_s-1} g_q^1 \int_{-\infty}^{\infty} n(t + jT_f + c_j^1 T_c + \tau_q^1) v(t)\, dt \tag{3.12}$$

3.4 SNR Computation

The signal at the input of the threshold comparator is $A(i) = \sum_{p=1}^{P} A_{q_p}(i)$. Therefore, using (3.12), the signal energy can be computed as

$$S = \mathrm{E}\left\{ \left(N_s R_{vw_{rec}}(\delta d_i^1) \sum_{p=1}^{P} {g_{q_p}^1}^2 \right)^2 \right\} = N_s^2 R_{vw_{rec}}^2(0) \left(\sum_{p=1}^{P} {g_{q_p}^1}^2 \right)^2 \tag{3.13}$$

where the ensemble average has been carried on d_i^1 assuming $\Pr.\{d_i^1 = 0\} = \Pr.\{d_i^1 = 1\} = \frac{1}{2}$. Here, by g_{q_p}, we mean that the pth strongest path of the user of interest is the q_pth arriving path in the corresponding multipath profile. The reader should notice that $R_{vw_{rec}}(0) = -R_{vw_{rec}}(\delta)$.

The interference arising from the non-selected paths of the user of interest plus those of other active users is represented by the term $\sum_{p=1}^{P} \sum_{j=iN_s}^{(i+1)N_s-1} \sum_{k=1}^{N_u} \sum_{m=0(k=1,m\neq q)}^{L^k-1} x(q,m,k)$, where

$$x(q,m,k) = g_q^1 g_m^k R_{vw_{rec}}(\delta D_j^k + \tau_0^k + (\lambda_m^k - \lambda_q^1) - (c_j^1 - c_j^k)T_c) \tag{3.14}$$

By taking the ensemble average of $(x(q,m,k))^2$ with respect to τ_0^k, we have

$$\mathrm{E}\{(x(q,m,k))^2\} = (g_q^1 g_m^k)^2 \frac{1}{T_f} \int_{-\frac{T_f}{2}}^{\frac{T_f}{2}} R_{vw_{rec}}^2(\delta D_j^k + x + (\lambda_m^k - \lambda_q^1) - (c_j^1 - c_j^k)T_c)\, dx \tag{3.15}$$

or

$$\mathrm{E}\{(x(q,m,k))^2\} = \frac{1}{T_f}(g_q^1 g_m^k)^2 \int_{-\frac{T_f}{2}+\delta D_j^k+(\lambda_m^k-\lambda_q^1)-(c_j^1-c_j^k)T_c}^{\frac{T_f}{2}+\delta D_j^k+(\lambda_m^k-\lambda_q^1)-(c_j^1-c_j^k)T_c} R_{vw_{rec}}^2(x)\, dx \tag{3.16}$$

Considering the restriction imposed on the hopping range earlier, the interval integral contains the support of $R_{vw_{rec}}(x)$, hence, it can be extended to the whole real line:

$$\mathrm{E}\{(x(q,m,k))^2\} = \frac{1}{T_f}(g_q^1 g_m^k)^2 \int_{-\infty}^{\infty} R_{vw_{rec}}^2(x)\, dx \tag{3.17}$$

The interference energy can be expressed as

$$I = N_s \sum_{p=1}^{P} \sum_{k=1}^{N_u} \sum_{m=0(k=1,m\neq 0)}^{L^k-1} \frac{1}{T_f} (g_q^1 g_m^k)^2 \int_{-\infty}^{\infty} R_{vw_{rec}}^2(x)\, dx \tag{3.18}$$

Since we normalized all the channels to have the same norm, i.e., $\sum_{m=0}^{L^k-1} (g_m^k)^2 = E = 1$ for all k's, the above expression can be simplified to

$$I = \frac{N_s}{T_f} \int_{-\infty}^{\infty} R_{vw_{rec}}^2(x)\, dx [\sum_{p=1}^{P} (g_{q_p}^1)^2 (N_u E - (g_{q_p}^1)^2)] \tag{3.19}$$

As can be seen, the multiple access interference is proportional to the number of pulses sent per data symbol, and inversely proportional to the frame duration. One should notice that (3.19) represents the multiple access interference variance, because $\mathrm{E}\{x(q,m,k)\} = \frac{1}{T_f} g_q^1 g_m^k \int_{-\infty}^{\infty} R_{vw_{rec}}(x)\, dx = 0$, where same techniques used in deriving (3.19), has been applied on the ensemble average of $x(q,m,k)$ with respect to τ_0^k. Due to propagation effects, $R_{vw_{rec}}$ is the derivative of a function which begins and ends at zero [67].

Finally, to compute the AWGN contribution at the input of the threshold comparator,

$$N = \mathrm{E}\left\{ \left(\sum_{p=1}^{P} \sum_{j=iN_s}^{(i+1)N_s-1} g_{q_p}^1 \int_{-\infty}^{\infty} n(t + jT_f + c_j^1 T_c + \tau_{q_p}^1) v(t)\, dt \right)^2 \right\} \tag{3.20}$$

or

$$N = \sum_{p=1}^{P}\sum_{p'=1}^{P}\sum_{j=iN_s}^{(i+1)N_s-1}\sum_{j'=iN_s}^{(i+1)N_s-1} g^1_{q_p} g^1_{q_{p'}} \int_{-\infty}^{\infty}\int_{-\infty}^{\infty} \mathrm{E}\{n(t)n(t')\} \\ v(t - jT_f - c^1_j T_c - \tau^1_{q_p}) v(t' - j'T_f - c^1_{j'} T_c - \tau^1_{q_{p'}})\, dt\, dt' \qquad (3.21)$$

Since $\mathrm{E}\{n(t)n(t')\} = \frac{N_0}{2}\delta(t-t')$,

$$N = \sum_{p=1}^{P}\sum_{p'=1}^{P}\sum_{j=iN_s}^{(i+1)N_s-1}\sum_{j'=iN_s}^{(i+1)N_s-1} g^1_{q_p} g^1_{q'_p} \int_{-\infty}^{\infty} \frac{N_0}{2} v(t - jT_f - c^1_j T_c - \tau^1_{q_p}) \\ v(t - j'T_f - c^1_{j'} T_c - \tau^1_{q_{p'}})\, dt \qquad (3.22)$$

Now only when $j = j'$, the above integral may be non-zero; therefore,

$$N = \sum_{p=1}^{P}\sum_{p'=1}^{P}\sum_{j=iN_s}^{(i+1)N_s-1} g^1_{q_p} g^1_{q'_p} \frac{N_0}{2} R_v(\tau^1_{q_{p'}} - \tau^1_{q_p}) dt = \\ N_s \sum_{p=1}^{P}\sum_{p'=1}^{P} g^1_{q_p} g^1_{q'_p} \frac{N_0}{2} R_v(\tau^1_{q_{p'}} - \tau^1_{q_p}) \qquad (3.23)$$

where $R_v(\tau) = \int_{-\infty}^{\infty} v(t)v(t-\tau)\, dt$. we can now express the SNR in the form

$$\mathrm{SNR}(N_u) = \frac{N_s^2 R^2_{vw_{rec}}(0)\left(\sum_{p=1}^{P} {g_q^1}^2\right)^2}{\frac{N_s}{T_f}\int_{-\infty}^{\infty} R^2_{vw_{rec}}(x)\, dx [\sum_{p=1}^{P} (g^1_{q_p})^2 (N_u E - (g^1_{q_p})^2)] + N} \qquad (3.24)$$

where N is given by (3.23) and $\mathrm{SNR}(N_u)$ accounts for the SNR when there are N_u active users communicating simultaneously.

Applying the Central Limit Theorem to the multiple access interference, the bit error rate performance can be computed as $P_e = Q(\sqrt{\mathrm{SNR}})$, where

$$Q(x) = \int_x^\infty \frac{1}{\sqrt{2\pi}} e^{-\frac{x^2}{2}}\, dx \tag{3.25}$$

Fig. 3.6 demonstrates the analytical results for the number of active users that can be supported simultaneously versus data rate given a specified bit error rate performance when the receiver selects the strongest path only, which in this case contains 25% of the total received energy contained in all the paths of the user of interest. As expected, by increasing the data rate, the likelihood of collisions due to using smaller frame durations goes up, hence, in order to maintain the bit error rate performance , less number of active users can be supported at the same time. In other words, for the same number of users, at higher data rates, performance degrades due to higher chance of collisions arising from smaller frame periods.

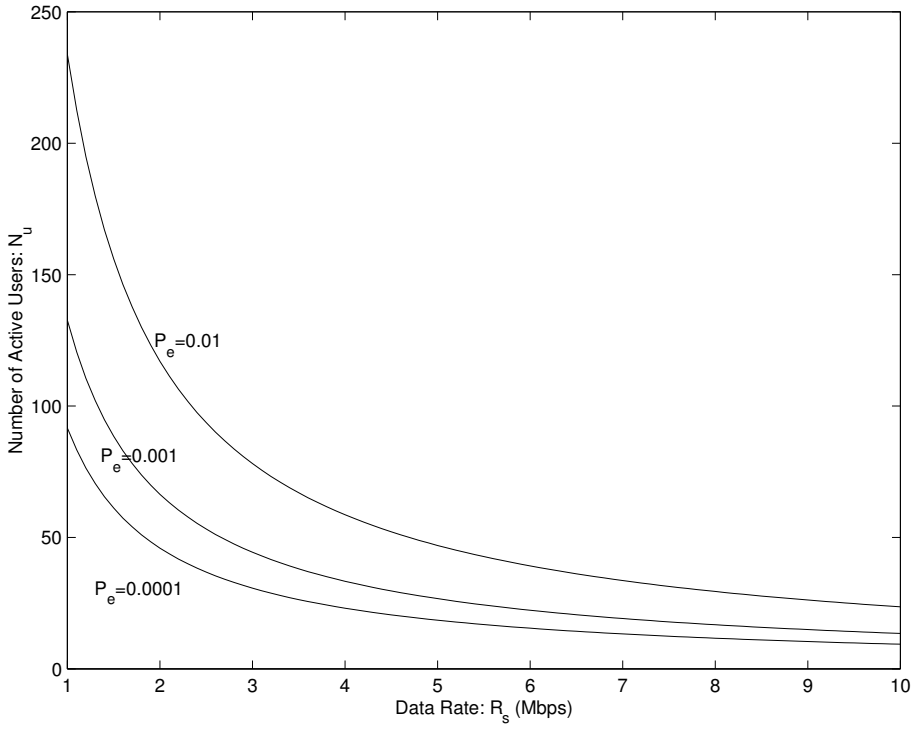

Figure 3.6: Number of active users versus data rate at given bit error rates

3.5 The Nature of Collisions

Consider a clean received pulse with normalized amplitude as $w_{rec}(t - \delta d)$. Here, d is the random data of the user of interest and could be zero or one with equal probability. We model the collision of this received signal with another waveform coming from any other users or multipath as receiving, $w_{rec}(t-\delta d)+\alpha w_{rec}(t-\beta)$. Here, α and β, are the amplitude and delay of the colliding pulse relative to the pulse of interest, respectively. The delay of the colliding pulse, β, is in $[-T_m, T_m+\delta]$. We investigate the effect of collision on the output of the

pulse correlator, $x = \int_0^{T_m+\delta} v(t)(w_{rec}(t-\delta d)+\alpha w_{rec}(t-\beta))\,dt$. In general there are two types of collisions, namely destructive and constructive. Destructive collisions are those who lead to either weakening or changing the polarity of the pulse correlator output. We call those subset of destructive collisions who change the polarity of x, as fatal or unrecoverable collisions. The rest of them who just weaken the magnitude of x without changing its polarity are called recoverable destructive collisions. Any collision which leads to increasing the magnitude of x without changing its polarity is called a constructive one. The results of this investigation show that as long as $|\alpha| < 1$, there will be no fatal collisions for any β. However for $|\alpha| > 1$, the fatality of the collisions depends on β and d. Fig. 3.7 shows the effect of collision versus β and parameterized by different α's when $d = 0$. The y-axis on this figure corresponds to the normalized effect of collision, which is $\frac{x}{\int_0^{T_m+\delta} v(t)w_{rec}(t-\delta d)\,dt}$. Therefor, 1 on this axis is equivalent to having no collision at all. Similar results are obtained when the transmitted data of the user of interest is one. Fig. 3.8 demonstrates the normalized collision effect for the case when the transmitted data is one. Due to the symmetrical nature of the problem, by looking at Fig. 3.7, for any α, half of the time the collisions are destructive and the other half are constructive. Also, as long as the colliding pulse is not stronger than the pulse of interest, i.e., $|\alpha| < 1$, all the destructive collisions are recoverable. Fatal collisions may happen only when the colliding pulse is stronger than the pulse

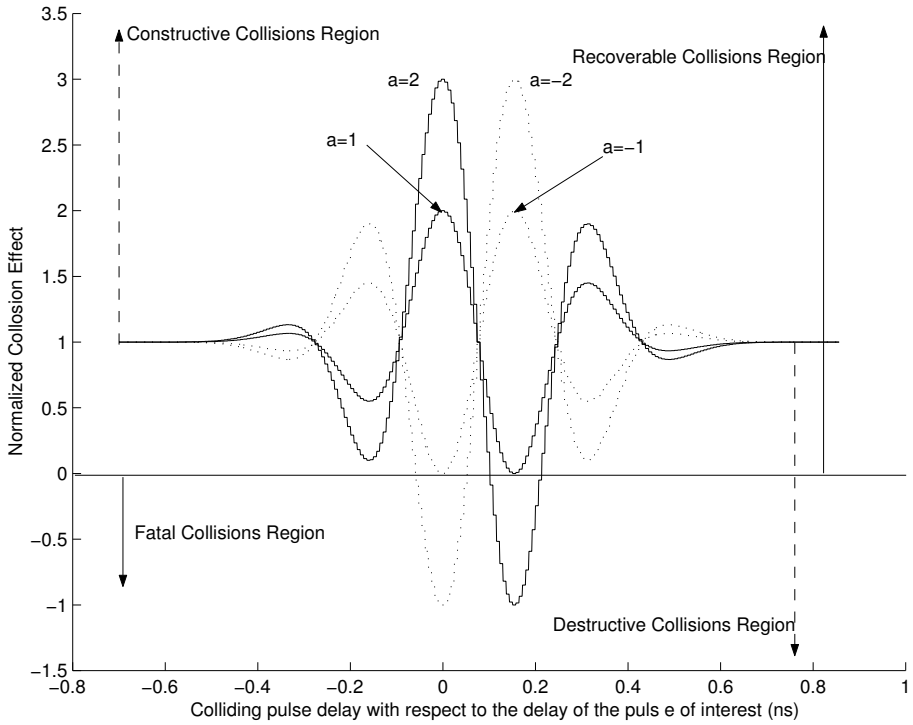

Figure 3.7: The effect of collision when the transmitted data of the user of interest is zero.

of interest, but they happen only a small fraction of the time depending on the strength and delay of the colliding pulse with respect to the victim pulse. For example, if the colliding pulse is 6 dB stronger than the pulse of interest, then only around 7% of the time a fatal collision happens. This shows that although collisions degrade the system performance, but most of the time they are recoverable.

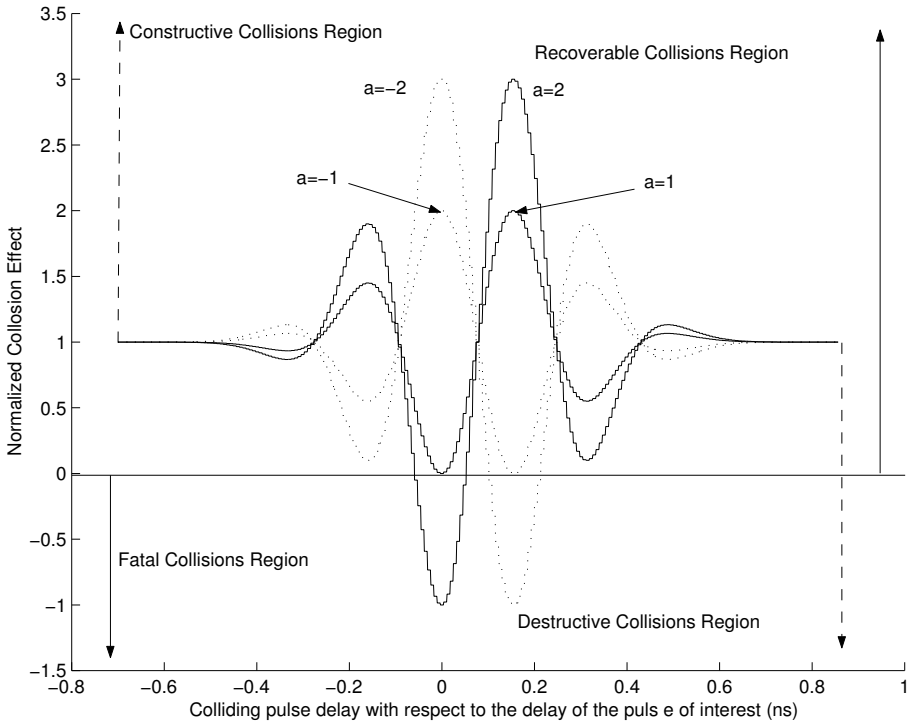

Figure 3.8: The effect of collision when the transmitted data of the user of interest is one.

3.6 Impulse Response of UWB Multipath Channels

Due to sending a sub-nanosecond pulse in each frame period, impulse radio enjoys a very high multipath resolution capability. This motivates the use of serial correlation search with half of a pulse width resolution in order to resolve individual paths in the multipath received signal. Fig. 3.9 shows a measured

UWB received signal in an indoor office environment. As can be seen, the multipath delay profile is very dense.

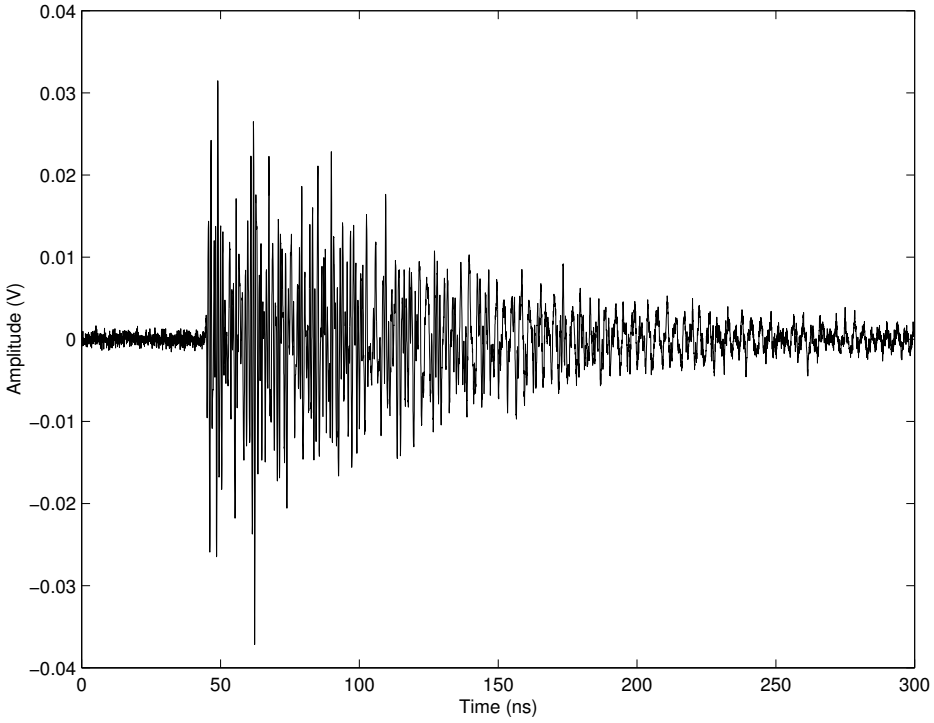

Figure 3.9: A typical indoor measurement of UWB received signal

After applying the serial correlation search to the measurement shown in Fig. 3.9, we ignore all the paths that are 20 dB weaker than the strongest path in order to prevent declaring a path due to noise. We shift all the delays by the delay of the first path so that the line of sight path delay is equal to zero. It is worth noting that the line of sight path is indeed the shortest path between the transmitter and the receiver, but if it is blocked by a medium in which the speed of the electromagnetic wave is considerably lower than the speed of

light in free space, then the first arriving path might not be the shortest path. After this delay shift, we normalize the impulse response of the UWB channel to have a unit norm. One normalized impulse response is shown in Fig. 3.10. Throughout the remaining of this chapter, we use such responses for different

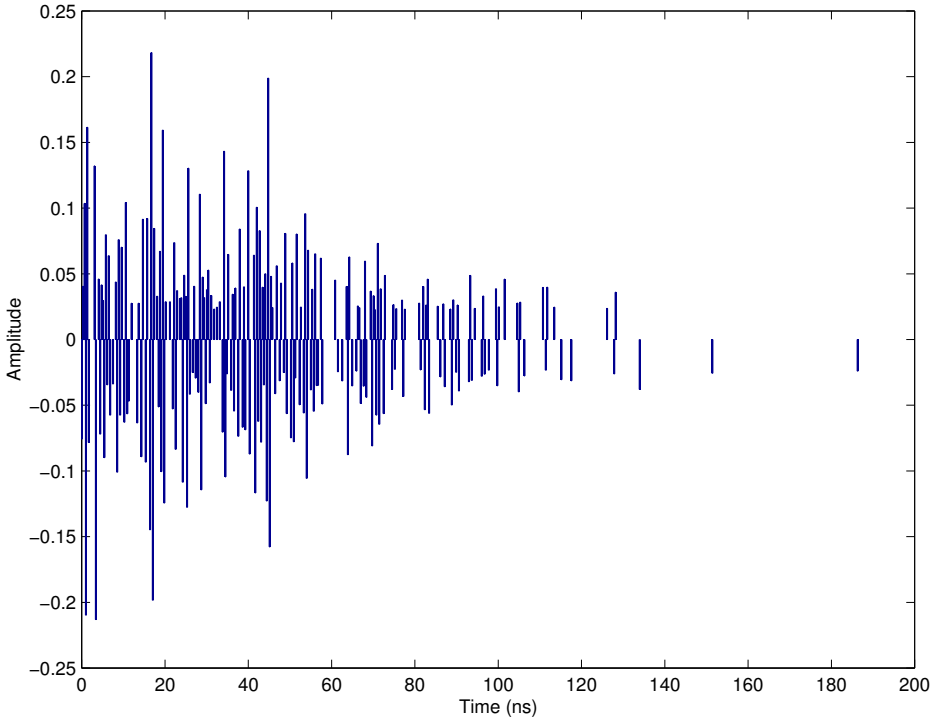

Figure 3.10: A normalized UWB Impulse Response

channels existing between each user's transmitter and the user of interest's receiver. We add a random asynchronous delay to each user with respect to the delay of the line of sight path of the user of interest. These delays are independent and uniformly distributed over one frame duration.

Fig. 3.11 compares the simulation and analytical results of uncoded bit error rate versus the number of pulses per data symbol for a scenario where 20 users are communicating at 1 Mbps data rate. Performance of multiple-access UWB radio in the presence of multipath is basically limited by the multiple-access interference. Therefore, the results shown here represent the case where the additive white gaussian noise is negligible or in other words when the thermal SNR is very high. As can be observed, after a few pulses

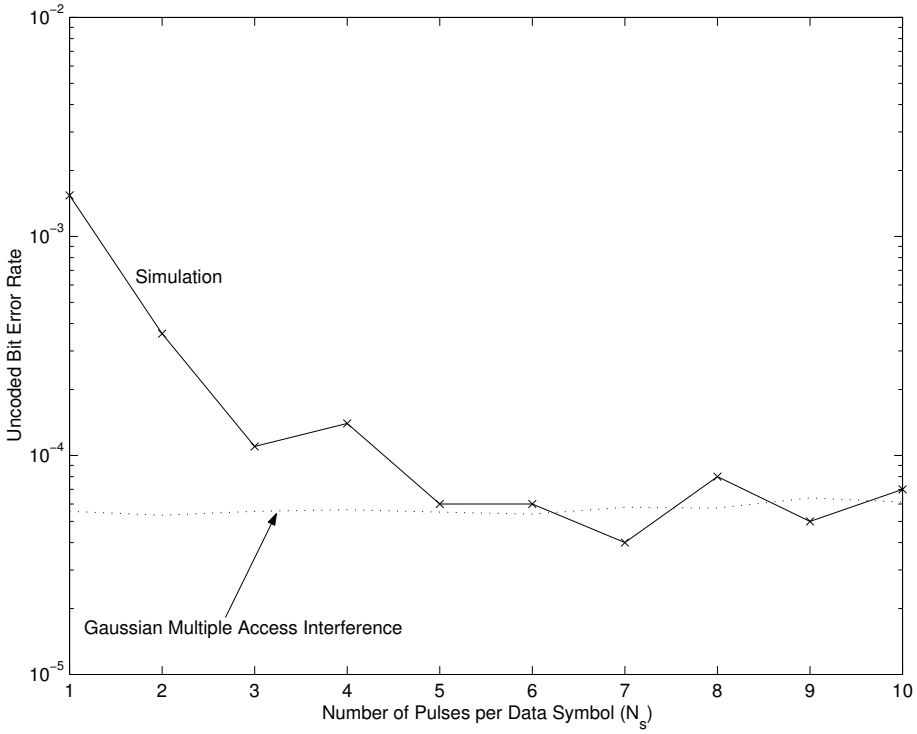

Figure 3.11: Analytical and simulation results comparison

sent per data symbol, specifically after $N_s = 5$ here, the two curves are very close to each other; however for fewer pulses transmitted per data symbol, the

two curves diverge more and more by decreasing N_s. This is due to the fact that analytical curve assumes a Gaussian multiple access collisions based on central limit theorem. With more pulses per data symbol, this assumption becomes valid. Whereas, for small N_s the requirements for the validity of central limit theorem become weak and the actual results based on simulations differ from those predicted by analysis.

Investigating the analytical results based on Gaussian multiple-access interference, one can see that these results may be used only when the central limit theorem applies to multiple-access interference distribution. Otherwise, the predictions based on these analytical solutions are not accurate enough to be used for system design purposes. However, such results may be used with more confidence when $\frac{N_u N_s \tilde{\tau}}{T_f} > 150$ as a rule of thumb. This rule of thumb is observed in all the curves given in Fig.'s 3.11 and 3.12.

Fig. 3.12 compares the simulation and analytical results based on Gaussian multiple-access interference for two different scenarios where 10 and 20 users are communicating at 2 Mbps and 1 Mbps data rates, respectively. Squares correspond to 20 users at 1 Mbps and circles represent 10 users at 2 Mbps. Again, not only do the analytical results become close to those of simulations when more pulses per data symbol are transmitted, but also the trade off between the number of users and data rate can be observed. By reducing

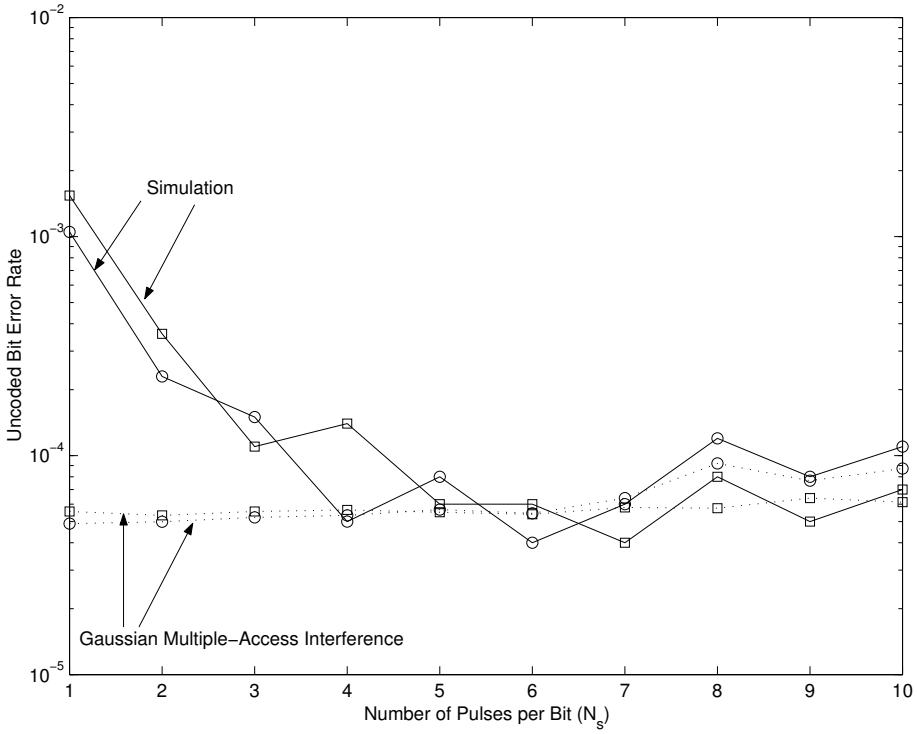

Figure 3.12: Analytical and simulation results at two different scenarios showing the trade off between the number of users and data rate

the data rate by a factor of two, number of supported users can be doubled for roughly the same bit error rate performance. It is worth noting that the simulated and semi-analytical results for SNR agree with each other.

Fig. 3.13 shows the simulation results for bit error rate versus the number of pulses transmitted per data symbol when 20 active users with roughly flat dense multipath channels over 200 ns delay spread are communicating at data rates of 1 and 2 Mbps. The hopping range has been set to 50% of one frame duration and the receiver selects the strongest path of the user of interest

only. At a fixed data rate, the number of pulses per data symbol times the

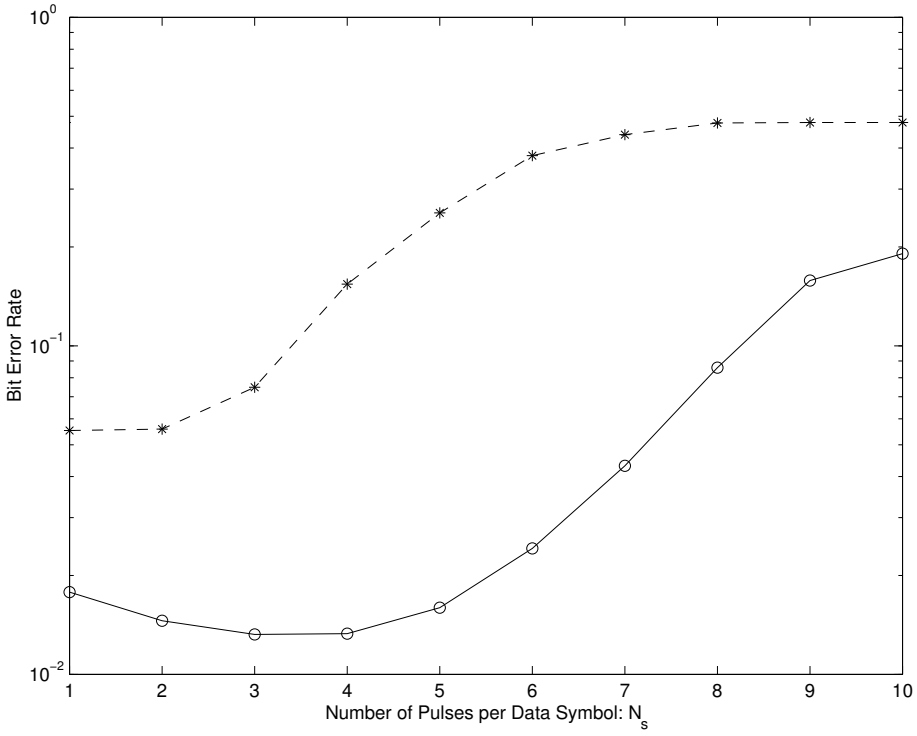

Figure 3.13: Bit error rate versus the number of pulses per data symbol with 20 active users at 1 and 2 Mbps data rates

frame duration is fixed; therefore, we have the freedom to vary these two factors subject to fixing their product. Increased frame duration implies a lower likelihood of collisions. However, with very large frame durations, even one strong destructive collision can result in a detection error. On the other hand, the number of pulses per data symbol is associated with the ability to mitigate the effect of collisions, e.g., if one of the pulses corresponding to the same data symbol of the user of interest gets destructively corrupted,

we can still recover the data symbol correctly utilizing a soft decision on the sum of all the pulses corresponding to the same data symbol. Albeit, if we choose a large number of pulses per symbol with a very short frame duration, we will have severe collisions at each frame period which may result in a detection error since all the pulses corresponding to the same data symbol are corrupted. Therefore, there is a trade off between the likelihood of collisions and mitigating the effect of collisions. As can be seen, at a 1 Mpbs data rate, sending three pulses per data symbol leads to a better bit error rate performance; however, at 2 Mbps, the best performance can be achieved only when one pulse is transmitted per data symbol. The reason is that when $N_s = 3$ and $R_s = 1$ Mbps, the frame duration is long enough compared to the delay spread; hence, the chance of fatal collisions is small. Then by transmitting this long frame three times per data symbol, we mitigate the effect of collisions by averaging over these three frames corresponding to the same data symbol. On the other hand, at 2 Mbps, at the same N_s, the frame duration is half of that of $R_s = 1$ Mbps, causing collisions with high likelihood at each frame duration. Therefore, the best performance can be achieved when we use the largest frame duration to make this likelihood of collisions smaller, which corresponds to $N_s = 1$. In fact, $N_s = 1.5$ at $R_s = 2$ Mbps leads to the same frame duration as $N_s = 3$ with $R_s = 1$ Mbps. However, since N_s should be an integer, $N_s = 1$ will lead to the best bit error rate for $R_s = 2$

Mbps scenario. Although with $N_s = 1$ at $R_s = 2$ Mbps , the frame duration is even bigger than $N_s = 3$ at $R_s = 1$ Mbps, but since we mitigate the effect of collisions by a factor of three more at $R_s = 1$ Mbps than that of $R_s = 2$ Mbps, the lower data rate case results in a better bit error rate performance. Generally speaking, with the same frame duration, the performance at lower data rates will be better due to better mitigation of collisions through larger N_s.

At a fixed data rate, $T_s = \frac{1}{R_s}$ is constant. Replacing T_f by $\frac{T_s}{N_s}$ in (3.24), we get

$$\mathrm{SNR}(N_u) = \frac{N_s^2 R_{vw_{rec}}^2(0)\left(\sum_{p=1}^{P} g_q^{1\,2}\right)^2}{\frac{N_s^2}{T_s}\int_{-\infty}^{\infty} R_{vw_{rec}}^2(x)\,dx\left[\sum_{p=1}^{p=P}\left(g_{q_p}^1\right)^2\left(N_u E - \left(g_{q_p}^1\right)^2\right)\right] + N_s\tilde{N}} \quad (3.26)$$

where $\tilde{N} = \sum_{p=1}^{P}\sum_{p'=1}^{P} g_{q_p}^1 g_{q_{p'}}^1 \frac{N_0}{2} R_v(\tau_{q_{p'}}^1 - \tau_{q_p}^1)$. This formula suggests that when N_s becomes larger, the SNR approaches a maximum asymptotically. However, when N_s becomes very large, T_f gets very small, which means that the above formula is not valid any more. Hence, in order to get a very good bit error rate performance predicted by (3.26), we need to choose the frame period long enough to satisfy the conditions under which we derived (3.24), and then we choose $N_s = \frac{T_s}{T_f}$. The value for T_f should be larger than two times the multipath delay spread. This conclusion agrees with the curves shown in Fig. 3.13.

Fig. 3.14 demonstrates the simulation results for bit error rate performance versus the hopping range of each user's time-hopping code under the best compromise between the number of pulses per data symbol and frame duration that leads to the best bit error rate performance over all hopping ranges and number of pulses per data symbol. Same channels as in Fig. 3.13 have been used here. Hopping range has been expressed in terms of a fraction of one

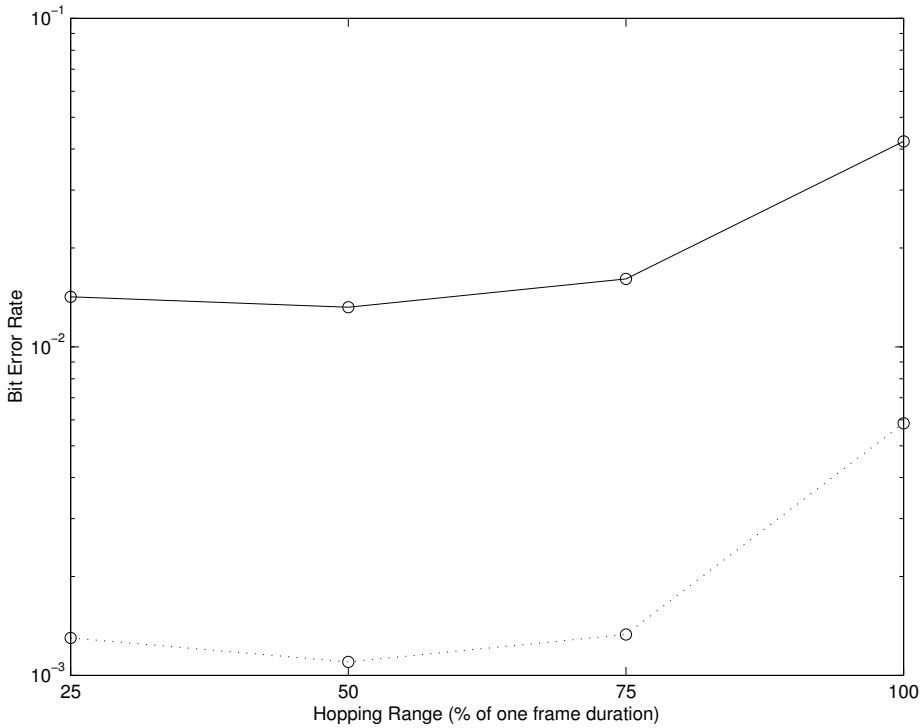

Figure 3.14: Bit error rate versus hopping range when 20 active users communicate at 0.5 and 1 Mbps data rates

frame duration. The solid and dotted curves in this figure corresponds to 20 users communicating simultaneously at 1 Mbps and 500 Kbps, respectively,

with only the strongest path of the user of interest selected at the receiver. As can be seen, at around 50% hopping range, we have enough hopping space for those users who are asynchronously closer to the user of interest to avoid multiple collisions and also, the strong collisions coming from the rest of the users are mitigated, therefore yielding good performance. At large hopping ranges, the inter-symbol interference of the user of interest becomes stronger and degrades the performance.

Selective RAKE reception of UWB signals in the presence of multipath without considering multiuser collisions has been investigated in [2, 69, 70, 68]. Fig. 3.15 illustrates the simulation results for bit error rate in terms of the number of paths combined at the receiver selectively or partially when 20 users with the same channels as in Fig. 3.13 are communicating simultaneously at 1 Mbps and only one pulse is transmitted per data symbol. Selective combining means to combine the most dominant paths with maximum ratio coefficients. However, by partial combining, we mean to combine the first few arriving paths of the user of interest with maximum ratio coefficients. The results show a very good payoff in terms of the bit error rate performance with increasing the receiver complexity through selective combining. Selecting only four more paths will result in more than 200 times better bit error rate performance. The performance gain does not continue with the same intensity after a few selected paths and we will reach a point where the complexity of the receiver

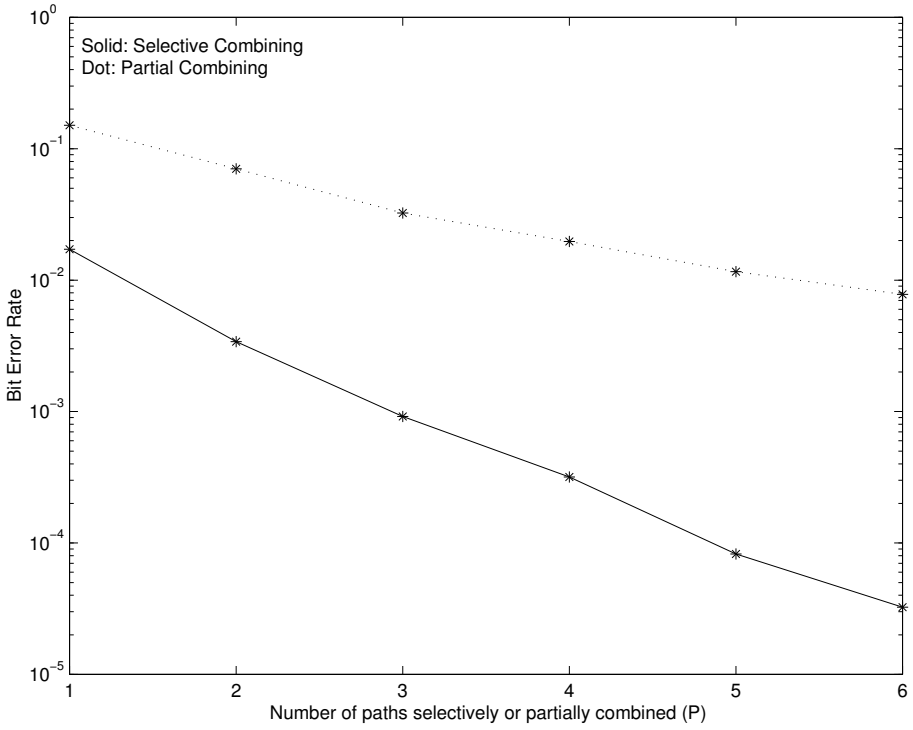

Figure 3.15: Bit error rate versus the number of paths selectively or partially combined at the receiver when 20 active users communicate at 1 Mbps

and more power consumption is not worth getting slightly better performance. After four or five selected paths the gain in performance is not worth trading off the receiver complexity and power consumption.

Transmitting only one pulse per bit will lead to detection errors in case of severe collisions; however, selecting more than one path of the user of interest compensates for these severe collisions in the way that not all the selected paths are severely corrupted on average. However, as can be seen, the same diversity gain does not exist with partial combining. This is due to the fact

that not only the first few arriving paths are not always the strongest ones, but also a strong destructive collision can corrupt the first few arriving paths of the user of interest simultaneously, since they are temporally adjacent to each other, hence, combining a few corrupted paths will not help the receiver in making a correct decision.

3.7 Direct Sequence UWB Radio

In this section, wireless multiple access digital impulse radio under multipath propagation conditions using direct sequence spreading is investigated. Using the same terminology as time-hopping UWB radio, the received signal is given by (3.2). Again, we assume $\tau_0^1 = 0$. The received signal of user k with no delay with respect to the line of sight path signal of the user of interest (User 1) is denoted by $S_{rec}^k(t)$, where

$$S_{rec}^k(t) = \sum_l a_l^k D_l^k w_{rec}(t - lT_f) \tag{3.27}$$

Again, each data symbol is transmitted repeatedly in N_s consecutive frames. Therefore, $D_{iN_s}^k = D_{iN_s+1}^k = \cdots = D_{(i+1)N_s-1}^k = d_i^k$ for all integer i's and $k = 1, 2, ..., N_u$. Here d_i^k is the ith transmitted symbol of user k and D_l^k is the ith repeated transmitted symbol of user k in the lth frame for $l =$

$iN_s, iN_s+1, ..., (i+1)N_s-1$ and $d_i^k \in \{+1, -1\}$. One pulse is transmitted at the beginning of each frame period. The polarity of each pulse is determined by the product of a_l^k and D_l^k, where a_l^k is the lth element of User k's spreading sequence, which is randomly chosen from {+1,-1}. The data modulation is antipodal as can be seen by the factor of D_l^k as a coefficient in (3.27).

Assuming a multiple selective combining receiver, the P dominant paths of the user of interest are selected [58, 45], and each is processed in a separate branch of the RAKE receiver. The following correlation is made at the branch corresponding to the qth selected path:

$$A_q(i) = \int_{t=iN_sT_f+\tau_q^1}^{(i+1)N_sT_f+\tau_q^1} r(t) \sum_{j=iN_s}^{(i+1)N_s-1} g_q^1 a_j^1 v(t - jT_f - \tau_q^1)\, dt \tag{3.28}$$

where

$$v(t) = w_{rec}(t) \tag{3.29}$$

is the template waveform used at the receiver. Using similar techniques used for time-hopping UWB radio,

$$A_q(i) = S_q(i) + M_q(i) + N_q(i) \tag{3.30}$$

where

$$S_q(i) = \sum_{j=iN_s}^{(i+1)N_s-1} {g_q^1}^2 {a_j^1}^2 D_j^1 R_{w_{rec}}(0) = N_s {g_q^1}^2 d_i^1 R_{w_{rec}}(0) \tag{3.31}$$

Since ${a_j^1}^2 = 1$ and $D_{iN_s}^1 = D_{iN_s+1}^1 = \cdots = D_{(i+1)N_s-1}^1 = d_i^1$. Also,

$$R_{w_{rec}}(\tau) = \int_{-\infty}^{\infty} w_{rec}(t) w_{rec}(t-\tau)\, dt \tag{3.32}$$

is the auto-correlation of the received pulse $w_{rec}(t)$ and can have non-zero values only on the interval $[-T_m, T_m]$, because the support of $w_{rec}(t)$ is $[0, T_m]$. The second term in the right hand side of (3.30) is

$$M_q(i) = \sum_{j=iN_s}^{(i+1)N_s-1} \sum_{k=1}^{N_u} \sum_{m=0(k=1,m\neq q)}^{L^k-1} \sum_{l=\lceil (j-1.5-\frac{\tilde{\tau}}{T_f}) \rceil}^{l=\lfloor (j+1.5+\frac{\tilde{\tau}}{T_f}) \rfloor} g_q^1 g_m^k$$
$$a_l^k a_j^1 R_{w_{rec}}((l-j)T_f + \beta^k + \lambda_m^k - \lambda_q^1) \tag{3.33}$$

where $\beta^k = \tau_0^k - \tau_0^1 \in [-\frac{T_f}{2}, \frac{T_f}{2}]$ is the asynchronous delay of User k with respect to that of User 1, and $\lambda_m^k = \tau_m^k - \tau_0^k$ is the User k's mth path excess delay. The term

$$N_q(i) = \sum_{j=iN_s}^{(i+1)N_s-1} \int_{-\infty}^{\infty} g_q^1 a_j^1 n(t+\tau_q^1) w_{rec}(t-jT_f)\, dt \tag{3.34}$$

accounts for AWGN contribution to the decision statistic.

If $A(i) = \sum_{p=1}^{P} A_{q_p}(i)$ is greater than zero we decide in favor of H_1, that is, the transmitted symbol d_i^1 has been a one, otherwise we decide the hypothesis H_{-1}. It is worth noting that in all the above signal processing, we have assumed that the receiver is synchronized to the first user's direct sequence and selected paths delays. Assuming $\frac{T_f}{2}$ to be much greater than δ and with careful inspection of the integral and summation intervals, considering:

(i) $w_{rec}(t) = 0$ for $t < 0$, or $t > T_m$

(ii) $T_f \geq 2\tilde{\tau} + 2T_m$

we can conclude

$$M_q(i) = \sum_{j=iN_s}^{(i+1)N_s-1} \sum_{k=1}^{N_u} \sum_{m=0(k=1,m\neq q)}^{L^k-1} g_q^1 g_m^k a_j^k a_j^1 d_i^k R_{w_{rec}}(\beta^k + \lambda_m^k - \lambda_q^1) \qquad (3.35)$$

The signal at the input of the threshold comparator is $A(i) = \sum_{p=1}^{P} A_{q_p}(i)$. Therefore, using (3.31), the signal energy can be computed as

$$S = \mathrm{E}\left\{ \left(N_s d_i^1 R_{w_{rec}}(0) \sum_{p=1}^{P} {g_{q_p}^1}^2 \right)^2 \right\} = N_s^2 R_{w_{rec}}^2(0) \left(\sum_{p=1}^{P} {g_{q_p}^1}^2 \right)^2 \qquad (3.36)$$

where the ensemble average has been carried on d_i^1 assuming $\Pr.\{d_i^1 = 0\} = \Pr.\{d_i^1 = 1\} = \frac{1}{2}$.

The interference arising from the non-selected paths of the user of interest plus those of other active users is represented by the term $\sum_{p=1}^{P} \sum_{j=iN_s}^{(i+1)N_s-1} \sum_{k=1}^{N_u} \sum_{m=0(k=1,m\neq q)}^{L^k-1} x(q,m,k)$, where

$$x(q,m,k) = g_q^1 g_m^k a_j^k a_j^1 d_i^k R_{w_{rec}}(\beta^k + \lambda_m^k - \lambda_q^1) \tag{3.37}$$

By taking the ensemble average of $(x(q,m,k))^2$ with respect to β^k, we have

$$\mathrm{E}\{(x(q,m,k))^2\} = (g_q^1 g_m^k)^2 \frac{1}{T_f} \int_{-\frac{T_f}{2}}^{\frac{T_f}{2}} R_{w_{rec}}^2(x + \lambda_m^k - \lambda_q^1)\, dx \tag{3.38}$$

Considering the restriction imposed on the frame length, the interval integral contains the support of $R_{w_{rec}}(x)$, hence, it can be extended to the whole real line:

$$\mathrm{E}\{(x(q,m,k))^2\} = \frac{1}{T_f}(g_q^1 g_m^k)^2 \int_{-\infty}^{\infty} R_{w_{rec}}^2(x)\, dx \tag{3.39}$$

The interference energy can be expressed as

$$I = N_s \sum_{p=1}^{P} \sum_{k=1}^{N_u} \sum_{m=0(k=1,m\neq 0)}^{L^k-1} \frac{1}{T_f}(g_q^1 g_m^k)^2 \int_{-\infty}^{\infty} R_{w_{rec}}^2(x)\, dx \tag{3.40}$$

Since we normalized all the channels to have the same norm, i.e., $\sum_{m=0}^{L^k-1}(g_m^k)^2 = E = 1$ for all k's, the above expression can be simplified to

$$I = \frac{N_s}{T_f}\int_{-\infty}^{\infty} R_{w_{rec}}^2(x)\,dx[\sum_{p=1}^{P}(g_{q_p}^1)^2(N_u E - (g_{q_p}^1)^2)] \tag{3.41}$$

To compute the AWGN contribution at the input of the threshold comparator,

$$N = \mathrm{E}\left\{\left(\sum_{p=1}^{P}\sum_{j=iN_s}^{(i+1)N_s-1} g_{q_p}^1 a_j^1 \int_{-\infty}^{\infty} n(t+\tau_{q_p}^1) w_{rec}(t-jT_f)\,dt\right)^2\right\} \tag{3.42}$$

or

$$N = \sum_{p=1}^{P}\sum_{p'=1}^{P}\sum_{j=iN_s}^{(i+1)N_s-1}\sum_{j'=iN_s}^{(i+1)N_s-1} g_{q_p}^1 g_{q_{p'}}^1 a_j^1 a_{j'}^1 \int_{-\infty}^{\infty}\int_{-\infty}^{\infty}\mathrm{E}\{n(t)n(t')\}$$
$$w_{rec}(t-jT_f-\tau_{q_p}^1) w_{rec}(t'-j'T_f-\tau_{q_{p'}}^1)\,dtdt' \tag{3.43}$$

Since $\mathrm{E}\{n(t)n(t')\} = \frac{N_0}{2}\delta(t-t')$,

$$N = \sum_{p=1}^{P}\sum_{p'=1}^{P}\sum_{j=iN_s}^{(i+1)N_s-1}\sum_{j'=iN_s}^{(i+1)N_s-1} g_{q_p}^1 g_{q'_p}^1 \int_{-\infty}^{\infty}\frac{N_0}{2} w_{rec}(t-jT_f-\tau_{q_p}^1)$$
$$w_{rec}(t-j'T_f-\tau_{q_{p'}}^1)\,dt \tag{3.44}$$

Now only when $j = j'$, the above integral may be non-zero; therefore,

$$N = \sum_{p=1}^{P} \sum_{p'=1}^{P} \sum_{j=iN_s}^{(i+1)N_s-1} g_{q_p}^1 g_{q'_p}^1 \int_{-\infty}^{\infty} \frac{N_0}{2} w_{rec}(t - jT_f - \tau_{q_p}^1)$$
$$w_{rec}(t - jT_f - \tau_{q_{p'}}^1)\, dt = N_s \sum_{p=1}^{P} \sum_{p'=1}^{P} g_{q_p}^1 g_{q'_p}^1 \frac{N_0}{2} R_{w_{rec}}(\tau_{q_{p'}}^1 - \tau_{q_p}^1) \tag{3.45}$$

We can now express the SNR in the form

$$\mathrm{SNR}(N_u) = \frac{N_s^2 R_{w_{rec}}^2(0) \left(\sum_{p=1}^{P} g_q^{1\,2} \right)^2}{\frac{N_s}{T_f} \int_{-\infty}^{\infty} R_{w_{rec}}^2(x)\, dx [\sum_{p=1}^{P} (g_{q_p}^1)^2 (N_u E - (g_{q_p}^1)^2)] + N} \tag{3.46}$$

where N is given by (3.45) and $\mathrm{SNR}(N_u)$ accounts for the SNR when there are N_u active users communicating simultaneously. Applying the Central Limit Theorem to the multiple access interference, the bit error rate performance can be computed as $P_e = Q(\sqrt{\mathrm{SNR}})$, where $Q(x)$ is given by (3.25).

Fig. 3.16 compares the analytical bit error rates of direct-sequence and time-hopping multiple access UWB radios as predicted by (3.24) and (3.46) assuming a Gaussian multiple access interference versus the number of active users communicating simultaneously at 10 Mbps when the selected path of the user of interest contains 25% of the total energy contained in all the user of interest's received paths. As can be seen, the performance of direct-sequence UWB radio is slightly better than that of time-hopping UWB radio at any

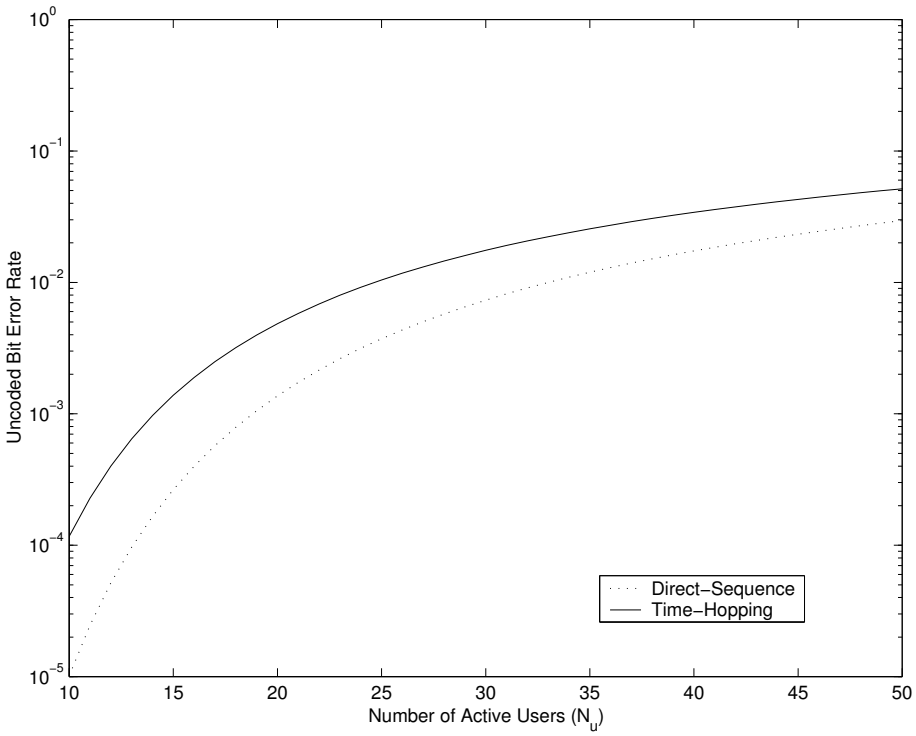

Figure 3.16: Direct-sequence and time-hopping bit error rate versus the number of active users

given number of active users. This is due to the antipodal nature of direct-sequence UWB radio as opposed to time shift modulation of time-hopping system. However, since the pulse position modulation parameter is optimized by (3.1), the difference in SNR for direct-sequence and time-hopping UWB radios is less than 3 dB. This means that under the circumstances when the performance is limited by multiple-access interference, the direct-sequence impulse radio may support 34% more users as compared to time-hopping pulse position modulation scheme.

3.8 Conclusion

UWB impulse radio promised a great multiple-access capacity under ideal propagation conditions [46, 77]. However, a typical wireless UWB channel has a huge delay spread compared to the transmitted pulse width. Therefore, performance of such wireless multiple-access scheme should be investigated under more realistic propagation conditions. Under the harsh assumption of flat multipath channels, the multiple-access capacity of UWB impulse radio is degraded by a factor of number of taps in the multipath channel [55]. To implement wireless multiple-access impulse radio communication systems, we need to predict the bit error rate performance of such systems under realistic multipath channels for a number of active users communicating simultaneously at a given data rate.

In this chapter, bit error rate performance of wireless multiple-access time-hopping digital impulse radio under realistic propagation conditions using real data obtained from experimental measurements is investigated. Bit error rate performance predictions based on analytical results are close to those obtained from simulations only when the multiple-access interference approaches a Gaussian distribution based on the central limit theorem. In other words, such predictions may be used only when enough number of users with enough number of pulses transmitted per data symbol at a given data rate are present.

Collisions are divided to destructive and constructive collisions. Not all the destructive collisions lead to an error. Those who contribute in the opposite polarity of the soft decision for the transmitted bit are called fatal collisions, whereas others are recoverable collisions. If we send only one pulse per bit, even with one fatal collision, a detection error will occur. Therefore, we need to send several pulses per bit in order to avoid errors in case of fatal collisions. There are two aspects of collisions associated to multiple-access performance of UWB digital impulse radio in the presence of multipath, namely, the likelihood of collisions and mitigating the effect of collisions. Likelihood of collisions is inversely proportional to the frame length; however, choosing the longest frame duration will cause a detection error even with only one fatal collision. Therefore, a few pulses per bit are needed in order for the receiver to be able to recover the collided bits. This suggests a trade-off between the frame length and the number of pulses per bit, hence, a local optimality between the values chosen for these quantities.

Restricting the time-hopping range can help mitigate the inter-symbol interference and remove some collisions arising from the users who are asynchronously apart enough with respect to the delay of the user of interest provided that the frame duration is long enough compared to a typical multipath channel delay spread. On the other hand, too much restricting the hopping range will result in frequent collisions between those users who are

asynchronously close to each other in each frame period, so worsening the performance. Again there is a locally optimal value for this range for different frame lengths.

Using a selective combining receiver will help attain a better performance when more number of dominant paths are selected; however, the gain in performance diminishes as more and more paths are selected. After the first few selected paths, the gain in performance is not worth the more power consumption and receiver complexity. While partial combining will eliminate the search for the few dominant paths at the receiver, it will degrade the system performance if a strong portion of any other user's multipath profile collides with the first few paths of the user of interest destructively. In that case, all the partial combining paths will be corrupted and we might not be able to make a correct soft decision based on those corrupted paths. In other words due to the correlation existing between the adjacent paths, partial combining provides less diversity gain as compared to selective combining.

Chapter 4

Narrow Band Interference Rejection

4.1 Introduction

Digital impulse radio enjoys an excellent multipath resolution capability up to a fraction of a nanosecond due to its huge bandwidth. On the other hand, occupying a vast amount of bandwidth causes new challenges for this kind of radio since there are many other communication systems working at different portions of UWB radio spectrum simultaneously [48, 56, 7, 11, 13, 15, 16, 26, 64, 79, 80]. This introduces external interference sources which cause performance degradation. It is important to know how a strong narrow band interferer degrades the UWB radio performance and how we can improve the performance in the presence of such interferers.

In this chapter, we analytically investigate SNR and bit error rate degradation in terms of the interference frequency and show how using different pulse shapes can mitigate some narrow bandwidth interferers. Moreover, we derive the relationship between gap time in doublet pulses and narrow bandwidth interference rejection, so that with careful design of such pulses we are able to mitigate a strong disturbing narrow band interference simultaneously present in the communication environment. It is shown how we can mitigate the effect of strong narrow band interferers by trying not to send information in those frequencies where such interferers are present.

Due to non ideal electronic circuits, we may not be able to generate ideal doublet pulses. Therefore, the effects of amplitude mismatches and gap time offset in a doublet pulse are also analyzed.

4.2 Mathematical Formulation

Sending one pulse in each frame period T_f [77, 58], the transmitted signal of the kth user with antipodal data modulation is

$$S^k_{trans}(t) = \sum_j D^k_j w_{trans}(t - jT_f - c^k_j T_c) \tag{4.1}$$

where $w_{trans}(t)$ is the transmitted waveform in the channel and c_j^k is the time-hopping code of the kth user in the jth frame with T_c representing a chip time. Also, D_j^k accounts for the kth user's symbol in the jth frame and $D_j^k \in \{-1, 1\}$. In order to obtain processing gain, we send N_s pulses per data symbol; therefore, $D_{iN_s}^k = D_{iN_s+1}^k = \cdots = D_{(i+1)N_s-1}^k = d_i^1$.

We model the received signal at the output of the receiver's antenna subsystem as

$$r(t) = \sum_{k=1}^{N_u} g_k S_{rec}^k(t - \tau_k) + I(t) + n(t) \tag{4.2}$$

where $S_{rec}^k(t) = \sum_j D_j^k w(t - jT_f - c_j^k T_c)$ is the kth user received signal with $w(t)$ representing the received waveform at the output of the receiver's antenna subsystem. The amplitude of the kth user is denoted as g_k. As (4.2) suggests, only one line of sight path signal has been assumed between each user's transmitter and the receiver of the user of interest. Fig. 4.1 shows the block diagram of the receiver. The received pulse shape scaled by the amplitude of the user of interest is used as template waveform [59] at the receiver's correlator. As can be seen, the receiver computes the decision statistic x_i for the ith data symbol as

$$x_i = \int_{t=iN_sT_f}^{t=(i+1)N_sT_f} r(t) \sum_{j=iN_s}^{(i+1)N_s-1} g_1 w(t - jT_f - c_j^1 T_c)\, dt \tag{4.3}$$

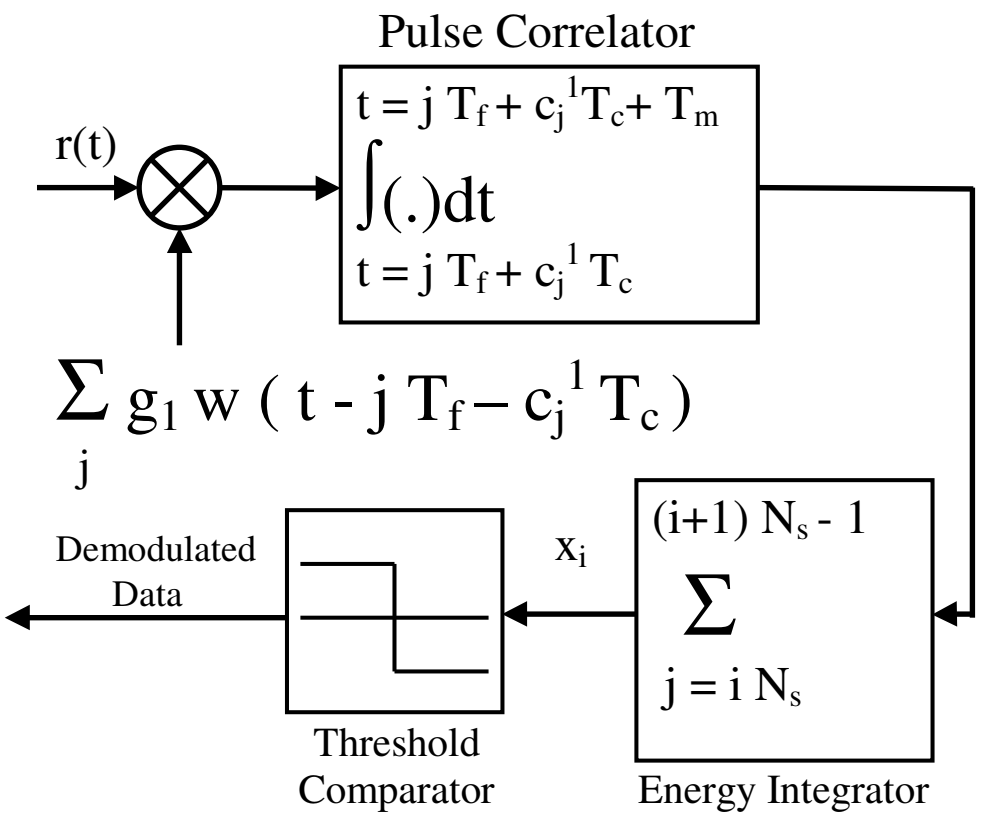

Figure 4.1: Receiver block diagram

If $x_i > 0$, then the decision will be in the favor of hypothesis H_1, i.e., the demodulated data is declared as a 1, otherwise hypothesis H_{-1} is stated to be true. Without loss of generality, we assume that the delay of the user of interest $\tau_1 = 0$, so each other user's delay with respect to the delay of the user

of interest can be written as $\tau_k = \alpha_k T_f + \beta_k$, where β_k is in $[\frac{-T_f}{2}, \frac{T_f}{2}]$. After some manipulations, we get

$$x_i = s_i + c_i + e_i + n_i \tag{4.4}$$

where

$$s_i = N_s g_1^2 d_i^1 R_w(0) \tag{4.5}$$

corresponds to the signal of the user of interest, and $R_w(\tau) = \int_{-\infty}^{\infty} w(t + \tau) w(t)\, dt$. The second term on the right hand side of (4.4),

$$c_i = \sum_{j=iN_s}^{(i+1)N_s-1} \sum_{k=2}^{N_u} g_1 g_k D_{j-\alpha_k}^k R_w((c_j^1 - c_{j-\alpha_k}^k)T_c - \beta_k) \tag{4.6}$$

accounts for the cross-talk due to the multiple-access interference. Also,

$$e_i = \sum_{j=iN_s}^{(i+1)N_s-1} \int_{iN_sT_f - jT_f - c_j^1 T_c}^{(i+1)N_sT_f - jT_f - c_j^1 T_c} g_1 I(t + jT_f + c_j^1 T_c) w(t)\, dt \tag{4.7}$$

represents the effect of the external interference. The last term on the right hand side of (4.4),

$$n_i = \sum_{j=iN_s}^{(i+1)N_s-1} \int_{iN_sT_f - jT_f - c_j^1 T_c}^{(i+1)N_sT_f - jT_f - c_j^1 T_c} g_1 n(t + jT_f + c_j^1 T_c) w(t)\, dt \tag{4.8}$$

is due to the random Gaussian noise with variance

$$\sigma_{n_i}^2 = N_s g_1^2 \frac{N_0}{2} R_w(0) \tag{4.9}$$

at the input of the threshold detector.

Since the support of $w(t)$ is $[0, T_m]$, and the interval integral $[iN_sT_f - jT_f - c_j^1 T_c, (i+1)N_sT_f - jT_f - c_j^1 T_c]$, contains this support for any integer j in $[iN_s, (i+1)N_s - 1]$, we can extend the integral interval in (4.7) to the whole real line, hence, the variance of e_i can be computed as

$$\lambda_i = \mathrm{E}\{e_i^2\} = g_1^2 \sum_{j=iN_s}^{(i+1)N_s-1} \sum_{j'=iN_s}^{(i+1)N_s-1} \int_{-\infty}^{\infty} R_I(\tau) R_w(\tau - (j-j')T_f - (c_j^1 - c_{j'}^1)T_c)\, d\tau \tag{4.10}$$

where $R_I(\tau) = \mathrm{E}\{I(t+\tau)I(t)\}$. Under certain circumstances when the time-hopping range is restricted to the interval $[0, \frac{T_f}{2} - T_m]$, and $R_I(\tau) = 0$ for $|\tau| > \frac{T_f}{2}$, $\mathrm{E}\{e_i^2\}$ can be simplified to

$$\mathrm{E}\{e_i^2\} = g_1^2 N_s \int_{-\infty}^{\infty} R_I(\tau) R_w(\tau)\, d\tau \tag{4.11}$$

The above formula is also valid without any restriction on the time-hopping range or any assumption on the autocorrelation function of $I(t)$, as long as $N_s = 1$.

Using Parseval's Theorem, (4.10) can be written as

$$\lambda_i = g_1^2 \sum_{j=iN_s}^{(i+1)N_s-1} \sum_{j'=iN_s}^{(i+1)N_s-1} \int_{-\infty}^{\infty} S_I(f) S_w(f) e^{j2\pi f((j-j')T_f + (c_j^1 - c_{j'}^1)T_c)}\, df \qquad (4.12)$$

This means that by careful design of the pulse shape $w(t)$, we can mitigate interference by generating nulls in the spectral density of the pulse shape around frequencies where the interference is strong.

Being perfectly synchronized to the time of arrival and time-hopping code of the user of interest at the receiver's correlator, the SNR at the output of the user of interest's receiver is computed as

$$\mathrm{SNR}(N_u) = \int_0^{\infty} \frac{N_s^2 g_1^4 R_w^2(0)}{P_{MAI} + \lambda + \sigma_{n_i}^2} f(\lambda)\, d\lambda \qquad (4.13)$$

where $f(\lambda)$ is the probability density function of the external interference variance given by (4.10), because this variance changes depending on the starting position of c_j^1. Here,

$$P_{\mathrm{MAI}} = \mathrm{E}\{c_i^2\} = N_s \sum_{k=2}^{N_u} (g_1 g_k)^2 \sigma^2 \qquad (4.14)$$

represents the multiple access interference variance when the time-hopping range is restricted to $[0, \frac{T_f}{2} - T_m]$ and

$$\sigma^2 = \frac{1}{T_f} \int_{-\infty}^{\infty} R_w^2(x)\, dx \tag{4.15}$$

Consider the case where

$$R_I(\tau) = \frac{{I_0}^2}{2} \cos(2\pi f_0 \tau) \tag{4.16}$$

which corresponds to the tone interference

$$I(t) = I_0 \cos(2\pi f_0 t) \tag{4.17}$$

Fig. 4.2 shows the effect of interference on SNR(20) as SNR degradation versus the signal to interference ratio (SIR) at the receiver's front end when the received pulse shape is the second order derivative of Gaussian shown in Fig. 4.3. Twenty active users are communicating at 1 Mbps data rate. The operating SNR(20) has been assumed 10 dB in the absence of interference.

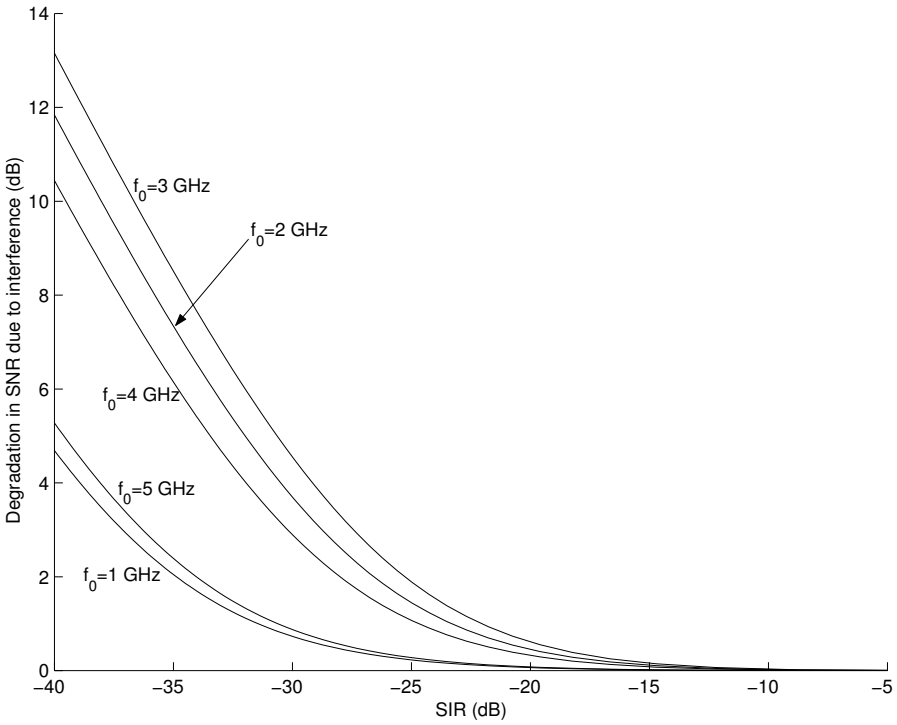

Figure 4.2: Effect of tone interference on the SNR

Due to the symmetry of the problem the bit error probability can be computed as

$$\Pr.\{\epsilon\} = \Pr.\{\epsilon | d_i^1 = 1\} = \Pr.\{x_i < 0 | d_i^1 = 1\} \tag{4.18}$$

Using (4.4) and (4.5) and replacing $d_i^1 = 1$,

$$\Pr.\{\epsilon\} = \Pr.\{c_i + e_i + n_i < -N_s g_1^2 R_w(0)\} \tag{4.19}$$

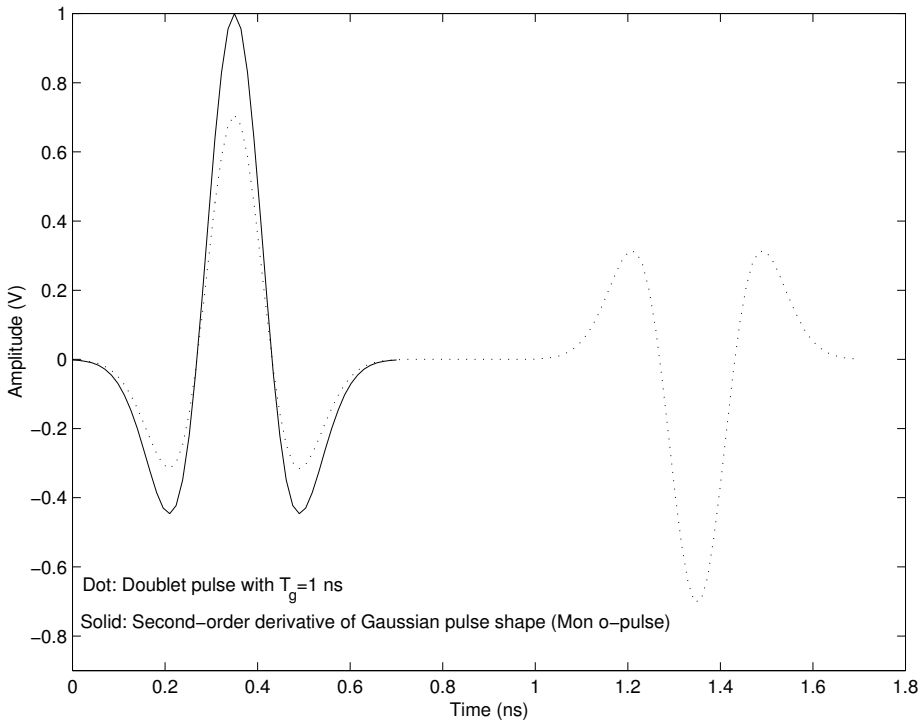

Figure 4.3: Second order derivative of Gaussian and doublet pulses

Applying the central limit theorem, and assuming perfect power control, i.e., $\frac{g_k^2}{g_1^2} = 1$, we get

$$\Pr.\{\epsilon\} = \int_0^\infty Q\left(\frac{R_w(0)}{\sqrt{\frac{(N_u-1)\sigma^2}{N_s} + \frac{\lambda}{g_1^4 N_s^2} + \frac{R_w(0)}{N_s g_1^2}\frac{N_0}{2}}}\right) f(\lambda)\, d\lambda \tag{4.20}$$

Fig. 4.4 shows the bit error rate performance of multiple-access digital impulse radio in the presence of an external tone interference with SIR around -37 dB versus the frequency of the interference when 20 users are communicating at 1 Mbps data rate. The bit error rate in the absence of interference is equal to

7.8270e-4, which corresponds to SNR(20) = 10 dB. The solid curve in Fig. 4.4

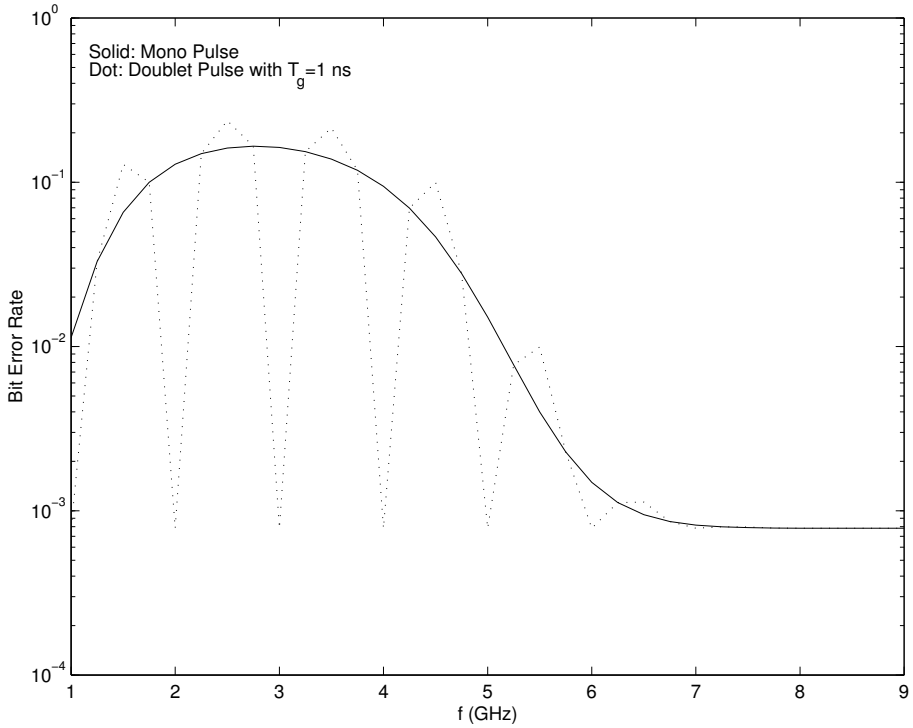

Figure 4.4: Bit error rate versus the interference frequency

corresponds to using a single second-order derivative of Gaussian pulse shape. As can be seen, the bit error rate performance in the presence of interference degrades more severely at frequencies where the spectral density of the second-order derivative of Gaussian pulse shape shown in Fig. 4.5 is stronger. The dotted curve in Fig. 4.4 corresponds to using a doublet pulse shape, which will be described in the next section.

Since $\mathrm{E}\{D_j^k\} = 0$, the discrete part of the power spectral density consisting of spectral lines at integer multiples of $\frac{1}{T_f}$ vanishes [66], and the spectral density of the modulated time-hopped signal

$$s(t) = \sum_{k=1}^{N_u} g_k \sum_j D_j^k w(t - jT_f - c_j^k T_c - \tau_k) \tag{4.21}$$

can be computed as

$$S_s(f) = \frac{|W(f)|^2}{T_f} \sum_{k=1}^{N_u} g_k^2 \tag{4.22}$$

Therefore, the shape of the spectral density of the received signal is just a scaled version of the energy spectral density of the received pulse shape $w(t)$.

As can be observed from Fig.'s 4.2 and 4.4, the tone interference degrades the performance differently depending on which portion of UWB radio operating bandwidth it hits. Fig. 4.5 demonstrates the normalized energy spectrum of the second-order derivative of Gaussian received pulse shape shown in Fig. 4.3. At around $f_0 = 3$ GHz, where the frequency content of the received pulse spectrum is very strong, the tone interference degrades the performance much more severely. Also at places where the frequency contents have almost the same strengths, e.g. at 1 GHz and 5 GHz, the degradations arising from the tone interferers are almost the same.

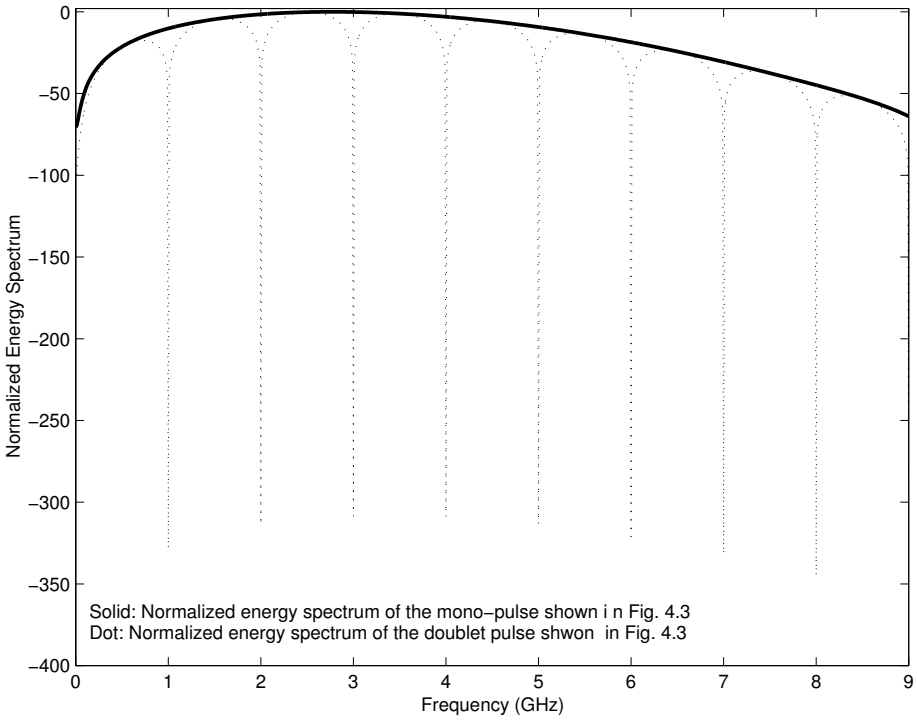

Figure 4.5: Normalized energy spectrum of mono and doublet waveforms shown in Fig. 4.3

4.3 Interference Rejection

A doublet pulse consists of two received waveforms separated from each other by T_g time shift and with opposite amplitudes, i.e.,

$$w_d(t) = \frac{1}{\sqrt{2}}(w(t) - w(t - T_g)) \tag{4.23}$$

Fig. 4.3 shows such a pulse. The spectral amplitude of such a pulse shape can be computed as

$$|W_d(f)|^2 = 2|W(f)|^2 \sin^2(\pi f T_g) \tag{4.24}$$

where $|W(f)|^2$ is the magnitude squared of a single received pulse spectrum. Therefore, the spectrum has nulls at $f = \frac{k}{T_g}$ for any integer k as illustrated in Fig. 4.5. By controlling T_g, we can generate nulls at specific frequencies to mitigate interferers around those frequencies. We can adjust the nulls by changing T_g in order to reject powerful narrow band interferers existing simultaneously at operating bandwidth of UWB radio in a particular environment. For example, if we set $T_g = 1$ ns, we can completely remove all the interferers whose frequencies are multiple integers of 1 GHz. This will lead to neither any SNR nor bit error rate performance degradation in Fig.'s 4.2 and 4.4 for $f_0 = 1, 2, 3, \cdots, 9$ GHz, regardless of how strong a tone interference at such frequencies is.

Fig. 4.6 shows the SNR degradation in the presence of an external interference with flat power spectral density over $B = 50$ MHz and $B = 100$ MHz bandwidth and 2 GHz center frequency when 20 UWB users are simultaneously communicating at 1 Mbps data rate. The operating SNR(20) has been assumed 10 dB in the absence of external interference. As can be seen,

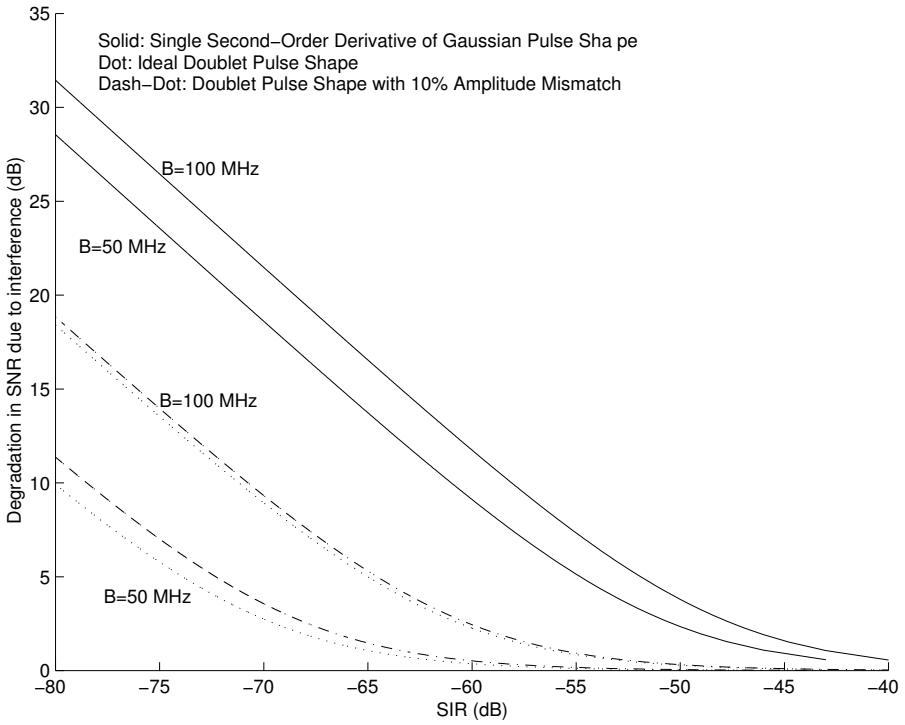

Figure 4.6: SNR degradation due to a narrow band interference with or without using a doublet pulse

there is a gain of 13 dB and 18.6 dB using a properly designed doublet pulse compared to just using a single pulse shape when the interference is 80 dB stronger than the signal of the user of interest with $B = 100$ MHz and $B = 50$ MHz bandwidth, respectively. It is worth noting that assuming a flat power spectral density for a narrow band interference over a fixed bandwidth at a specific center frequency, actually represents a harsh situation, because the interference power is equally spread over its bandwidth, which hurts our system more severely if the generated notch by a doublet pulse is not wide enough in the frequency domain. On the contrary, a narrow band interference over a

fixed bandwidth with power mostly concentrated around its center frequency, can be easily mitigated by adjusting the notch sharply in the middle of its bandwidth.

It can be shown that the asymptotic performance gain in Fig. 4.6, obtained by using a proper doublet pulse, $w_d(t)$, over a mono-pulse, $w(t)$, when the interference becomes very strong is

$$G = 10 \log \left(\frac{\int_{B1}^{B2} S_w(f) df}{\int_{B1}^{B2} S_{w_d}(f)\, df} \right) \tag{4.25}$$

where $\frac{B1+B2}{2}$ is the narrow band interference center frequency with bandwidth $B = B2 - B1$. This asymptotic gain is 13.1 dB and 19.1 dB for the cases of $B = 100$ MHz and $B = 50$ MHz shown in Fig. 4.6, respectively.

To mitigate two different external interferers at two different frequencies, we can design

$$T_g = \frac{1}{G.C.D.\{f_1, f_2\}} \tag{4.26}$$

where G.C.D. represents the greatest common devisor operation over those external interferers' center frequencies.

4.4 Effect of Mismatches

In this section, the effect of mismatches in the positive and negative amplitudes of a doublet pulse along with having an offset in the gap time from its nominal value are investigated. To model these effects, doublet pulse is expressed in the form:

$$w_d(t) = w(t) - \alpha w(t - \beta T_g) \tag{4.27}$$

where $w(t)$ is the received pulse shape and α and β are used to model amplitude mismatch and gap time offset in the doublet pulse, respectively. Therefore, the spectral amplitude squared of the doublet pulse is

$$|W_d(f)|^2 = |W(f)|^2 C(f) \tag{4.28}$$

where

$$C(f) = [1 - 2\alpha \cos(2\pi\beta T_g f) + \alpha^2] \tag{4.29}$$

In order to generate perfect nulls at some frequency f_0, we need to have $C(f_0) = 0$ for an arbitrary pulse shape $w(t)$. Hence,

$$C(f_0) = 0 \Rightarrow \cos(2\pi\beta T_g f_0) = \frac{1+\alpha^2}{2\alpha} \tag{4.30}$$

Since α is a number around 1 to represent the amplitude mismatch between the positive and negative polarities in the doublet pulse; therefore, $\alpha > 0$, and $\frac{1+\alpha^2}{2\alpha} \geq 1$. This means that perfect nulls can be generated only when there is no amplitude mismatch or when $\alpha = 1$; however, by finding the minima of $C(f)$, we can locate the position of deep nulls in the frequency spectrum:

$$\frac{dC(f)}{df} = 0 \Rightarrow f = \frac{k}{2\beta T_g} \tag{4.31}$$

where k is an integer.

When k is an even integer, we get

$$\left|W_d(\frac{k}{2\beta T_g})\right|^2 = \left|W(\frac{k}{2\beta T_g})\right|^2 (1-\alpha)^2 \tag{4.32}$$

and when k is an odd integer

$$C(\frac{k}{2\beta T_g}) = (1+\alpha)^2 \tag{4.33}$$

which corresponds to the local maxima of $C(f)$. Hence, nulls can be generated only at even multiples of $\frac{1}{2\beta T_g}$, which is equivalent to any integer multiple of $\frac{1}{\beta T_g}$. Fig. 4.6 shows that little performance degradation is observed when using a non-ideal doublet pulse.

4.5 Conclusion

Using a huge bandwidth, digital impulse radio has to face interference from external sources working at different portions of its bandwidth. Interference coming from these external sources degrades the UWB radio performance. Depending on the frequency of narrow band interferers, they degrade the performance differently. Those with frequencies concentrated at regions where the UWB radio pulse has stronger frequency contents, degrade the performance more severely. By careful design of UWB pulse shape, we can mitigate the narrow bandwidth interference. This can be achieved with careful design of gap time between the two single pulses in a doublet pulse in order to generate nulls in the frequency domain where the interference is present; therefore, with this technique, we do not need to use any additional expensive filter to reject narrow bandwidth interference.

Studies of amplitude mismatches and gap time offset show how the location and magnitude of the nulls are affected by these factors when a doublet pulse is

used in order to avoid narrow bandwidth interference. The results obtained in this chapter are general and not limited to the pulse shapes shown in Fig. 4.3, and can be applied to any arbitrary pulse shape as may be required to meet spectral masked imposed by regulatory authorities.

Chapter 5

Power Spectral Density of Multiple Access Digital Impulse Radio in the Presence of Multipath

5.1 Introduction

In this chapter, the Power Spectral Density (PSD) of multiple access digital impulse radio utilizing direct-sequence or time-hopping spreading technique with bit-flipping or pulse position data modulation is investigated. According to Federal Communication Commission's Report and Order on Ultra Wide Bandwidth (UWB) systems, the transmitted power radiated by such devices should be restricted within spectral masks associated to different UWB applications. For an indoor wireless multiuser scenario the aggregate interference

should comply with these regulations. This motivates investigating the power spectral density of multiple access UWB impulse radio under realistic propagation conditions for system design and power control issues.

In other words, it is important to know the effects of realistic multipath channels on the UWB power spectral density in order to estimate the power level fluctuations in typical UWB applications. If these fluctuations are very high, then the spurious emission levels radiated by such UWB devices may severely degrade the reliable performance of other narrow band communication systems working simultaneously at different portions of UWB radio spectrum.

5.2 Power Spectral Density of a Finite Power Random Signal

The following approach is taken in computing the power spectral density, $S(f)$, of a finite power signal, $s(t)$, throughout this chapter.

$$S(f) = \lim_{T \to \infty} \frac{\mathrm{E}\{|\mathrm{F}\{s_{2T}(t)\}|^2\}}{2T} \tag{5.1}$$

where F$\{s(t)\}$ represents the Fourier Transform of $s_{2T}(t)$ and

$$s_{2T}(t) = s(t), t \in [-T, T] \tag{5.2}$$

and $s_{2T}(t) = 0$ outside the above interval. This approach can be used regardless of a stochastic process being wide sense stationary or not. Albeit, the power spectral density of a wide sense stationary process computed using (5.1) is equivalent to the Fourier transform of its autocorrelation function. The method used in [65, 66] computes the power spectral density of a time-hopping system based on computing the autocorrelation function of a single user scenario under ideal propagation conditions. In this chapter, we derive closed form formulas for both time-hopping and direct-sequence multiple-access power spectral densities. The effects of UWB multipath on the power spectral density is also investigated.

5.3 Direct-Sequence Spreading with Bit-Flipping Modulation

The wireless multiple access digital impulse radio signal under multipath propagation conditions utilizing direct-sequence spreading with bit-flipping data modulation can be represented as

$$s(t) = \sum_{k=1}^{N_u} \sum_{m=0}^{L^k-1} g_m^k f^k(t - \tau_m^k) \tag{5.3}$$

where

$$f^k(t) = \sum_{l} a_l^k d_{\lfloor \frac{l}{N_s} \rfloor}^k w(t - lT_f) \tag{5.4}$$

is the transmitted signal of User k with no asynchronous delay. The mth path's delay of the kth user is represented by $\tau_m^k = \tau_0^k + \lambda_m^k$, where λ_m^k is the excess delay of the kth user's mth path and τ_0^k is his/her corresponding asynchronous delay. The amplitude of the mth path of the kth user is denoted by g_m^k. We assume there are N_u active users simultaneously present and that User k has a multipath channel with L^k taps. Each transmitted data is repeated N_s times, therefore, the kth user's data at the lth frame is shown as $d_{\lfloor \frac{l}{N_s} \rfloor}$. The transmitted data $d_i^k \in \{+1, -1\}$ and there is an additional direct-sequence

spreading modulation, a_l^k, which represents the polarity of user k's spreading sequence at the lth frame. The spreading sequences are assumed random. At the beginning of each frame duration, T_f, one pulse, $w(t)$, is transmitted.

The first step toward power spectral density computation is to take the Fourier Transform of $s_{2nT_f}(t)$ using (5.3).

$$\mathrm{F}\{s_{2nT_f}(t)\} = \sum_{k=1}^{N_u} \sum_{m=0}^{L^k-1} g_m^k F_{2nT_f}^k(f) e^{-j2\pi f \tau_m^k} \tag{5.5}$$

where $F_{2nT_f}^k(f)$ is the Fourier Transform of $f_{2nT_f}^k(t)$. But using (5.4),

$$F_{2nT_f}^k(f) = \sum_{l=-n}^{n-1} a_l^k d_{[\frac{l}{N_s}]}^k W(f) e^{-j2\pi f l T_f} \tag{5.6}$$

where $W(f)$ represents the Fourier Transform of $w(t)$. Note that the support of $w(t)$ is much less than one frame duration. To compute $|\mathrm{F}\{s_{2nT_f}(t)\}|^2$, we have

$$|\mathrm{F}\{s_{2nT_f}(t)\}|^2 = \sum_{k=1}^{N_u} \sum_{k'=1}^{N_u} \sum_{m=0}^{L^k-1} \sum_{m'=0}^{L^{k'}-1} g_m^k g_{m'}^{k'} F_{2nT_f}^k(f) F_{2nT_f}^{k'}(f)^* e^{-j2\pi f \tau_m^k} e^{+j2\pi f \tau_{m'}^{k'}} \tag{5.7}$$

Using (5.6)

$$F^k_{2nT_f}(f)F^{k'}_{2nT_f}(f)^* = \sum_{l=-n}^{n-1}\sum_{l'=-n}^{n-1} a^k_l a^{k'}_{l'} d^k_{\lfloor \frac{l}{N_s} \rfloor} d^{k'}_{\lfloor \frac{l'}{N_s} \rfloor} |W(f)|^2 e^{-j2\pi f(l-l')T_f} \tag{5.8}$$

Therefore, $\mathrm{E}\{|\mathrm{F}\{s_{2nT_f}(t)\}|^2\}$ can be computed as

$$\mathrm{E}\{|\mathrm{F}\{s_{2nT_f}(t)\}|^2\} = \sum_{k=1}^{N_u}\sum_{k'=1}^{N_u}\sum_{m=0}^{L^k-1}\sum_{m'=0}^{L^{k'}-1} g^k_m g^{k'}_{m'} \sum_{l=-n}^{n-1}\sum_{l'=-n}^{n-1} \mathrm{E}\{X(k,k',m,m',l,l')\}|W(f)|^2 \tag{5.9}$$

where

$$X(k,k',m,m',l,l') = a^k_l a^{k'}_{l'} d^k_{\lfloor \frac{l}{N_s} \rfloor} d^{k'}_{\lfloor \frac{l'}{N_s} \rfloor} e^{-j2\pi f(l-l')T_f} e^{-j2\pi f(\tau^k_m - \tau^{k'}_{m'})} \tag{5.10}$$

Since different users have independent random direct sequences, a^k_l is independent from $a^{k'}_{l'}$ for $k \neq k'$, and even for the same user, a^k_l is independent from $a^k_{l'}$ when $l \neq l'$. From this observation and from the fact that $\Pr.\{a^k_l = +1\} = \Pr.\{a^k_l = -1\} = \frac{1}{2}$, we conclude that $\mathrm{E}\{X(k,k',m,m',l,l')\} = 0$ when $k \neq k'$ and/or $l \neq l'$. Hence,

$$\mathrm{E}\{|\mathrm{F}\{s_{2nT_f}(t)\}|^2\} = \sum_{k=1}^{N_u}\sum_{m=0}^{L^k-1}\sum_{m'=0}^{L^k-1} g^k_m g^k_{m'} \sum_{l=-n}^{n-1} \mathrm{E}\{X(k,k,m,m',l,l)\}|W(f)|^2 \tag{5.11}$$

where

$$\mathrm{E}\{X(k,k,m,m',l,l)\} = e^{-j2\pi f(\lambda_m^k - \lambda_{m'}^k)} \tag{5.12}$$

since ${a_l^k}^2 = 1$ and ${d^k_{\lfloor \frac{l}{N_s} \rfloor}}^2 = 1$ and ,$\tau_m^k - \tau_{m'}^k = \lambda_m^k - \lambda_{m'}^k$. Hence,

$$\mathrm{E}\{|\mathrm{F}\{s_{2nT_f}(t)\}|^2\} = \sum_{k=1}^{N_u} \sum_{m=0}^{L^k-1} \sum_{m'=0}^{L^k-1} g_m^k g_{m'}^k 2n|W(f)|^2 e^{-j2\pi f(\lambda_m^k - \lambda_{m'}^k)} \tag{5.13}$$

Using (5.1) with $T = nT_f$, we have

$$S(f) = \lim_{n\to\infty} \frac{\sum_{k=1}^{N_u} \sum_{m=0}^{L^k-1} \sum_{m'=0}^{L^k-1} g_m^k g_{m'}^k 2n|W(f)|^2 e^{-j2\pi f(\lambda_m^k - \lambda_{m'}^k)}}{2nT_f} \tag{5.14}$$

or the power spectral density of multiple access digital impulse radio utilizing direct-sequence spreading with bit-flipping data modulation under multipath propagation conditions is given by

$$S(f) = \frac{|W(f)|^2}{T_f} \sum_{k=1}^{N_u} \left| \sum_{m=0}^{L^k-1} g_m^k \, e^{-j2\pi f \lambda_m^k} \right|^2 \tag{5.15}$$

As can be seen, there are no discrete parts present in the power spectral density of a direct-sequence signal utilizing antipodal data modulation. As expected, the multiuser power spectral density is simply the sum of individual power spectral densities corresponding to different users and the effect of kth user's

multipath channel is demonstrated through $\left|\sum_{m=0}^{L^k-1} g_m^k e^{-j2\pi f \lambda_m^k}\right|^2$. There is also a scale factor of $\frac{1}{T_f}$ in the power spectral density formula.

5.4 Time-Hopping Spreading with Pulse Position Modulation

The wireless multiple access digital impulse radio signal under multipath propagation conditions utilizing time-hopping spreading with pulse position data modulation can be represented as

$$r_{2nN_sT_f}(t) = \sum_{k=1}^{N_u} \sum_{m=0}^{L^k-1} g_m^k S_{2nN_sT_f}^k (t - \tau_m^k) \tag{5.16}$$

where

$$S_{2nN_sT_f}^k(t) = \sum_{l=-nN_s}^{nN_s-1} w(t - lT_f - c_l^k T_c - \delta d_{\lfloor \frac{l}{N_s} \rfloor}^k) \tag{5.17}$$

Taking the Fourier Transform of $r_{2nN_sT_f}(t)$,

$$R_{2nN_sT_f}(f) = \sum_{k=1}^{N_u} \sum_{m=0}^{L^k-1} g_m^k \sum_{l=-nN_s}^{nN_s-1} W(f) e^{-j2\pi f (lT_f + c_l^k T_c + \delta d_{\lfloor \frac{l}{N_s} \rfloor}^k + \tau_m^k)} \tag{5.18}$$

Therefore, considering $\tau_m^k = \lambda_m^k + \tau_0^k$,

$$|R_{2nN_sT_f}(f)|^2 = \sum_{k=1}^{N_u}\sum_{k'=1}^{N_u}\sum_{m=0}^{L^k-1}\sum_{m'=0}^{L^{k'}-1} g_m^k g_{m'}^{k'} e^{-j2\pi f(\lambda_m^k - \lambda_{m'}^{k'})} \sum_{l=-nN_s}^{nN_s-1}\sum_{l'=-nN_s}^{nN_s-1}$$
$$|W(f)|^2 e^{-j2\pi f((l-l')T_f)} e^{-j2\pi f(c_l^k - c_{l'}^{k'})T_c} e^{-j2\pi f\delta(d^k_{\lfloor \frac{l}{N_s}\rfloor} - d^{k'}_{\lfloor \frac{l'}{N_s}\rfloor})} e^{-j2\pi f(\tau_0^k - \tau_0^{k'})} \quad (5.19)$$

First, we show that when $k \neq k'$, $\lim_{n\to\infty} \frac{\mathrm{E}\{|R_{2nN_sT_f}(f)|^2\}}{2nN_sT_f} = 0$. For convenience, such terms are denoted by $|R_{2nN_sT_f}(f; k \neq k')|^2$.

$$\lim_{n\to\infty} \frac{\mathrm{E}\{|R_{2nN_sT_f}(f;k\neq k')|^2\}}{2nN_sT_f} = \lim_{n\to\infty} \sum_{k=1}^{N_u}\sum_{k'=1,k'\neq k}^{N_u}\sum_{m=0}^{L^k-1}\sum_{m'=0}^{L^{k'}-1} g_m^k g_{m'}^{k'}$$
$$e^{-j2\pi f(\lambda_m^k - \lambda_{m'}^{k'})} |W(f)|^2 \sum_{l=-nN_s}^{nN_s-1}\sum_{l'=-nN_s}^{nN_s-1} \frac{1}{2nN_s} e^{-j2\pi f((l-l')T_f)} \mathrm{E}\{e^{-j2\pi f c_l^k T_c}\}$$
$$\mathrm{E}\{e^{j2\pi f c_{l'}^{k'} T_c}\}\mathrm{E}\{e^{-j2\pi f\delta d^k_{\lfloor \frac{l}{N_s}\rfloor}}\}\mathrm{E}\{e^{j2\pi f\delta d^{k'}_{\lfloor \frac{l'}{N_s}\rfloor}}\}\mathrm{E}\{e^{-j2\pi f\tau_0^k}\}\mathrm{E}\{e^{j2\pi f\tau_0^{k'}}\} \quad (5.20)$$

Since

$$\mathrm{E}\{e^{-j2\pi f c_l^k T_c}\} = \sum_{h=0}^{N_h-1} \frac{1}{N_h} e^{-j2\pi f h T_c} = \frac{1}{N_h}\frac{1-e^{-j2\pi f N_h T_c}}{1-e^{-j2\pi f T_c}} \quad (5.21)$$

where N_h is an integer for which $N_hT_c \leq T_f$ and $0 \leq c_l^k < N_h$ and

$$\mathrm{E}\{e^{-j2\pi f\delta d^k_{\lfloor \frac{l}{N_s}\rfloor}}\} = \frac{1}{2} + \frac{e^{-j2\pi f\delta}}{2} \quad (5.22)$$

and

$$\mathrm{E}\{e^{-j2\pi f\tau_0^k}\} = \frac{1}{T_f}\int_{\frac{-T_f}{2}}^{\frac{T_f}{2}} e^{-j2\pi fx}\,dx = \mathrm{sinc}(fT_f) \tag{5.23}$$

where $\mathrm{sinc}(x) = \frac{\sin(\pi x)}{\pi x}$, we can conclude that

$$\begin{aligned}\lim_{n\to\infty}\frac{\mathrm{E}\{|R_{2nN_sT_f}(f;k\neq k')|^2\}}{2nN_sT_f} = \lim_{n\to\infty}\sum_{k=1}^{N_u}\sum_{k'=1,k'\neq k}^{N_u}\sum_{m=0}^{L^k-1}\sum_{m'=0}^{L^{k'}-1} g_m^k g_{m'}^{k'} \\ e^{-j2\pi f(\lambda_m^k-\lambda_{m'}^{k'})}|W(f)|^2\sum_{l=-nN_s}^{nN_s-1}\sum_{l'=-nN_s}^{nN_s-1}\frac{1}{2nN_sT_f}e^{-j2\pi f((l-l')T_f)} \\ \frac{1}{N_h^2}\frac{2-2\cos(2\pi fN_hT_c)}{2-2\cos(2\pi fT_c)}\frac{2+2\cos(2\pi f\delta)}{4}\mathrm{sinc}^2(fT_f)\end{aligned} \tag{5.24}$$

From the identity (see Appendix C)

$$\sum_{l=-nN_s}^{nN_s-1}\sum_{l'=-nN_s}^{nN_s-1} e^{-j2\pi f((l-l')T_f)} = \frac{\sin^2(2\pi fT_fnN_s)}{\sin^2(\pi fT_f)} \tag{5.25}$$

and considering that (see Appendix D)

$$\lim_{n\to\infty}\frac{1}{2nN_s}\frac{\sin^2(2\pi fT_fnN_s)}{\sin^2(\pi fT_f)} = \frac{1}{T_f}\sum_{i=-\infty}^{\infty}\delta_D(f-\frac{i}{T_f}) \tag{5.26}$$

we have

$$\lim_{n\to\infty}\frac{\mathrm{E}\{|R_{2nN_sT_f}(f;k\neq k')|^2\}}{2nN_sT_f}=\sum_{k=1}^{N_u}\sum_{k'=1,k'\neq k}^{N_u}\sum_{m=0}^{L^k-1}\sum_{m'=0}^{L^{k'}-1}g_m^k g_{m'}^{k'}e^{-j2\pi f(\lambda_m^k-\lambda_{m'}^{k'})}$$
$$|W(f)|^2\frac{1}{2nN_sT_f^2N_h^2}\frac{\sin^2(\pi fN_hT_c)}{\sin^2(\pi fT_c)}\cos^2(\pi f\delta)\mathrm{sinc}^2(fT_f)$$
$$\sum_{i=-\infty}^{\infty}\delta_D(f-\frac{i}{T_f}) \tag{5.27}$$

or

$$\lim_{n\to\infty}\frac{\mathrm{E}\{|R_{2nN_sT_f}(f;k\neq k')|^2\}}{2nN_sT_f}=\sum_{k=1}^{N_u}\sum_{k'=1,k'\neq k}^{N_u}\sum_{m=0}^{L^k-1}\sum_{m'=0}^{L^{k'}-1}g_m^k g_{m'}^{k'}\sum_{i=-\infty}^{\infty}$$
$$e^{-j2\pi\frac{i}{T_f}(\lambda_m^k-\lambda_{m'}^{k'})}|W(\frac{i}{T_f})|^2\frac{1}{2nN_sT_f^2N_h^2}\frac{\sin^2(\pi\frac{i}{T_f}N_hT_c)}{\sin^2(\pi\frac{i}{T_f}T_c)}\cos^2(\pi\frac{i}{T_f}\delta)$$
$$\mathrm{sinc}^2(i)\delta_D(f-\frac{i}{T_f})=0 \tag{5.28}$$

Since $\mathrm{sinc}^2(i)=0$ for any $i\neq 0$ and $W(0)=0$ due to propagation effects. Hence,

$$\lim_{n\to\infty}\frac{\mathrm{E}\{|R_{2nN_sT_f}(f)|^2\}}{2nN_sT_f}=\lim_{n\to\infty}\frac{1}{2nN_sT_f}\sum_{k=1}^{N_u}\sum_{m=0}^{L^k-1}\sum_{m'=0}^{L^{k'}-1}g_m^k g_{m'}^{k}e^{-j2\pi f(\lambda_m^k-\lambda_{m'}^{k})}$$
$$|W(f)|^2\sum_{l=-nN_s}^{nN_s-1}\sum_{l'=-nN_s}^{nN_s-1}e^{-j2\pi f(l-l')T_f}\mathrm{E}\{e^{-j2\pi f(c_l^k-c_{l'}^k)T_c}\}\mathrm{E}\{e^{-j2\pi f\delta(d^k_{\lfloor\frac{l}{N_s}\rfloor}-d^k_{\lfloor\frac{l'}{N_s}\rfloor})}\} \tag{5.29}$$

or

$$\lim_{n\to\infty}\frac{\mathrm{E}\{|R_{2nN_sT_f}(f)|^2\}}{2nN_sT_f}=\lim_{n\to\infty}\frac{1}{2nN_sT_f}\sum_{k=1}^{N_u}\sum_{m=0}^{L^k-1}\sum_{m'=0}^{L^{k'}-1}g_m^k g_{m'}^k e^{-j2\pi f(\lambda_m^k-\lambda_{m'}^k)}$$
$$|W(f)|^2[(\sum_{l=l'=-nN_s}^{nN_s-1}1)+\sum_{l,l'=-nN_s(l'\neq l)}^{nN_s-1}e^{-j2\pi f((l-l')T_f)}\mathrm{E}\{e^{-j2\pi f c_l^k T_c}\}$$
$$\mathrm{E}\{e^{j2\pi f c_{l'}^k T_c}\}\mathrm{E}\{e^{-j2\pi f\delta(d^k_{\lfloor\frac{l}{N_s}\rfloor}-d^k_{\lfloor\frac{l'}{N_s}\rfloor})}\}] \qquad (5.30)$$

We divide the case for $l\neq l'$ into two disjoint subsets, namely, $l\neq l'$ and $\lfloor\frac{l}{N_s}\rfloor=\lfloor\frac{l'}{N_s}\rfloor$ and the case where $l\neq l'$ while $\lfloor\frac{l}{N_s}\rfloor\neq\lfloor\frac{l'}{N_s}\rfloor$. Therefore,

$$\lim_{n\to\infty}\frac{\mathrm{E}\{|R_{2nN_sT_f}(f)|^2\}}{2nN_sT_f}=\sum_{k=1}^{N_u}\sum_{m=0}^{L^k-1}\sum_{m'=0}^{L^{k'}-1}g_m^k g_{m'}^k e^{-j2\pi f(\lambda_m^k-\lambda_{m'}^k)}|W(f)|^2$$
$$(\frac{1}{T_f}+\lim_{n\to\infty}\frac{1}{2nN_sT_f}\sum_{l=-nN_s}^{nN_s-1}\sum_{l'=-nN_s(l'\neq l,\lfloor\frac{l}{N_s}\rfloor=\lfloor\frac{l'}{N_s}\rfloor)}^{nN_s-1}e^{-j2\pi f(l-l')T_f}$$
$$\frac{1}{N_h^2}\frac{\sin^2(\pi fN_hT_c)}{\sin^2(\pi fT_c)}+\lim_{n\to\infty}\frac{1}{2nN_sT_f}\sum_{l=-nN_s}^{nN_s-1}\sum_{l'=-nN_s(l'\neq l,\lfloor\frac{l}{N_s}\rfloor\neq\lfloor\frac{l'}{N_s}\rfloor)}^{nN_s-1}e^{-j2\pi f(l-l')T_f}$$
$$\frac{1}{N_h^2}\frac{\sin^2(\pi fN_hT_c)}{\sin^2(\pi fT_c)}\cos^2(\pi f\delta)) \qquad (5.31)$$

To proceed, we need to compute

$$\sum_{l=-nN_s}^{nN_s-1}\sum_{l'=-nN_s(l'\neq l,\lfloor\frac{l}{N_s}\rfloor=\lfloor\frac{l'}{N_s}\rfloor)}^{nN_s-1}e^{-j2\pi f(l-l')T_f}=2n\sum_{i=1}^{N_s-1}(N_s-i)(e^{j2\pi ifT_f}+e^{-j2\pi ift_f}) \qquad (5.32)$$

which simplifies to

$$\sum_{l=-nN_s}^{nN_s-1} \sum_{l'=-nN_s (l' \neq l, \lfloor \frac{l}{N_s} \rfloor = \lfloor \frac{l'}{N_s} \rfloor)}^{nN_s-1} e^{-j2\pi f(l-l')T_f} = 4n \sum_{i=1}^{N_s-1} (N_s - i) \cos(2\pi i f T_f) \tag{5.33}$$

Also,

$$\sum_{l=-nN_s}^{nN_s-1} \sum_{l'=-nN_s (l' \neq l, \lfloor \frac{l}{N_s} \rfloor \neq \lfloor \frac{l'}{N_s} \rfloor)}^{nN_s-1} e^{-j2\pi f(l-l')T_f} = \sum_{l=-nN_s}^{nN_s-1} \sum_{l'=-nN_s}^{nN_s-1} e^{-j2\pi f(l-l')T_f} - \sum_{l=l'=-nN_s}^{nN_s-1} 1 - \sum_{l=-nN_s}^{nN_s-1} \sum_{l'=-nN_s (l' \neq l, \lfloor \frac{l}{N_s} \rfloor = \lfloor \frac{l'}{N_s} \rfloor)}^{nN_s-1} e^{-j2\pi f(l-l')T_f} \tag{5.34}$$

or

$$\sum_{l=-nN_s}^{nN_s-1} \sum_{l'=-nN_s (l' \neq l, \lfloor \frac{l}{N_s} \rfloor \neq \lfloor \frac{l'}{N_s} \rfloor)}^{nN_s-1} e^{-j2\pi f(l-l')T_f} = \frac{\sin^2(2\pi f T_f n N_s)}{\sin^2(\pi f T_f)} - 2nN_s - 4n \sum_{i=1}^{N_s-1} (N_s - i) \cos(2\pi i f T_f) \tag{5.35}$$

Therefore,

$$\lim_{n\to\infty}\frac{\mathrm{E}\{|R_{2nN_sT_f}(f)|^2\}}{2nN_sT_f}=\sum_{k=1}^{N_u}\sum_{m=0}^{L^k-1}\sum_{m'=0}^{L^{k'}-1}g_m^k g_{m'}^k e^{-j2\pi f(\lambda_m^k-\lambda_{m'}^k)}|W(f)|^2$$
$$\{\frac{1}{T_f}+\frac{2}{N_h^2N_sT_f}\frac{\sin^2(\pi fN_hT_c)}{\sin^2(\pi fT_c)}\sum_{i=1}^{N_s-1}(N_s-i)\cos(2\pi ifT_f)+\frac{1}{N_h^2}\frac{\sin^2(\pi fN_hT_c)}{\sin^2(\pi fT_c)}$$
$$\cos^2(\pi f\delta)(\frac{1}{T_f^2}\sum_{i=-\infty}^{\infty}\delta_D(f-\frac{i}{T_f})-\frac{1}{T_f}-\frac{2}{N_sT_f}\sum_{i=1}^{N_s-1}(N_s-i)\cos(2\pi ifT_f))\} \tag{5.36}$$

After carrying on some manipulations, the power spectral density of multiple access time-hopping digital impulse radio with pulse position modulation in the presence of multipath can be given by

$$S(f)=\sum_{k=1}^{N_u}\left|\sum_{m=0}^{L^k-1}g_m^k e^{-j2\pi f\lambda_m^k}W(f)\right|^2\{\frac{1}{T_f}+\frac{2\sin^2(\pi f\delta)}{N_h^2N_sT_f}\frac{\sin^2(\pi fN_hT_c)}{\sin^2(\pi fT_c)}$$
$$\sum_{i=1}^{N_s-1}(N_s-i)\cos(2\pi ifT_f)-\frac{\cos^2(\pi f\delta)}{N_h^2T_f}\frac{\sin^2(\pi fN_hT_c)}{\sin^2(\pi fT_c)}+$$
$$\frac{1}{N_h^2T_f^2}\sum_{i=-\infty}^{\infty}\frac{\sin^2(\pi i\frac{T_c}{T_f}N_h)}{\sin^2(\pi i\frac{T_c}{T_f})}\cos^2(\pi\frac{i}{T_f}\delta)\delta_D(f-\frac{i}{T_f})\} \tag{5.37}$$

One should note that when $N_hT_c=T_f$, i.e., when the hopping range is equal to one frame duration, the discrete parts of the power spectral density will vanish.

5.5 Investigating the Effects of Multipath on UWB Power Spectral Density

In this section, the power spectral density fluctuations of single user and multiuser UWB radio in the presence of multipath channels is studied [60].

Fig. 5.1 demonstrates the power spectral density of single user direct-sequence UWB radio considering only the fist few arriving paths. This PSD has been normalized by the $\max_f \frac{|W(f)|^2}{T_f}$. As can be seen, the power spectral

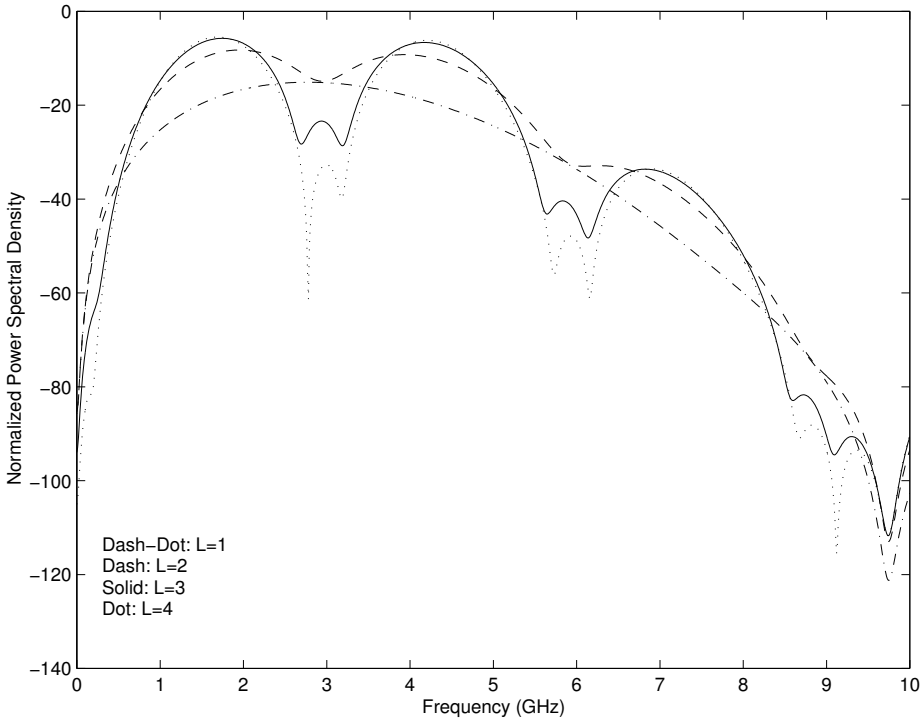

Figure 5.1: Single user PSD assuming only the first few arriving paths

density assuming only the first arriving path is proportional to the energy

spectral density of the pulse shape used. This pulse shape and its energy spectral density is shown in Fig. 4.3 and 4.5, respectively. Considering the first two arriving paths, the PSD distorts a little bit with respect to the energy spectral density of the pulse shape. Adding the third and fourth paths, we see the frequency selectivity phenomenon and the fluctuations range between roughly -45 to 15 dB compared to the no multipath scenario. This suggests the careful design of UWB systems such that under realistic propagation conditions the radiated power level does not exceed the limits imposed by regulatory authorities. Fig. 5.2 shows these fluctuations using all the paths of the received signal. This figure illustrates PSD fluctuations between -27 and 21 dB as compared with the no multipath scenario. Fig. 5.3 investigates the power spectral density of multiuser UWB radio. Curves for both single user and 10 user scenarios are given for comparison. Here, all the paths have been considered for each user's independent multipath channel. As can be observed, the multiple access power spectral density is smoother than that of the single user due to the aggregation of different users's PSD's which somehow averages out sharp fluctuations. However, the multiple access PSD is 10 dB stronger than the single user case. This aggregate PSD should be designed such that it meets the spectral mask requirements imposed by regulatory authorities.

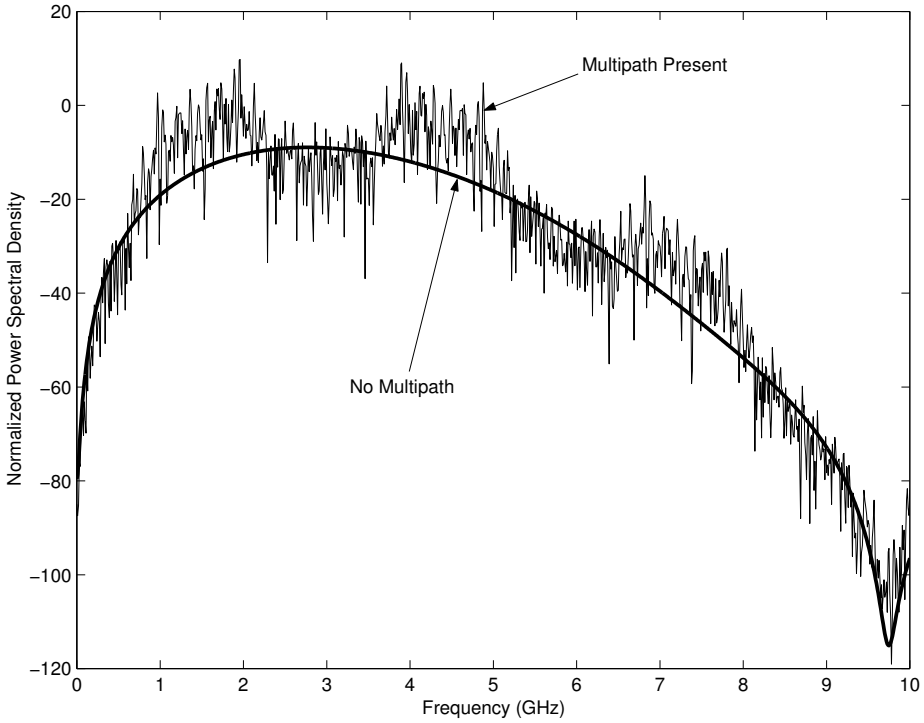

Figure 5.2: Single user PSD under ideal and realistic propagation conditions

5.6 Conclusion

It is important to know the effects of typical UWB multipath channels on UWB impulse radio power spectral density in order to investigate the spurious emissions from such radios on other narrow band systems working simultaneously at different portions of UWB radio spectrum. This power Spectral density in the presence of multipath demonstrates frequency selectivity on the order of ± 20 dB fluctuations. These fluctuations should be considered in designing

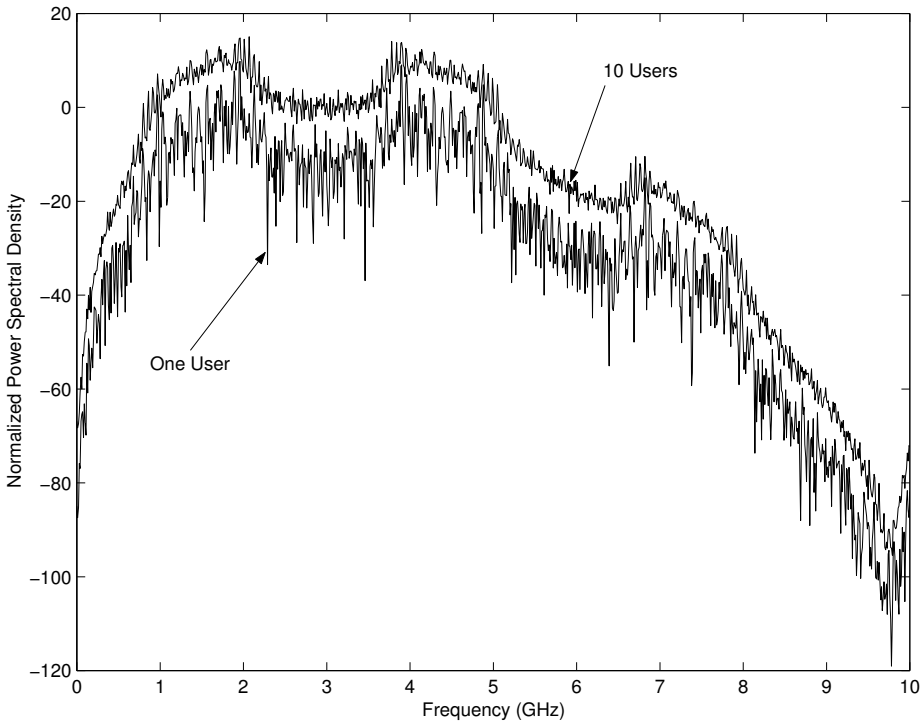

Figure 5.3: Single user and multiuser PSD comparison

UWB transmitters so as not to cause intolerable spurious emission levels on traditional narrow band systems.

The power spectral density of a multiple-access UWB impulse radio communication system has higher levels proportional to the number of active users communicating at the same time. This suggests reduction in transmitted power levels based on the total number of active users such that the aggregate interference is restricted within specific spectral masks imposed by regulatory authorities. Although the power spectral density levels are higher for

multiple-access systems, the power spectral density fluctuations due to multi-path phenomenon are smoother because of aggregating different users's power spectral densities which somehow averages such fluctuations.

Chapter 6

UWB Radio under F.C.C. Regulations

6.1 Introduction

Ultra Wide Bandwidth (UWB) digital impulse radio occupies huge amount of bandwidth up to a few GHz due to using extremely narrow pulses in time domain, which are typically only a fraction of a nanosecond wide. Many traditional communication systems operate on different regions of UWB radio bandwidth. In order to mitigate the effects of interference caused by UWB devices on traditional narrow band systems, the regulatory authorities imposed restrictions on the pulse spectrum and transmitted power of such devices. In this chapter, the practical UWB systems under these new laws are investigated.

6.2 UWB Spectral Mask

Many traditional UWB systems use a Gaussian pulse shape with sub nanosecond width. These pulses do not comply with the spectral masked imposed by regulatory authorities. Fig. 6.1 shows this spectral mask [8]. The vertical axis

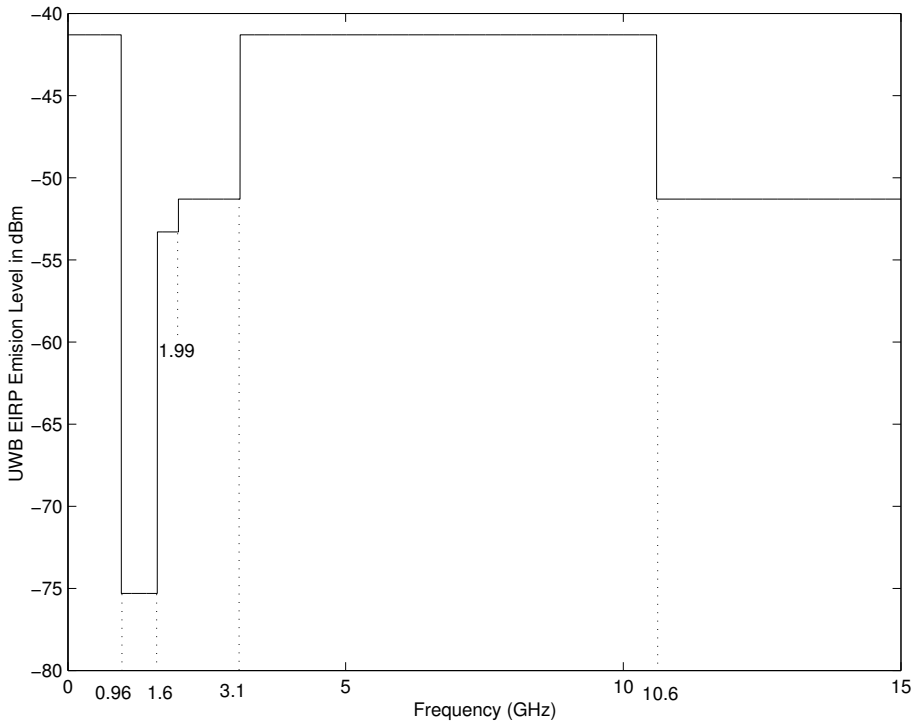

Figure 6.1: FCC spectral mask for indoor UWB devices

in Fig. 6.1 is the UWB Equivalent Isotropic Radiation Power (EIRP) emission level in dBm per MHz measured at a distance of 3 meters from the UWB transmitter antenna. The maximum allowable level is -41.25 dBm. In order to

understand this mask better, we derive this maximum allowable EIRP. According to FCC regulations, all UWB devices should comply with specific spurious emission limits. This limit is $500\frac{\mu V}{m}$ in RMS electric field strength measured in one MHz bandwidth at 3 meters from the UWB transmitter antenna. This limit should be met at any direction from the transmitter antenna measured by a spectrum analyzer with 1 MHz resolution bandwidth. This unintentional spurious emission limit should be valid for any 1 MHz of frequency spectrum.

If we represent the electric field intensity by $\mathbf{e}(t)$ with units of $\frac{V}{m}$, and if $\mathbf{h}(t)$ represents the magnetic filed intensity, then

$$|\mathbf{e}(t)| = \eta|\mathbf{h}(t)| \tag{6.1}$$

where $\mathbf{e}(t) \perp \mathbf{h}(t)$. The magnetic field intensity, $\mathbf{h}(t)$, is expressed in Amperes per meter squared. The impedance of the medium through which the electromagnetic wave is travelling, is represented by η in Ohms. The Poynting vector is defined as

$$\mathbf{p}(t) = \mathbf{e}(t) \times \mathbf{h}(t) \tag{6.2}$$

where $\times$ indicates vector cross product. Poynting vector is the power radiated through a unit surface area at the point of measurement in $\frac{W}{m^2}$ and is perpendicular to this area. Considering

$$e(t) = E\cos(2\pi f_c t) \tag{6.3}$$

then

$$P = \frac{|E|^2}{2\eta} \tag{6.4}$$

where P represents the root mean squared value of radiated power per unit surface area of the wave front in $\frac{W}{m^2}$. Equivalently

$$P = \frac{|E_{rms}|^2}{\eta} \tag{6.5}$$

where E_{rms} accounts for the RMS value of the electric field strength. For free space,

$$\eta = 120\pi = 377\Omega \tag{6.6}$$

The 500 $\frac{\mu V}{m^2}$ RMS electric field strength at 3 meters from the UWB transmitter antenna translates to

$$P = \frac{500 \times 10^{-6}}{377} = 6.63 \times 10^{-10} \frac{\mathrm{W}}{\mathrm{m}^2} \tag{6.7}$$

The total radiated power is bounded from above by the isotropic radiated power, which sends energy equally in all directions. For a sphere with a radius of 3 meters this means

$$P_{\text{total}} \leq (4\pi 3^2) 6.63 \times 10^{-10} = 7.5 \times 10^{-8} \frac{\mathrm{W}}{\mathrm{m}^2} \tag{6.8}$$

or

$$P_{\text{total}} \leq 10 \log_{10}(7.5 \times 10^{-8}) = -71.25\text{dBW} = -41.25\text{dBm} \tag{6.9}$$

It is worth noting that EIRP is the maximum radiated power and if we use directional antennas, we must base our computation on the strongest power density direction. In other words, EIRP is greater than actual radiated power for directional antennas and doing the computations for EIRP will be conservative. Mathematically,

$$\text{EIRP} = \max_{\theta_{\text{az.}}, \theta_{\text{el.}}} \{4\pi R^2 P(\theta_{\text{azimuth}}, \theta_{\text{elevation}})\} \tag{6.10}$$

where R represents the measurement distance from the transmitter antenna and $P(\theta_{\text{azimuth}}, \theta_{\text{elevation}})$ accounts for power density at spherical coordinates of $(R, \theta_{\text{azimuth}}, \theta_{\text{elevation}})$. The maximization in (6.10) is carried on with respect to $\theta_{\text{azimuth}}, \theta_{\text{elevation}}$ at distance R from the transmitter antenna.

6.3 Pulse Shape Design

A Gaussian pulse can be mathematically represented as

$$w(t) = \frac{A}{\sqrt{(2\pi)\sigma^2}} e^{-\frac{t^2}{2}} \tag{6.11}$$

By taking the derivatives of a Gaussian pulse, the following recursive relationship for the derivatives of a Gaussian pulse can be obtained [49]

$$w^{(n)}(t) = \frac{1-n}{\sigma^2} w^{(n-2)}(t) - \frac{t}{\sigma^2} w^{(n-1)}(t) \tag{6.12}$$

where $w^{(n)}(t)$ represents the nth order derivative of a Gaussian pulse. Taking the Fourier transform of $w^{(n)}(t)$,

$$W^{(n)}(f) = A(2\pi f)^n e^{-\frac{(2\pi f\sigma)^2}{2}} \tag{6.13}$$

where $W^{(n)}(f)$ represents the Fourier transform of the nth derivative of Gaussian pulse shape. To find the maximum value of $W^{(n)}(f)$,

$$\frac{\partial W^{(n)}(f)}{\partial f} = 0 \Rightarrow f_{max} = \frac{\sqrt{n}}{2\pi\sigma} \tag{6.14}$$

which corresponds to a maximum value of

$$W^n(f_{max}) = A\frac{n}{\sigma^2}^{\frac{n}{2}} e^{-\frac{n}{2}} \tag{6.15}$$

Designing the pulse shape such that its normalized power spectral density is 10 dB below its maximum at 10.6 GHz and investigating different values for n leads us to obtain $n = 6$ with $\sigma = 53$ picoseconds as a good candidate meeting all the F.C.C. spectral masked requirements [49]. This pulse has been shown in Fig. 6.2.

Fig. 6.3 shows a typical UWB channel measurement. This measurement has been normalized to have a unit energy. This multipath channel measurement is one of many taken by Intel Corporation in the frequency domain between 2 GHz to 8 GHz with 3.75 MHz resolution bandwidth. Inverse fast Fourier transform has been applied to this frequency domain measurement to get the time domain representation of Fig. 6.3. Since higher frequencies do not have the same penetration capability as lower frequencies and the attenuation

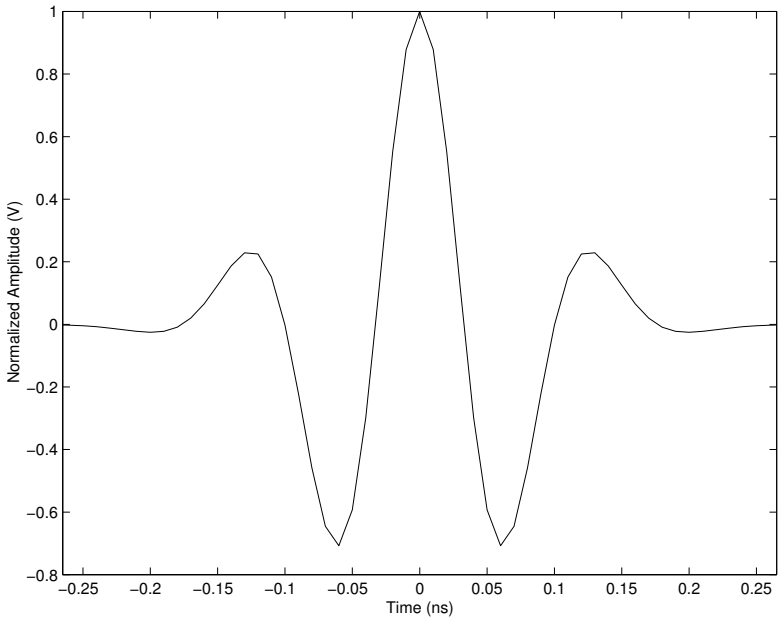

Figure 6.2: Sixth order derivative of Gaussian pulse shape

is higher at such frequencies, the channel model in Fig. 6.3 represents lower number of paths per unit time and the delay spread is much less than that of Fig. 3.10. Throughout this chapter we use multipath channel responses as in Fig. 6.3 with a sixth order derivative of Gaussian pulse shape shown in Fig. 6.2 for studying multiple access digital impulse radio.

6.4 Simulation Results

Fig. 6.4 shows the simulation results for the uncoded bit error rate versus the number of pulses per bit and parameterized by different hopping ranges

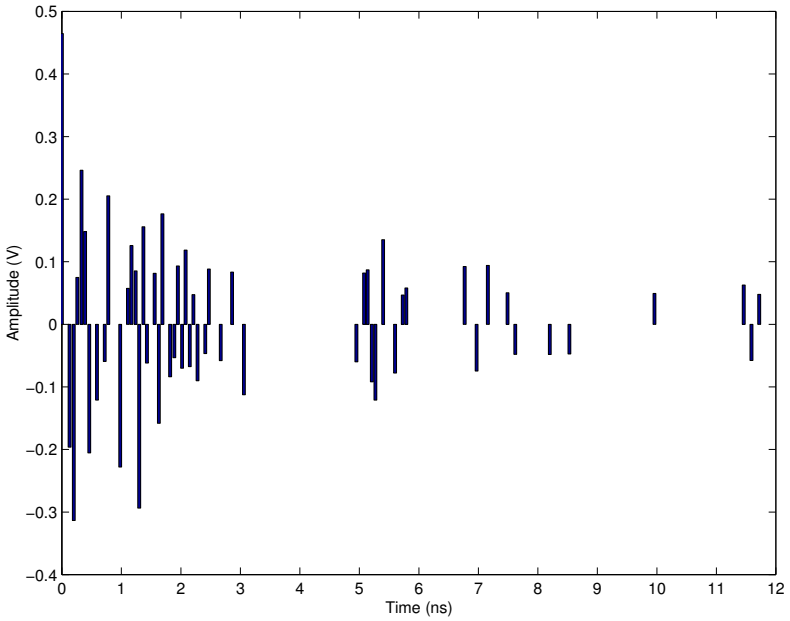

Figure 6.3: A typical indoor UWB Channel

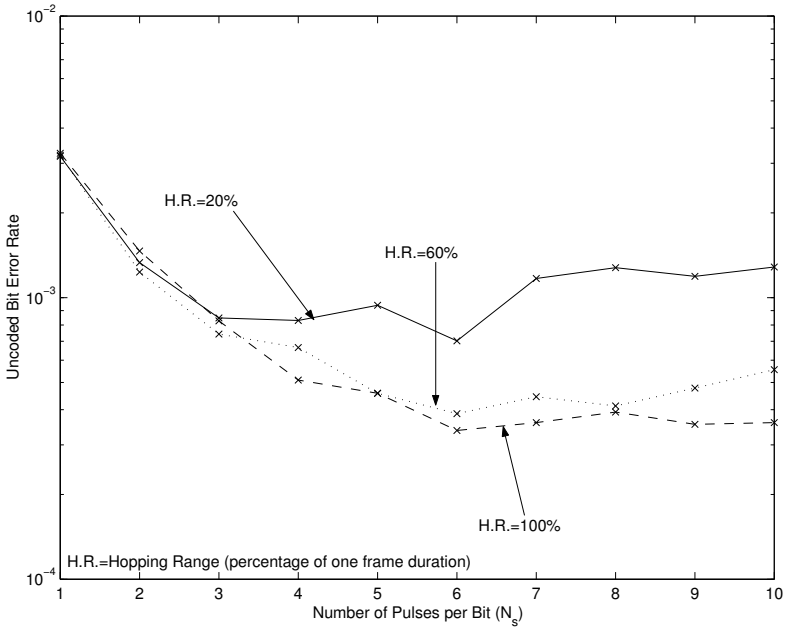

Figure 6.4: Uncoded bit error rate versus the number of pulses per bit and parameterized by different hopping ranges

when 10 users are communicating at 5 Mbps data rate simultaneously. Hopping range is expressed in terms of the percentage of one frame duration. As can be seen, at higher frame durations, restricting the hopping range leads to a better performance due to eliminating the inter-symbol interference and mitigating the collisions arising from those users who are asynchronously apart enough from the asynchronous delay of the user of interest. However, this restriction does not help at small frame durations, since we need adequate hopping spaces to mitigate the multiple access collisions. Also, a local optimality exists in choosing an appropriate frame duration. At lower number of pulses per data symbol, although the likelihood of collisions are smaller due to longer frame durations, with just few destructive collisions, we can not recover the corrupted transmitted bit of the user of interest using the corrupted soft decision statistic. On the other hand, at large number of pulses per bit, the effect of collisions is better mitigated due to averaging over a large number of pulses per data symbol, but the likelihood of collisions are so high that averaging over many severely corrupted pulses associated to the same transmitted bit does not help the receiver in making a correct decision. Therefore, there is a locally optimal value for choosing the frame duration, where the chance of collisions and mitigating the effect of collisions are jointly optimized.

Fig. 6.5 demonstrates the simulation results for the near far problem when five users are communicating at 5 Mbps simultaneously. The horizontal axis

shows the single interferer power to the power of the user of interest's signal. For example, 3 dB on this axis means that each of the other four interferers is two times stronger than the user of interest. While the uncoded bit error rate for the case with no near-far problem, i.e., the leftmost point on the curve, is 3.75×10^{-5}, the performance degrades to 1.4×10^{-3} when each interferer is 10 dB stronger than the user of interest's signal. This problem is significant

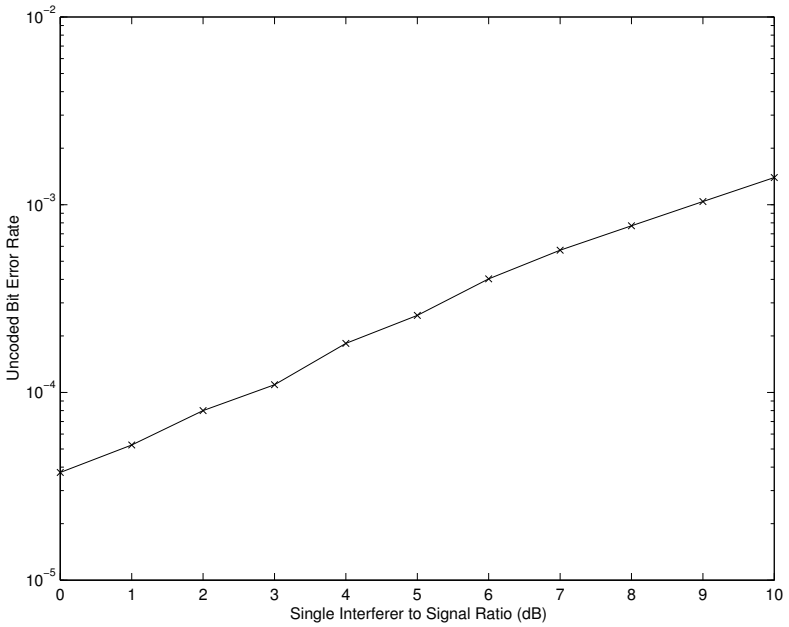

Figure 6.5: Near-far problem

in determining the absolute power level for the user of interest that not only complies with FCC maximum emission levels, but also maintains a reliable communication in the presence of strong interferers.

Fig. 6.6 investigates the simulation results for bit error rate performance at different frame durations and hopping ranges when 10 users are communicating at 10 Mbps simultaneously. Similar conclusions as drawn from Fig. 6.4 are observed by investigating Fig. 6.6 carefully. However, due to smaller frame duration at each N_s compared to the frame duration at the same N_s in Fig. 6.4, the bit error rate is higher. Also, for the same reason, the bit error rate is

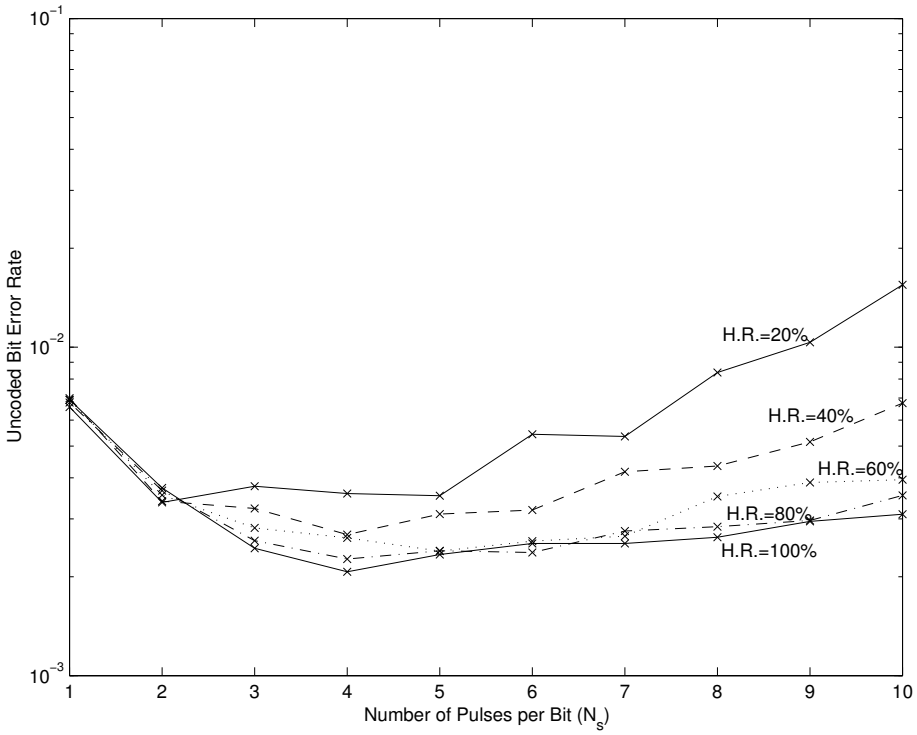

Figure 6.6: Uncoded bit error rate at different frame durations and hopping ranges

minimum at a lower number of pulses per data symbol.

Given a fixed number of users, N_u, we may design the frame duration, T_f, such that the bit error performance at a given data rate, R_s, is better. We describe such design rules of thumb as follows. Representing a typical multipath channel delay spread as $\tilde{\tau}$, frame duration may be chosen as

$$T_f = \frac{N_u \tilde{\tau}}{10} \tag{6.16}$$

Therefore,

$$N_s = \frac{1}{R_s T_f} \tag{6.17}$$

These rules can be explained by the following sentence. Repeat a long frame period, but not longer, as many times as possible. Repetition is good. It gives us processing gain. However, sending many pulses per data symbol at very short frame durations corrupted by lots of collisions at each frame period, does not help mitigate the effect of collisions. A long enough frame should be repeated as many times as possible so that not all the frames corresponding to the same bit are severely corrupted by multiple-access collisions. In that case, averaging over all those not so corrupted frames as many times as possible, leads to a better performance. Fig.'s 6.7 and 6.8 are such examples to illustrate these design rules of thumb.

Fig. 6.7 shows the simulation results for bit error rate performance versus the number of pulses transmitted per data symbol for 10 users when they are communicating at two different data rates. The dash curve corresponds to 10 Mbps data rate while the solid curve demonstrates the 5 Mbps data rate. As can be observed, the best performance can be achieved when the frame duration is roughly the size of a typical multipath channel delay spread in both cases.

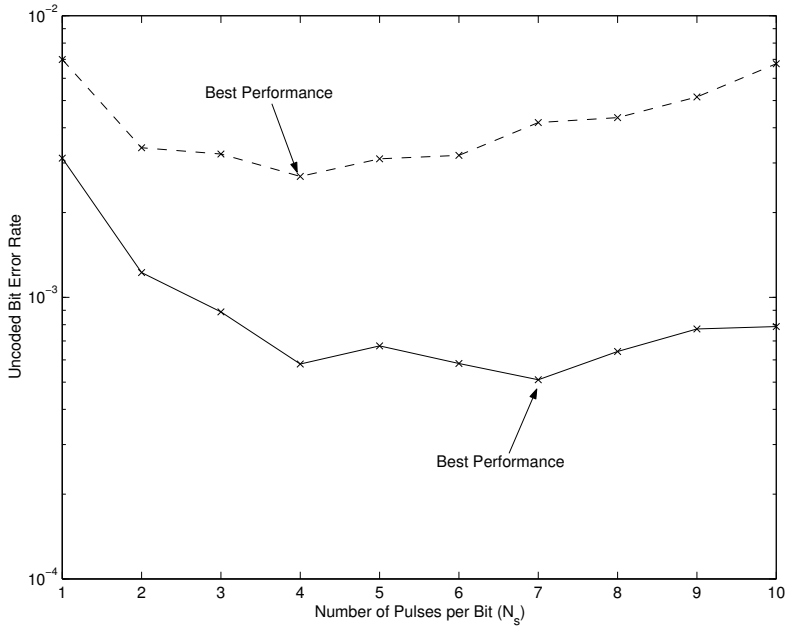

Figure 6.7: Uncoded bit error rate at different frame durations for different data rates with fixed number of users

Fig. 6.8 demonstrates the simulation results for bit error rate versus the number of pulses sent per data symbol when users are communicating at 5 Mbps data rate. The solid curve corresponds to 10 users while the dash curve

sketches the 20 user case. Again, for 10 users the best performance is achieved when the frame period is on the order of the delay spread; however, the frame period is almost doubled where the best performance is obtained for 20 users at the same data rate.

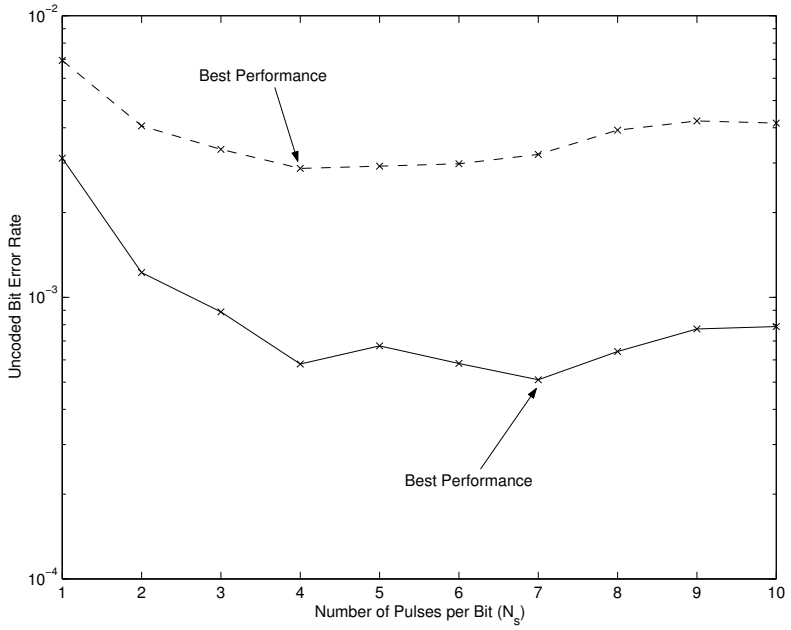

Figure 6.8: Uncoded bit error rate at different frame durations for different number of users at a fixed data rate

6.5 Conclusion

In order to achieve a better bit error rate performance for UWB multiple-access digital impulse radio in the presence of multipath propagation conditions, several parameters should be considered to design such systems. These

parameters are chosen based on the number of active users, data rate, and a typical multipath channel delay spread. System design rules of thumb based on running a lot of simulations for different scenarios are proposed.

At a given data rate, it is better to send as many pulses as possible per data symbol in order to attain processing gain at the receiver. However, transmitting too many pulses with very short frame durations results in making a soft decision based on averaging over many severely corrupted pulses corresponding to the same data symbol, which does not necessarily lead to the best achievable bit error rate performance.

Choosing a long enough frame duration compared to the multipath channel delay spread and sending as many such frames as possible per data symbol ensures a good soft decision by averaging over those not so collided frames. In this case, a better bit error rate performance for the same number of users communicating at a fixed data rate is feasible.

Restricting the hopping range when the frame period is large enough compared to the multipath channel delay spread helps mitigate the inter-symbol interference and collisions from those users who are asynchronously apart enough with respect to the user of interest. On the other hand, this restriction may not lead to a better performance for shorter frame durations since there is not

enough room for different users to hop around in order to avoid multiple-access collisions.

Chapter 7

Future Work

7.1 Introduction

The regulatory authorities have recently imposed new rules for UWB communication devices under which transmitted power is restricted by spectral masks specifically designed for different UWB applications operating at different frequency bandwidths. These new regulations motivate conducting research on studying and investigating the behavior of UWB systems under such circumstances. Also, some other system design aspects of UWB digital impulse radio such as fast acquisition synchronization and tracking loops, UWB channel estimation, and pseudo random sequence design should be investigated in the frame work of UWB specific characteristics and applications. In this chapter, some of the future research topics of interest are addressed.

7.2 Designing Efficient Pulse Shapes

According to the spectral mask shown in Fig. 6.1, an efficient pulse shape for indoor UWB devices may be designed such that its spectral density contents is as close to a rectangular spectrum over the frequency range from 3.1 GHz to 10.6 GHz as possible. This optimization should be done under some other constraints such as good synchronization properties of the pulse and the feasibility of generating the sub nanosecond pulse fairly easy with current technology. This is a challenging research area, which needs complex mathematical analysis along with considering some practical engineering restrictions.

7.3 Fast Synchronization Algorithms

As the name UWB implies, the system uses extremely narrow pulses on the order of tenths of a nanosecond. This requires very fast synchronizing algorithms [9, 26, 32, 33, 34] that not only acquire the frame clock, but also synchronize to the time-hopping or direct sequence associated to the user of interest in the harsh multipath propagation conditions along with having many users communicating simultaneously. Due to the multipath phenomenon, energy can be detected along the delay spread, and specially when the line of sight path is not the strongest path, detecting the leading edge of the delay spread is not

such an easy task. Presence of several users at the same time, hopping around the frame period, makes this task even harder for we have to synchronize to the user of interest and not just any of them.

7.4 UWB Channel Statistical Modelling at the Frequency Range of Interest

According to F.C.C. Report and Order on UWB systems, frequency range of interest for indoor UWB devices is mainly limited between 3.1 GHz to 10.6 GHz. This may suggest that new channel measurement campaign at this specific frequency range complied with F.C.C. spectral mask should be carried on in order to develop accurate models for indoor UWB channel based on new rules. These measurements should represent the statistical properties of a typical indoor UWB multipath channel with regard to delay spread, multipath intensity profile, and coherency of the channel. Therefore, many measurements at different scenarios should be made, so that each scenario characterizes one or more statistics of UWB multipath channels on average.

7.5 Optimal Design for Combining Ranging and Communication Capabilities

Due to the fine multipath resolution of UWB radio, accurate ranging with fine precision is feasible [30, 12]. Developing optimal UWB channel estimation algorithms based on combining communication and ranging capabilities results in compact multipurpose UWB devices with promising market potentials.

7.6 Pseudo-Random Sequence Design with Favorable Correlation Properties

Designing spectrally flat time-hopping sequences with minimum correlation between different sequences associated to different users in the presence of multipath is another research topic on developing UWB impulse radio [47, 28, 35]. These sequences should be designed not only to minimize the chance of collisions between different users under ideal propagation conditions, but also to separate different users apart enough from each other such that in realistic multipath propagation scenarios, the overlap between different users's delay spreads are also minimized.

7.7 Fast Low Bit Quantization Algorithms

To achieve high precision, we need as many bits for quantization as possible; however, due to the huge bandwidth of UWB radio, this requires very fast technology to take billions of samples per second. This is not feasible by current advances in analog to digital converters. Therefore, channelized receivers [38, 39] should be deployed to overcome this problem. Designing such receivers with low complexity and enough precision is another research area to overcome hardware limitations by developing feasible quantization algorithms.

Reference List

[1] Dajana Cassioli, Moe Z. Win, Andreas F. Molisch, *"A Statistical Model for the UWB Indoor Channel,"* IEEE Vehicular Technology Conference, VOL. 2, Spring 2001.

[2] Dajana Cassioli, Moe Z. Win, Francesco Vatalaro, Andreas F. Molisch, *"Performance of Low-Complexity Rake Reception in a Realistic UWB Channel,"* IEEE International Conference on Communications, NO. 1, April 2002.

[3] Ward Cheney, and David Kincaid, "Numerical Mathematics and Computing," Fourth Edition, Brooks/Cole Publishing Company, 1999.

[4] J. M. Cramer, R. A. Scholtz, M. Z. Win, *"On the analysis of UWB communication channels,"* IEEE Military Communications Conference, NO. 1, October 1999.

[5] J. M. Cramer, R. A. Scholtz, M.Z. Win, *"Spatio-Temporal Diversity in Ultra-Wideband Radio,"* IEEE Wireless Communications and Networking Conference, NO. 1, September 1999.

[6] R. Jean-Marc Cramer, Moe Z. Win, Robert A. Scholtz, *"Evaluation of the Multipath Characteristics of the Impulse Radio Channel,"* The Ninth IEEE International Symposium on Personal, Indoor and Mobile Radio Communications, VOL. 2, September 1998.

[7] Douglas A. Cummings, *"Aggregate Ultra Wideband Impact On Global Positioning System Receivers,"* IEEE Radio and Wireless Conference, 2001.

[8] Federal Communication Commission, *"Revision of Part 15 of the Commission's Rules Regarding Ultra-wideband Transmission Systems, First Report and Order,"* FCC, February 2002.

[9] Robert Fleming, Cherie Kushner, Gary Roberts, Uday Nandiwada, *"Rapid Acquisition for Ultra-Wideband Localizers,"* IEEE Conference on Ultra Wideband Systems and Technologies, Baltimore, MD, May 2002.

[10] Jeffrey R. Foerster, *"The Effects of Multipath Interference on the Performance of UWB Systems in an Indoor Wireless Channel,"* IEEE Vehicular Technology Conference, VOL. 2, Spring 2001.

[11] Robert Fontana, *"An Insight into UWB Interference Suppression in Time-Hopping Impulse Radio Systems,"* IEEE Conference on Ultra Wideband Systems and Technologies, Baltimore, MD, May 2002.

[12] Robert Fontana, Steve Gunderson, *"Ultra-Wideband Precision Asset Location System,"* IEEE Conference on Ultra Wideband Systems and Technologies, Baltimore, MD, May 2002.

[13] Matti Hamalainen, Jari Iinatti, Veikko Hovinen, Matti Latva-aho, *"In-Band Interference of Three Kind of UWB Signals in GPS L1 Band and GSM900 Uplink Band,"* 12th IEEE International Symposium on Personal, Indoor and Mobile Radio Communications, VOL. 1, September 2001.

[14] M. Hamalainen, V. Hovinen, J. Iinatti, M. Latva-aho, *"In-Band Interference Power Caused by Different Kinds of UWB Signals at UMTS/WCDMA Frequency Bands,"* IEEE Radio and Wireless Conference, 2001.

[15] M. Hamalainen, V. Hovinen, R. Tesi, J. H. J. Iinatti, M. Latva-aho, *"On the UWB system Performance with GSM900, UMTS/WCDMA, and GPS,"* IEEE Journal on Selected Areas in Communications, VOL. 20, NO. 9, December 2002.

[16] M. Hamalainen, Raffaello Tesi, Jari Iinatti, *"On the UWB System Performance Studies in AWGN Channel with Interference in UMTS Band,"* IEEE Conference on Ultra Wideband Systems and Technologies, Baltimore, MD, May 2002.

[17] Homayoun Hashemi, *"A Study of Temporal and Spatial Variations of the Indoor Radio Propagation Channel,"* 5th IEEE International Symposium on Personal, Indoor and Mobile Radio Communications, VOL. 1, September 1994.

[18] Homayoun Hashemi, *"Impulse Response Modeling of Indoor Radio Propagation Channels,"* IEEE Journal on Selected Areas in Communications, VOL. 11, NO. 7, September 1993.

[19] Homayoun Hashemi, *"The Indoor Radio Propagation Channel,"* Proceedings of the IEEE, VOL. 81, Issue: 7, July 1993.

[20] Homayoun Hashemi, Michael McGuire, Thomas Vlasschaert, David Tholl, *"Measurements and Modeling of Temporal Variations of the Indoor Radio Propagation Channel,"* IEEE Transactions on Vehicular Technology, VOL. 43, NO. 3, August 1994.

[21] Homayoun Hashemi, Daniel Lee, Dale Ehman, *"Statistical Modeling of the Indoor Radio Propagation Channel - Part II,"* IEEE Vehicular Technology Conference, May 1992.

[22] Homayoun Hashemi, David Tholl, *"Statistical Modeling and Simulation of the RMS Delay Spread of Indoor Radio Propagation Channels,"* IEEE Transactions on Vehicular Technology, VOL. 43, Issue: 1, February 1994.

[23] Homayoun Hashemi, David Tholl, Gerald Morrison, *"Statistical Modeling of the Indoor Radio Propagation Channel - Part I,"* IEEE Vehicular Technology Conference, May 1992.

[24] Homayoun Hashemi, David Tholl, Thomas Vlasschaert, *"A Study of CW Spatial Fading of the Indoor Radio Propagation Channel,"* Fourth IEEE International Conference on Universal Personal Communications, November 1995.

[25] Simon S. Haykin, "Adaptive Filter Theory," Third Edition, Prentice Hall, 1995.

[26] Eric Homier, Robert A. Scholtz, *"Rapid Acquisition of Ultra-Wideband Signals in the Dense Multipath Channel,"* IEEE Conference on Ultra Wideband Systems and Technologies, Baltimore, MD, May 2002.

[27] Maria Stella Iacobucci, Maria Gabriella Di Benedetto, *"Radio Frequency Interference Issues in Impulse Radio Multiple Access Communication Systems,"* IEEE Conference on Ultra Wideband Systems and Technologies, Baltimore, MD, May 2002.

[28] D. C. Laney, G. M. Maggio, F. Lehmann, L. Larson, *"Multiple Access for UWB Impulse Radio with Pseudochaotic Time Hopping,"* IEEE Journal on Selected Areas in Communications, VOL. 20, NO. 9, December 2002.

[29] Hojoon Lee, Byungchil Han, Yoan Shin, Sungbin Im, *"Multipath Characteristics of Impulse Radio Channels,"* IEEE Vehicular Technology Conference Proceedings, VOL. 3, Spring 2000.

[30] J.-Y. Lee, R. A. Scholtz, *"Ranging in a Dense Multipath Environment Using an UWB Radio Link,"* IEEE Journal on Selected Areas in Communications, VOL. 20, NO. 9, December 2002.

[31] James S. Lehnert, Michael B. Pursley, *"Multipath Diversity Reception of Spread-Spectrum Multiple-Access Communications,"* IEEE Transactions on Communications, VOL. Com-35, NO. 11, November 1987.

[32] W. M. Lovelace, J. K. Townsend, *"The Effects of Timing Jitter and Tracking on the Performance of Impulse Radio,"* IEEE Journal on Selected Areas in Communications, VOL. 20, NO. 9, December 2002.

[33] William Lovelace, J. Keith Townsend, *"The Effects of Timing Jitter on the Performance of Impulse Radio,"* IEEE Conference on Ultra Wideband Systems and Technologies, Baltimore, MD, May 2002.

[34] Yao Ma, S. Pasupathy, *"Acquisition Performance of an Ultra Wide-band Communications System over a Multiple-Access Fading Channel,"* IEEE Conference on Ultra Wideband Systems and Technologies, Baltimore, MD, May 2002.

[35] Gian Mario Maggio, Nikola Rulkov, Luca Reggiani, *"Psedo-Chaotic Time Hopping For UWB Impulse Radio,"* IEEE Transactions on Circuits and Systems-I: Fundamental Theory and Applications, VOL. 48, NO. 12, December 2001.

[36] Jerry M. Mendel, "Lessons in Estimation Theory for Signal Processing, Communications, and Control," Prentice Hall, 1995.

[37] Fernando Ramirez-Mireles, *"On the Perfromance of Ultra-Wide-Band Signals in Gaussian Noise and Dense Multipath,"* IEEE Transactions on Vehicular Technology, VOL. 50, NO. 1, January 2001.

[38] Won Namgoong, *"A Channelized DSSS Ultra-Wideband Receiver,"* IEEE 2001.

[39] Won Namgoong, *"Channelized Digital Receivers for Impulse Radio,"* To be appeared in IEEE International Conference on Communications, June 2003.

[40] Homayoun Nikookar, Homayoun Hashemi, *"Phase Modeling of Indoor Radio Propagation Channels,"* IEEE Transactions on Vehicular Technology, VOL. 49, NO. 2, March 2000.

[41] Homayoun Nikookar, Homayoun Hashemi, *"Statistical Modeling of Signal Amplitude Fading of Indoor Radio Propagation Channels,"* 2nd International Conference on Universal Personal Communications, VOL. 1, October 1993.

[42] Robert C. Qui, *"A Theoretical Study of the Ultra-Wideband Wireless Propagation Channel Based on the Scattering Centers,"* IEEE Vehicular Technology Conference 1998.

[43] R. C. Qui, *"A Study of the Ultra-Wideband Wireless Propagation Channel and Optimum UWB Receiver Design,"* IEEE Journal on Selected Areas in Communications, VOL. 20, NO. 9, December 2002.

[44] Robert C. Qui, I-Tai Lu, *"Multipath resolving with frequency dependence for wide-band wireless channel modeling,"* IEEE Transactions on Vehicular Technology, VOL. 48, NO. 1, January 1999.

[45] Theodore S. Rappaport, "Wireless Communications," Prentice Hall, 1996.

[46] R. A. Scholtz, *"Multiple Access with Time-Hopping Impulse Radio,"* IEEE Military Communications Conference, VOL. 2, Boston, MA, October 1993.

[47] R. A. Scholtz, P. Vijay Kumar, Carlos J. Corrado-Bravo, *"Signal Design for Ultra-wideband Radio,"* Sequences and Their Applications - SETA'01, Springer-Verlag 2002.

[48] R. A. Scholtz, R. Weaver, E. Homier, J. Lee, P. Hilms, A. Taha, R. Wilson, *"UWB Radio Deployment Challenges,"* IEEE Personal Indoor Mobile Radio Communications, London, U.K., September 2000.

[49] Hongsan Sheng, Philip Orlik, Alexander M. Haimovich, Leonard J. Cimini, Jinyun Zhang, *"On the Spectral and Power Requirements for Ultra-Wideband Transmission,"* Submitted to IEEE International Conference on Communications, June 2003.

[50] Kazimierz Siwiak, Alan Petroff, *"A Path Link Model for Ultra Wide Band Pulse Transmissions,"* IEEE Vehicular Technology Conference, VOL. 2, Spring 2001.

[51] Kazimierz Siwiak, *"Impact of Ultra Wide Band Transmissions on a Generic Receiver,"* IEEE Vehicular Technology Conference, VOL. 2, Spring 2001.

[52] Kazimierz Siwiak, *"Ultra-Wide Band Radio: Introducing a New Technology,"* IEEE Vehicular Technology Conference, VOL. 2, Spring 2001.

[53] Kazimierz Siwiak, Paul Withington, Susan Phelan, *"Ultra-Wide Band Radio: The Emergence of an Important Introducing New Technology,"* IEEE Vehicular Technology Conference, VOL. 2, Spring 2001.

[54] Gilbert Strang, "Linear Algebra and Its Applications," Harcourt College Publishers, 1988.

[55] Ali Taha, *"Multiple Access Capacity and Receiver Processing of Impulse Radio in the Presence of Multipath,"* Ph.D. Proposal, Communication Sciences Institute, Department of Electrical Engineering-Systems, University of Southern California, February 2001.

[56] Ali Taha, Keith M. Chugg, *"A Theoretical Study on the Effects of Interference on UWB Multiple Access Impulse Radio,"* 36th Asilomar Conference, Pacific Grove, CA, Novemeber 3-6, 2002.

[57] Ali Taha, Keith M. Chugg, *"Multiple Access Capacity of Digital Impulse Radio in the Presence of Multipath Fading,"* URSI 2001, Boulder, Colorado, January 2001.

[58] Ali Taha, Keith M. Chugg, *"Multipath Diversity Reception of Wireless Multiple Access Time-Hopping Digital Impulse Radio,"* IEEE Conference on Ultra Wideband Systems and Technologies, Baltimore, MD, May 2002.

[59] Ali Taha, Keith M. Chugg, *"On Designing the Optimal Template Waveform for UWB Impulse Radio in the Presence of Multipath,"* IEEE Conference on Ultra Wideband Systems and Technologies, Baltimore, MD, May 2002.

[60] Ali Taha, Keith M. Chugg, *"On the Power Spectral Density of Wireless Multiple-Access UWB Impulse Radio under Realistic Propagation Conditions,"* Submitted to IEEE Vehicular Technology Conference, Orlando, FL, October 2003.

[61] Ali Taha, Keith M. Chugg, *"Wireless Multiple Access UWB Radio Under Realistic Propagation Conditions,"* To be submitted to IEEE Transactions on Communications.

[62] C. L. Weber, G. K. Huth, and B. H. Batson, *"Performance Considerations of Code Division Multiple-Access Systems,"* IEEE Transactions on Vehicular Technology, VOL. VT-30, NO. 1, February 1981.

[63] Matthew L. Welborn, *"System Considerations for Ultra-Wideband Wireless Networks,"* IEEE Radio and Wireless Conference, 2001.

[64] R. D. Wilson, R. D. Weaver, M.-H. Chung, R. A. Scholtz, *"Ultra Wideband Interference on an Amateur Radio Receiver,"* IEEE Conference on Ultra Wideband Systems and Technologies, Baltimore, MD, May 2002.

[65] Moe Z. Win, *"A Unified Spectral Analysis of Generalized Time-Hopping Spread Spectrum Signals in the Presence of Timing Jitter,"* IEEE Journal on Selected Areas in Communications, VOL. 20, NO. 9, December 2002.

[66] Moe Z. Win, *"Spectral Density of Random Time-Hopping Spread-Spectrum UWB Signals with Uniform Timing Jitter,"* IEEE Military Communications Conference Proceedings, VOL. 2, 1999.

[67] Moe Z. Win, *Ultra-Wide Bandwidth Spread-Spectrum Techniques for Wireless Multiple-Access Communications,* Ph.D. Thesis, Communication Sciences Institute, University of Southern California, May 1998.

[68] Moe Z. Win, George Chrisikos, Nelson R. Sollenberger, *"Performance of Rake Reception in Dense Multipath Channels: Implications of Spreading Bandwidth and Selection Diversity Order,"* IEEE Journal on Selected Areas in Communications, VOL. 18, NO. 8, August 2000.

[69] Moe Z. Win, Zoran A. Kostic, *"Impact of Spreading Bandwidth on Rake Reception in Dense Multipath Channels,"* IEEE Journal on Selected Areas in Communications, VOL. 17, NO. 10, October 1999.

[70] Moe Z. Win, Zoran A. Kostic, *"Virtual Path Analysis of Selective Rake Receiver in Dense Multipath Channels,"* IEEE Communications Letters, VOL. 3, NO. 11, November 1999.

[71] Moe Z. Win, Fernando Ramirez-Mireles, Robert A. Scholtz, *"Ultra-Wide Bandwidth (UWB) Signal Propagation for 0utdoor Wireless Communications,"* IEEE Vehicular Technology Conference, VOL. 1, May 1997.

[72] Moe Z. Win, Robert A. Scholtz, *"Comparisons of Analog and Digital Impulse Radio for Wireless Multiple-Access Communications,"* IEEE International Conference on Communications-Montreal, Canada, June 1997.

[73] Moe Z. Win, Robert A. Scholtz, *"Energy Capture vs. Correlator Resources in Ultra-Wide Bandwidth Indoor Wireless Communications Channels,"* in Proc. Military Communications Conference, VOL. 3, Monterey, CA., pp. 1277-1281, November 1997.

[74] Moe Z. Win, Robert A. Scholtz, *"Impulse Radio: How it works,"* IEEE Communications Letters, VOL. 2, NO. 1, January 1998.

[75] Moe Z. Win, Robert A. Scholtz, *"On the Robustness of Ultra-Wide Bandwidth Signals in Dense Multipath Environments,"* IEEE Communications Letters, Vol. 2, No. 2, February 1998.

[76] Moe Z. Win, Robert A. Scholtz, *"Ultrta-Wide Bandwidth Signal Propagation for Indoor Wirelss Communications,"* IEEE International Conference on Communications-Montreal, Canada, June 1997.

[77] M. Z. Win, R. A. Scholtz, *"Ultra-Wide Bandwidth Time-Hopping Spread Spectrum Impulse Radio for Wireless Multiple-Access Communications,"* IEEE Transactions on Communications, VOL. 48, NO. 4, April 2000.

[78] Moe Z. Win, Robert A. Scholtz, Larry W. Fullerton, *"Time-Hopping SSMA Techniques for Impulse Radio with an Analog Modulated Data Subcarrier,"* IEEE 4th International Symposium on Spread Spectrum Techniques and Applications Proceedings, VOL. 1, September 1996.

[79] L. Zhao, A. M. Haimovich, *"Performance of Ultra-Wideband Communications in the Presence of Interference,"* IEEE Journal on Selected Areas in Communications, VOL. 20, NO. 9, December 2002.

[80] Li Zhao, Alxander M. Haimovich, Haim Grebel, *"Performance of Ultra-Wideband Communications in the Presence of Interference,"* IEEE International Conference on Communications, VOL 10, 2001.

[81] P. Withington, R. Reinhardt, R. Stanley, *"Preliminary Results of an Ultra-Wideband (Impulse) Scanning Receiver"* IEEE Military Communications Conference Proceedings, VOL. 2, 1999.

Appendix A

Obtaining the Lower and Upper Limits of the $\sum_l$ in (3.9)

Function $R_{vw_{rec}}((l-j)T_f + (c_l^k - c_j^1)T_c + \delta D_l^k + \tau_m^k - \tau_q^1)$ may be not equal to zero, only for the terms for which

$$-T_m < (l-j)T_f + (c_l^k - c_j^1)T_c + \delta D_l^k + \tau_m^k - \tau_q^1 < T_m + \delta \qquad \text{(A.1)}$$

or

$$A < l < B \qquad \text{(A.2)}$$

where

$$A = \frac{-T_m - (c_l^k - c_j^1)T_c - \delta D_l^k - \tau_0^k - (\lambda_m^k - \lambda_q^1)}{T_f} + j \qquad \text{(A.3)}$$

and

$$B = \frac{T_m + \delta - (c_l^k - c_j^1)T_c - \delta D_l^k - \tau_0^k - (\lambda_m^k - \lambda_q^1)}{T_f} + j \qquad \text{(A.4)}$$

and we have used the fact that $\tau_m^k = \tau_0^k + \lambda_m^k$ and $\tau_0^1 = 0$. The lower limit of l is minimized as

$$\min(A) = \frac{-T_m - (T_f - T_c) - \delta - \frac{T_f}{2} - \tilde{\tau}}{T_f} + j \qquad \text{(A.5)}$$

where $\tilde{\tau}$ is the maximum delay spread of multipath profiles and $\max[(c_l^k - c_j^1)T_c] = T_f - T_c$. The asynchronous delay τ_0^k is uniformly distributed over $[-\frac{T_f}{2}, \frac{T_f}{2}]$. Therefore,

$$\min(A) = j - 1.5 - \frac{\tilde{\tau}}{T_f} \qquad \text{(A.6)}$$

assuming $T_c = T_m + \delta$. Similarly the upper limit of l is maximized as

$$\max(B) = \frac{T_m + \delta - (-(T_f - T_c)) - 0 - (-\frac{T_f}{2}) - (-\tilde{\tau})}{T_f} + j \qquad \text{(A.7)}$$

Hence,

$$j - 1.5 - \frac{\tilde{\tau}}{T_f} < l < j + 1.5 + \frac{\tilde{\tau}}{T_f} \tag{A.8}$$

Appendix B

Proof of Simplifying the $\sum_l$ in (3.9) to $l = j$ in (3.12)

Similar to Appendix A, the lower and upper limits for l for which $R_{vw_{rdc}}((l-j)T_f + (c_l^k - c_j^1)T_c + \delta D_l^k + \tau_m^k - \tau_q^1)$ may be nonzero, Taking into account the time-hopping range restriction given as the third condition stated at the top of page 47, can be minimized and maximized ,respectively as

$$\min(A) = \frac{-T_m - (\frac{T_f}{2} - \tilde{\tau} - 2T_m - \delta) - \delta - \frac{T_f}{2} - \tilde{\tau}}{T_f} + j \qquad \text{(B.1)}$$

$$\max(B) = \frac{T_m + \delta + (\frac{T_f}{2} - \tilde{\tau} - 2T_m - \delta) - 0 + \frac{T_f}{2} + \tilde{\tau}}{T_f} + j \qquad \text{(B.2)}$$

Hence,

$$j - 1 + \frac{T_m}{T_f} < l < j + 1 - \frac{T_m}{T_f} \tag{B.3}$$

Since $T_f \gg T_m$ in a typical multiuser scenario, we can conclude that

$$j \leq l \leq j \tag{B.4}$$

which means that only terms with $l = j$ may lead to nonzero terms on the right hand side of (3.9); therefore (3.12) is obtained.

Appendix C

Proof of (5.25)

The left hand side of (5.25) can be written as

$$\sum_{l=-nN_s}^{nN_s-1} \sum_{l'=-nN_s}^{nN_s-1} e^{-j2\pi f((l-l')T_f)} = \left| \sum_{l=-nN_s}^{nN_s-1} x^{-l} \right|^2 \tag{C.1}$$

where

$$x = e^{-j2\pi f T_f} \tag{C.2}$$

Using the geometric series sum formula

$$\sum_{l=-nN_s}^{nN_s-1} x^{-l} = \frac{x^{-nN_S}(1-x^{2nN_s})}{1-x} = \frac{x^{-nN_S}-x^{nN_s}}{1-x} \tag{C.3}$$

After carrying on some manipulations and replacing x by $e^{-j2\pi fT_f}$

$$\sum_{l=-nN_s}^{nN_s-1} x^{-l} = \frac{\sin(2\pi fT_f nN_s)}{1-\cos(2\pi fT_f)+j\sin(2\pi fT_f)} \tag{C.4}$$

or

$$\left|\sum_{l=-nN_s}^{nN_s-1} x^{-l}\right|^2 = \frac{4\sin^2(2\pi fT_f nN_s)}{2(1-\cos(2\pi fT_f)} \tag{C.5}$$

Therefore,

$$\sum_{l=-nN_s}^{nN_s-1}\sum_{l'=-nN_s}^{nN_s-1} e^{-j2\pi f((l-l')T_f)} = \frac{\sin^2(2\pi fT_f nN_s)}{\sin^2(2\pi fT_f)} \tag{C.6}$$

Appendix D

Proof of (5.26)

The function

$$g(f) = \frac{1}{2nN_s} \frac{\sin^2(2\pi f T_f n N_s)}{\sin^2(\pi f T_f)} \tag{D.1}$$

is periodic in f with period $f_0 = \frac{1}{T_f}$. To investigate the behavior of this function, we investigate the period $[-\frac{1}{2T_f}, \frac{1}{2T_f}]$. This function has a bounded value at all $f \in [-\frac{1}{2T_f}, \frac{1}{2T_f}] - \{0\}$. Therefore,

$$\lim_{n \to \infty} g(f) = 0 \tag{D.2}$$

for any $f \in [-\frac{1}{2T_f}, \frac{1}{2T_f}] - \{0\}$, because a bounded value is divided by infinity at such frequencies. To investigate the above limit at $f = 0$,

$$\lim_{n\to\infty} \lim_{f\to 0} g(f) = \lim_{n\to\infty} \lim_{f\to 0} \frac{1}{2nN_s} \frac{4\pi^2 f^2 {T_f}^2 n^2 {N_s}^2}{\pi^2 f^2 {T_f}^2} = \infty \tag{D.3}$$

we compute the surface area under this function around $f = 0$.

$$\lim_{n\to\infty} \int_{-\epsilon}^{\epsilon} g(f)df = \lim_{n\to\infty} \int_{-\epsilon}^{\epsilon} 2nN_s \frac{\sin^2(2\pi f T_f n N_s)}{(2nN_s \pi f T_f)^2} \tag{D.4}$$

or

$$\lim_{n\to\infty} \int_{-\epsilon}^{\epsilon} g(f)df = \lim_{n\to\infty} \frac{1}{T_f} \int_{-2nN_s\epsilon T_f}^{2nN_s\epsilon T_f} \mathrm{sinc}^2(x)dx = \frac{1}{T_f} \tag{D.5}$$

where $\mathrm{sinc}(x) = \frac{\sin(\pi x)}{\pi x}$. Therefore,

$$\lim_{n\to\infty} g(f) = \frac{1}{T_f}\delta_D(f) \tag{D.6}$$

when $f \in [-\frac{1}{2T_f}, \frac{1}{2T_f}]$ and $\delta_D(f)$ is the Dirac delta function. Since $g(f)$ is periodic with period $\frac{1}{T_f}$,

$$\lim_{n\to\infty} g(f) = \frac{1}{T_f} \sum_{i=-\infty}^{\infty} \delta_D(f - \frac{i}{T_f}) \tag{D.7}$$